

# **Generalizations of the Kerr-Newman solution**



# Contents

<b>1</b>	<b>Topics</b>	<b>423</b>
1.1	ICRANet Participants . . . . .	423
1.2	Ongoing collaborations . . . . .	423
1.3	Students . . . . .	424
<b>2</b>	<b>Brief description</b>	<b>425</b>
<b>3</b>	<b>Introduction</b>	<b>427</b>
<b>4</b>	<b>The general static vacuum solution</b>	<b>429</b>
4.1	Line element and field equations . . . . .	430
4.2	Static solution . . . . .	431
<b>5</b>	<b>Stationary generalization</b>	<b>435</b>
5.1	Ernst representation . . . . .	435
5.2	Representation as a nonlinear sigma model . . . . .	437
5.3	Representation as a generalized harmonic map . . . . .	439
5.4	Dimensional extension . . . . .	444
5.5	The general solution . . . . .	446
<b>6</b>	<b>Comparison of vacuum static quadrupolar metrics</b>	<b>451</b>
6.1	Introduction . . . . .	451
6.2	General properties of static and axisymmetric vacuum solutions	453
6.3	Static vacuum metrics with quadrupole . . . . .	457
6.4	Physical conditions . . . . .	460
6.5	Multipole moments . . . . .	463
6.6	Remarks . . . . .	467
<b>7</b>	<b>Observers in Kerr spacetimes: the ergoregion on the equatorial plane</b>	<b>469</b>
7.1	Introduction . . . . .	469
7.2	Ergoregion properties in the Kerr spacetime . . . . .	475

*Contents*

---

7.3	Stationary observers and light surfaces . . . . .	479
7.3.1	The frequencies $\omega_{\pm}$ . . . . .	480
7.3.2	Light surfaces . . . . .	491
7.4	Zero angular momentum observers . . . . .	494
7.5	Remarks . . . . .	501
	<b>Bibliography</b>	<b>513</b>

# 1 Topics

- Generalizations of the Kerr-Newman solution
- Properties of Kerr-Newman spacetimes
- Quadrupolar metrics

## 1.1 ICRANet Participants

- Donato Bini
- Andrea Geralico
- Roy P. Kerr
- Hernando Quevedo
- Jorge A. Rueda
- Remo Ruffini

## 1.2 Ongoing collaborations

- Medeu Abishev (Kazakh National University - KazNU, Kazakhstan)
- Kuantay Boshkayev (Kazakh National University - KazNU, Kazakhstan)
- Antonio C. Gutierrez (University of Bolivar, Colombia)
- Orlando Luongo (University of Naples, Italy)
- Daniela Pugliese (Silesian University in Opava, Czech Republic)
- Saken Toktarbay (Kazakh National University - KazNU, Kazakhstan)

## 1.3 Students

- Viridiana Pineda (UNAM PhD, Mexico)
- Pedro Sánchez (UNAM PhD, Mexico)
- Bakytzhan Zhami (KazNU PhD, Kazakhstan)

## 2 Brief description

One of the most important metrics in general relativity is the Kerr-Newman solution that describes the gravitational and electromagnetic fields of a rotating charged mass. For astrophysical purposes, however, it is necessary to take into account the effects due to the moment of inertia of the object. To attack this problem we investigate new exact solutions of Einstein-Maxwell equations which possess an infinite set of gravitational and electromagnetic multipole moments and contain the Kerr-Newman solution as special case.

In particular, we investigate the properties of static and axisymmetric vacuum solutions of Einstein equations which generalize the Schwarzschild spherically symmetric solution to include a quadrupole parameter. We test all the solutions with respect to elementary and asymptotic flatness and curvature regularity. Analyzing their multipole structure, according to the relativistic invariant Geroch definition, we show that all of them are equivalent up to the level of the quadrupole. We conclude that the quadrupolar metric ( $q$ -metric), a variant of the Zipoy-Voorhees metric, is the simplest generalization of the Schwarzschild metric, containing a quadrupole parameter. This is of particular importance for the investigation of the physical effects due to the quadrupole moment, especially in the framework of relativistic astrophysics.

To explore the physical characteristics of black hole spacetimes, we perform a detailed analysis of the properties of stationary observers located on the equatorial plane of the ergosphere in a Kerr spacetime, including light-surfaces. This study highlights crucial differences between black hole and the super-spinner sources. In the case of Kerr naked singularities, the results allow us to distinguish between “weak” and “strong” singularities, corresponding to spin values close to or distant from the limiting case of extreme black holes, respectively. We derive important limiting angular frequencies for naked singularities. We especially study very weak singularities as resulting from the spin variation of black holes. We also explore the main properties of zero angular momentum observers for different classes of black hole and naked singularity spacetimes.



### 3 Introduction

It is hard to overemphasize the importance of the Kerr geometry not only for general relativity itself, but also for the very fundamentals of physics. It assumes this position as being the most physically relevant rotating generalization of the static Schwarzschild geometry. Its charged counterpart, the Kerr-Newman solution, representing the exterior gravitational and electromagnetic fields of a charged rotating object, is an exact solution of the Einstein-Maxwell equations.

Its line element in Boyer-Lindquist coordinates can be written as

$$\begin{aligned}
 ds^2 = & \frac{r^2 - 2Mr + a^2 + Q^2}{r^2 + a^2 \cos^2 \theta} (dt - a \sin^2 \theta d\phi)^2 \\
 & - \frac{\sin^2 \theta}{r^2 + a^2 \cos^2 \theta} [(r^2 + a^2)d\phi - a dt]^2 \\
 & - \frac{r^2 + a^2 \cos^2 \theta}{r^2 - 2Mr + a^2 + Q^2} dr^2 - (r^2 + a^2 \cos^2 \theta) d\theta^2, \quad (3.0.1)
 \end{aligned}$$

where  $M$  is the total mass of the object,  $a = J/M$  is the specific angular momentum, and  $Q$  is the electric charge. In this particular coordinate system, the metric functions do not depend on the coordinates  $t$  and  $\phi$ , indicating the existence of two Killing vector fields  $\zeta^I = \partial_t$  and  $\zeta^{II} = \partial_\phi$  which represent the properties of stationarity and axial symmetry, respectively.

An important characteristic of this solution is that the source of gravity is surrounded by two horizons situated at a distance

$$r_{\pm} = M \pm \sqrt{M^2 - a^2 - Q^2} \quad (3.0.2)$$

from the origin of coordinates. Inside the interior horizon,  $r_-$ , a ring singularity is present which, however, cannot be observed by any observer situated outside the exterior horizon. If the condition  $M^2 < a^2 + Q^2$  is satisfied, no horizons are present and the Kerr-Newman spacetime represents the exterior field of a naked singularity.

Despite of its fundamental importance in general relativity, and its theoretical and mathematical interest, this solution has not been especially useful for describing astrophysical phenomena, first of all, because observed astrophysical objects do not possess an appreciable net electric charge. Furthermore, the limiting Kerr metric takes into account the mass and the rotation, but does not consider the moment of inertia of the object. For astrophysical applications it is, therefore, necessary to use more general solutions with higher multipole moments which are due not only to the rotation of the body but also to its shape. This means that even in the limiting case of a static spacetime, a solution is needed that takes into account possible deviations from spherically symmetry.

## 4 The general static vacuum solution

In general relativity, stationary axisymmetric solutions of Einstein's equations [1] play a crucial role for the description of the gravitational field of astrophysical objects. In particular, the black hole solutions and their generalizations that include Maxwell fields are contained within this class.

This type of exact solutions has been the subject of intensive research during the past few decades. In particular, the number of known exact solutions drastically increased after Ernst [2] discovered an elegant representation of the field equations that made it possible to search for their symmetries. These studies lead finally to the development of solution generating techniques [1] which allow us to find new solutions, starting from a given seed solution. In particular, solutions with an arbitrary number of multipole moments for the mass and angular momentum were derived in [3] and used to describe the gravitational field of rotating axially symmetric distributions of mass.

The first analysis of stationary axially symmetric gravitational fields was carried out by Weyl [4] in 1917, soon after the formulation of general relativity. In particular, Weyl discovered that in the static limit the main part of the vacuum field equations reduces to a single linear differential equation. The corresponding general solution can be written in cylindrical coordinates as an infinite sum with arbitrary constant coefficients. A particular choice of the coefficients leads to the subset of asymptotically flat solutions which is the most interesting from a physical point of view. In this section we review the main properties of stationary axisymmetric gravitational fields. In particular, we show explicitly that the main field equations in vacuum can be represented as the equations of a nonlinear sigma model in which the base space is the 4-dimensional spacetime and the target space is a 2-dimensional conformally Euclidean space.

## 4.1 Line element and field equations

Although there exist in the literature many suitable coordinate systems, stationary axisymmetric gravitational fields are usually described in cylindrical coordinates  $(t, \rho, z, \varphi)$ . Stationarity implies that  $t$  can be chosen as the time coordinate and the metric does not depend on time, i.e.  $\partial g_{\mu\nu}/\partial t = 0$ . Consequently, the corresponding timelike Killing vector has the components  $\delta_t^\mu$ . A second Killing vector field is associated to the axial symmetry with respect to the axis  $\rho = 0$ . Then, choosing  $\varphi$  as the azimuthal angle, the metric satisfies the conditions  $\partial g_{\mu\nu}/\partial \varphi = 0$ , and the components of the corresponding spacelike Killing vector are  $\delta_\varphi^\mu$ .

Using further the properties of stationarity and axial symmetry, together with the vacuum field equations, for a general metric of the form  $g_{\mu\nu} = g_{\mu\nu}(\rho, z)$ , it is possible to show that the most general line element for this type of gravitational fields can be written in the Weyl-Lewis-Papapetrou form as [4, 5, 6]

$$ds^2 = f(dt - \omega d\varphi)^2 - f^{-1} \left[ e^{2\gamma}(d\rho^2 + dz^2) + \rho^2 d\varphi^2 \right], \quad (4.1.1)$$

where  $f$ ,  $\omega$  and  $\gamma$  are functions of  $\rho$  and  $z$ , only. After some rearrangements which include the introduction of a new function  $\Omega = \Omega(\rho, z)$  by means of

$$\rho \partial_\rho \Omega = f^2 \partial_z \omega, \quad \rho \partial_z \Omega = -f^2 \partial_\rho \omega, \quad (4.1.2)$$

the vacuum field equations  $R_{\mu\nu} = 0$  can be shown to be equivalent to the following set of partial differential equations

$$\frac{1}{\rho} \partial_\rho (\rho \partial_\rho f) + \partial_z^2 f + \frac{1}{f} [(\partial_\rho \Omega)^2 + (\partial_z \Omega)^2 - (\partial_\rho f)^2 - (\partial_z f)^2] = 0, \quad (4.1.3)$$

$$\frac{1}{\rho} \partial_\rho (\rho \partial_\rho \Omega) + \partial_z^2 \Omega - \frac{2}{f} (\partial_\rho f \partial_\rho \Omega + \partial_z f \partial_z \Omega) = 0, \quad (4.1.4)$$

$$\partial_\rho \gamma = \frac{\rho}{4f^2} [(\partial_\rho f)^2 + (\partial_\rho \Omega)^2 - (\partial_z f)^2 - (\partial_z \Omega)^2], \quad (4.1.5)$$

$$\partial_z \gamma = \frac{\rho}{2f^2} (\partial_\rho f \partial_z f + \partial_\rho \Omega \partial_z \Omega). \quad (4.1.6)$$

It is clear that the field equations for  $\gamma$  can be integrated by quadratures,

once  $f$  and  $\Omega$  are known. For this reason, the equations (4.1.3) and (4.1.4) for  $f$  and  $\Omega$  are usually considered as the main field equations for stationary axisymmetric vacuum gravitational fields. In the following subsections we will focus on the analysis of the main field equations, only. It is interesting to mention that this set of equations can be geometrically interpreted in the context of nonlinear sigma models [7].

Let us consider the special case of static axisymmetric fields. This corresponds to metrics which, apart from being axially symmetric and independent of the time coordinate, are invariant with respect to the transformation  $\varphi \rightarrow -\varphi$  (i.e. rotations with respect to the axis of symmetry are not allowed). Consequently, the corresponding line element is given by (4.1.1) with  $\omega = 0$ , and the field equations can be written as

$$\partial_\rho^2 \psi + \frac{1}{\rho} \partial_\rho \psi + \partial_z^2 \psi = 0, \quad f = \exp(2\psi), \quad (4.1.7)$$

$$\partial_\rho \gamma = \rho \left[ (\partial_\rho \psi)^2 - (\partial_z \psi)^2 \right], \quad \partial_z \gamma = 2\rho \partial_\rho \psi \partial_z \psi. \quad (4.1.8)$$

We see that the main field equation (4.1.7) corresponds to the linear Laplace equation for the metric function  $\psi$ .

## 4.2 Static solution

The general solution of Laplace's equation is known and, if we demand additionally asymptotic flatness, we obtain the Weyl solution which can be written as [4, 1]

$$\psi = \sum_{n=0}^{\infty} \frac{a_n}{(\rho^2 + z^2)^{\frac{n+1}{2}}} P_n(\cos \theta), \quad \cos \theta = \frac{z}{\sqrt{\rho^2 + z^2}}, \quad (4.2.1)$$

where  $a_n$  ( $n = 0, 1, \dots$ ) are arbitrary constants, and  $P_n(\cos \theta)$  represents the Legendre polynomials of degree  $n$ . The expression for the metric function  $\gamma$  can be calculated by quadratures by using the set of first order differential equations (4.1.8). Then

$$\gamma = - \sum_{n,m=0}^{\infty} \frac{a_n a_m (n+1)(m+1)}{(n+m+2)(\rho^2 + z^2)^{\frac{n+m+2}{2}}} (P_n P_m - P_{n+1} P_{m+1}). \quad (4.2.2)$$

Since this is the most general static, axisymmetric, asymptotically flat vacuum solution, it must contain all known solution of this class. In particular, one of the most interesting special solutions which is Schwarzschild's spherically symmetric black hole spacetime must be contained in this class. To see this, we must choose the constants  $a_n$  in such a way that the infinite sum (4.2.1) converges to the Schwarzschild solution in cylindric coordinates. But, or course, this representation is not the most appropriate to analyze the interesting physical properties of Schwarzschild's metric.

In fact, it turns out that to investigate the properties of solutions with multiple moments it is more convenient to use prolate spheroidal coordinates  $(t, x, y, \varphi)$  in which the line element can be written as

$$ds^2 = f dt^2 - \frac{\sigma^2}{f} \left[ e^{2\gamma} (x^2 - y^2) \left( \frac{dx^2}{x^2 - 1} + \frac{dy^2}{1 - y^2} \right) + (x^2 - 1)(1 - y^2) d\varphi^2 \right]$$

where

$$x = \frac{r_+ + r_-}{2\sigma}, \quad (x^2 \geq 1), \quad y = \frac{r_+ - r_-}{2\sigma}, \quad (y^2 \leq 1) \quad (4.2.3)$$

$$r_{\pm}^2 = \rho^2 + (z \pm \sigma)^2, \quad \sigma = \text{const}, \quad (4.2.4)$$

and the metric functions are  $f$ ,  $\omega$ , and  $\gamma$  depend on  $x$  and  $y$ , only. In this coordinate system, the general static solution which is also asymptotically flat can be expressed as

$$f = \exp(2\psi), \quad \psi = \sum_{n=0}^{\infty} (-1)^{n+1} q_n P_n(y) Q_n(x), \quad q_n = \text{const}$$

where  $P_n(y)$  are the Legendre polynomials, and  $Q_n(x)$  are the Legendre functions of second kind. In particular,

$$\begin{aligned} P_0 &= 1, \quad P_1 = y, \quad P_2 = \frac{1}{2}(3y^2 - 1), \dots \\ Q_0 &= \frac{1}{2} \ln \frac{x+1}{x-1}, \quad Q_1 = \frac{1}{2} x \ln \frac{x+1}{x-1} - 1, \\ Q_2 &= \frac{1}{2} (3x^2 - 1) \ln \frac{x+1}{x-1} - \frac{3}{2} x, \dots \end{aligned}$$

The corresponding function  $\gamma$  can be calculated by quadratures and its general expression has been explicitly derived in [8]. The most important special cases contained in this general solution are the Schwarzschild metric

$$\psi = -q_0 P_0(y) Q_0(x), \quad \gamma = \frac{1}{2} \ln \frac{x^2 - 1}{x^2 - y^2},$$

and the Erez-Rosen metric [9]

$$\psi = -q_0 P_0(y) Q_0(x) - q_2 P_2(y) Q_2(x), \quad \gamma = \frac{1}{2} \ln \frac{x^2 - 1}{x^2 - y^2} + \dots$$

In the last case, the constant parameter  $q_2$  turns out to determine the quadrupole moment. In general, the constants  $q_n$  represent an infinite set of parameters that determines an infinite set of mass multipole moments.



## 5 Stationary generalization

The solution generating techniques [12] can be applied, in particular, to any static seed solution in order to obtain the corresponding stationary generalization. One of the most powerful techniques is the inverse method (ISM) developed by Belinski and Zakharov [13]. We used a particular case of the ISM, which is known as the Hoenselaers–Kinnersley–Xanthopoulos (HKX) transformation to derive the stationary generalization of the general static solution in prolate spheroidal coordinates.

### 5.1 Ernst representation

In the general stationary case ( $\omega \neq 0$ ) with line element

$$ds^2 = f(dt - \omega d\varphi)^2 - \frac{\sigma^2}{f} \left[ e^{2\gamma}(x^2 - y^2) \left( \frac{dx^2}{x^2 - 1} + \frac{dy^2}{1 - y^2} \right) + (x^2 - 1)(1 - y^2)d\varphi^2 \right]$$

it is useful to introduce the the Ernst potentials

$$E = f + i\Omega, \quad \xi = \frac{1 - E}{1 + E},$$

where the function  $\Omega$  is now determined by the equations

$$\sigma(x^2 - 1)\Omega_x = f^2\omega_y, \quad \sigma(1 - y^2)\Omega_y = -f^2\omega_x.$$

Then, the main field equations can be represented in a compact and symmetric form:

$$(\bar{\xi}\xi^* - 1) \left\{ [(x^2 - 1)\bar{\xi}_x]_x + [(1 - y^2)\bar{\xi}_y]_y \right\} = 2\bar{\xi}^* [(x^2 - 1)\xi_x^2 + (1 - y^2)\xi_y^2].$$

This equation is invariant with respect to the transformation  $x \leftrightarrow y$ . Then, since the particular solution

$$\zeta = \frac{1}{x} \rightarrow \Omega = 0 \rightarrow \omega = 0 \rightarrow \gamma = \frac{1}{2} \ln \frac{x^2 - 1}{x^2 - y^2}$$

represents the Schwarzschild spacetime, the choice  $\zeta^{-1} = y$  is also an exact solution. Furthermore, if we take the linear combination  $\zeta^{-1} = c_1 x + c_2 y$  and introduce it into the field equation, we obtain the new solution

$$\zeta^{-1} = \frac{\sigma}{M} x + i \frac{a}{M} y, \quad \sigma = \sqrt{M^2 - a^2},$$

which corresponds to the Kerr metric in prolate spheroidal coordinates.

In the case of the Einstein-Maxwell theory, the main field equations can be expressed as

$$(\zeta \zeta^* - \mathcal{F} \mathcal{F}^* - 1) \nabla^2 \zeta = 2(\zeta^* \nabla \zeta - \mathcal{F}^* \nabla \mathcal{F}) \nabla \zeta,$$

$$(\zeta \zeta^* - \mathcal{F} \mathcal{F}^* - 1) \nabla^2 \mathcal{F} = 2(\zeta^* \nabla \zeta - \mathcal{F}^* \nabla \mathcal{F}) \nabla \mathcal{F}$$

where  $\nabla$  represents the gradient operator in prolate spheroidal coordinates. Moreover, the gravitational potential  $\zeta$  and the electromagnetic  $\mathcal{F}$  Ernst potential are defined as

$$\zeta = \frac{1 - f - i\Omega}{1 + f + i\Omega}, \quad \mathcal{F} = 2 \frac{\Phi}{1 + f + i\Omega}.$$

The potential  $\Phi$  can be shown to be determined uniquely by the electromagnetic potentials  $A_t$  and  $A_\varphi$ . One can show that if  $\zeta_0$  is a vacuum solution, then the new potential

$$\zeta = \zeta_0 \sqrt{1 - e^2}$$

represents a solution of the Einstein-Maxwell equations with effective electric charge  $e$ . This transformation is known in the literature as the Harrison transformation [10]. Accordingly, the Kerr-Newman solution in this representation acquires the simple form

$$\zeta = \frac{\sqrt{1 - e^2}}{\frac{\sigma}{M} x + i \frac{a}{M} y}, \quad e = \frac{Q}{M}, \quad \sigma = \sqrt{M^2 - a^2 - Q^2}.$$

In this way, it is very easy to generalize any vacuum solution to include the case of electric charge. More general transformations of this type can be used in order to generate solutions with any desired set of gravitational and electromagnetic multipole moments [11].

## 5.2 Representation as a nonlinear sigma model

Consider two (pseudo)-Riemannian manifolds  $(M, \gamma)$  and  $(N, G)$  of dimension  $m$  and  $n$ , respectively. Let  $M$  be coordinatized by  $x^a$ , and  $N$  by  $X^\mu$ , so that the metrics on  $M$  and  $N$  can be, in general, smooth functions of the corresponding coordinates, i.e.,  $\gamma = \gamma(x)$  and  $G = G(X)$ . A harmonic map is a smooth map  $X : M \rightarrow N$ , or in coordinates  $X : x \mapsto X$  so that  $X$  becomes a function of  $x$ , and the  $X$ 's satisfy the motion equations following from the action [14]

$$S = \int d^m x \sqrt{|\gamma|} \gamma^{ab}(x) \partial_a X^\mu \partial_b X^\nu G_{\mu\nu}(X), \quad (5.2.1)$$

which sometimes is called the “energy” of the harmonic map  $X$ . The straightforward variation of  $S$  with respect to  $X^\mu$  leads to the motion equations

$$\frac{1}{\sqrt{|\gamma|}} \partial_b \left( \sqrt{|\gamma|} \gamma^{ab} \partial_a X^\mu \right) + \Gamma_{\nu\lambda}^\mu \gamma^{ab} \partial_a X^\nu \partial_b X^\lambda = 0, \quad (5.2.2)$$

where  $\Gamma_{\nu\lambda}^\mu$  are the Christoffel symbols associated to the metric  $G_{\mu\nu}$  of the target space  $N$ . If  $G_{\mu\nu}$  is a flat metric, one can choose Cartesian-like coordinates such that  $G_{\mu\nu} = \eta_{\mu\nu} = \text{diag}(\pm 1, \dots, \pm 1)$ , the motion equations become linear, and the corresponding sigma model is linear. This is exactly the case of a bosonic string on a flat background in which the base space is the 2-dimensional string world-sheet. In this case the action (5.2.1) is usually referred to as the Polyakov action [16].

Consider now the case in which the base space  $M$  is a stationary axisymmetric spacetime. Then,  $\gamma^{ab}$ ,  $a, b = 0, \dots, 3$ , can be chosen as the Weyl-Lewis-Papapetrou metric (4.1.1), i.e.

$$\gamma_{ab} = \begin{pmatrix} f & 0 & 0 & -f\omega \\ 0 & -f^{-1}e^{2k} & 0 & 0 \\ 0 & 0 & -f^{-1}e^{2k} & 0 \\ -f\omega & 0 & 0 & f\omega^2 - \rho^2 f^{-1} \end{pmatrix}. \quad (5.2.3)$$

Let the target space  $N$  be 2-dimensional with metric  $G_{\mu\nu} = (1/2)f^{-2}\delta_{\mu\nu}$ ,  $\mu, \nu = 1, 2$ , and let the coordinates on  $N$  be  $X^\mu = (f, \Omega)$ . Then, it is straightforward to show that the action (5.2.1) becomes

$$S = \int \mathcal{L} dt d\varphi d\rho dz, \quad \mathcal{L} = \frac{\rho}{2f^2} \left[ (\partial_\rho f)^2 + (\partial_z f)^2 + (\partial_\rho \Omega)^2 + (\partial_z \Omega)^2 \right], \quad (5.2.4)$$

and the corresponding motion equations (5.2.2) are identical to the main field equations (4.1.3) and (4.1.4).

Notice that the field equations can also be obtained from (5.2.4) by a direct variation with respect to  $f$  and  $\Omega$ . This interesting result was obtained originally by Ernst [2], and is the starting point of what today is known as the Ernst representation of the field equations.

The above result shows that stationary axisymmetric gravitational fields can be described as a  $(4 \rightarrow 2)$ -nonlinear harmonic map, where the base space is the spacetime of the gravitational field and the target space corresponds to a 2-dimensional conformally Euclidean space. A further analysis of the target space shows that it can be interpreted as the quotient space  $SL(2, R)/SO(2)$  [15], and the Lagrangian (5.2.4) can be written explicitly [17] in terms of the generators of the Lie group  $SL(2, R)$ . Harmonic maps in which the target space is a quotient space are usually known as nonlinear sigma models [14].

The form of the Lagrangian (5.2.4) with two gravitational field variables,  $f$  and  $\Omega$ , depending on two coordinates,  $\rho$  and  $z$ , suggests a representation as a harmonic map with a 2-dimensional base space. In string theory, this is an important fact that allows one to use the conformal invariance of the base space metric to find an adequate representation for the set of classical solutions. This, in turn, facilitates the application of the canonical quantization procedure. Unfortunately, this is not possible for the Lagrangian (5.2.4). Indeed, if we consider  $\gamma^{ab}$  as a 2-dimensional metric that depends on the parameters  $\rho$  and  $z$ , the diagonal form of the Lagrangian (5.2.4) implies that  $\sqrt{|\gamma|}\gamma^{ab} = \delta^{ab}$ . Clearly, this choice is not compatible with the factor  $\rho$  in front of the Lagrangian. Therefore, the reduced gravitational Lagrangian (5.2.4) cannot be interpreted as corresponding to a  $(2 \rightarrow n)$ -harmonic map. Nevertheless, we will show in the next section that a modification of the definition of harmonic maps allows us to “absorb” the unpleasant factor  $\rho$  in the metric of the target space, and to use all the advantages of a 2-dimensional base space.

Notice that the representation of stationary fields as a nonlinear sigma model becomes degenerate in the limiting case of static fields. Indeed, the underlying geometric structure of the  $SL(2, R)/SO(2)$  nonlinear sigma models requires that the target space be 2-dimensional, a condition which is not satisfied by static fields. We will see below that by using a dimensional extension of generalized sigma models, it will be possible to treat the special static case, without affecting the underlying geometric structure.

The analysis performed in this section for stationary axisymmetric fields can be generalized to include any gravitational field containing two commuting Killing vector fields [1]. This is due to the fact that for this class of gravitational fields it is always possible to find the corresponding Ernst representation in which the Lagrangian contains only two gravitational variables which depend on only two spacetime coordinates.

### 5.3 Representation as a generalized harmonic map

Consider two (pseudo-)Riemannian manifolds  $(M, \gamma)$  and  $(N, G)$  of dimension  $m$  and  $n$ , respectively. Let  $x^a$  and  $X^\mu$  be coordinates on  $M$  and  $N$ , respectively. This coordinatization implies that in general the metrics  $\gamma$  and  $G$  become functions of the corresponding coordinates. Let us assume that not only  $\gamma$  but also  $G$  can explicitly depend on the coordinates  $x^a$ , i.e. let  $\gamma = \gamma(x)$  and  $G = G(X, x)$ . This simple assumption is the main aspect of our generalization which, as we will see, lead to new and nontrivial results.

A smooth map  $X : M \rightarrow N$  will be called an  $(m \rightarrow n)$ -generalized harmonic map if it satisfies the Euler-Lagrange equations

$$\frac{1}{\sqrt{|\gamma|}} \partial_b \left( \sqrt{|\gamma|} \gamma^{ab} \partial_a X^\mu \right) + \Gamma_{\nu\lambda}^\mu \gamma^{ab} \partial_a X^\nu \partial_b X^\lambda + G^{\mu\lambda} \gamma^{ab} \partial_a X^\nu \partial_b G_{\lambda\nu} = 0, \quad (5.3.1)$$

which follow from the variation of the generalized action

$$S = \int d^m x \sqrt{|\gamma|} \gamma^{ab}(x) \partial_a X^\mu \partial_b X^\nu G_{\mu\nu}(X, x), \quad (5.3.2)$$

with respect to the fields  $X^\mu$ . Here the Christoffel symbols, determined by the metric  $G_{\mu\nu}$ , are calculated in the standard manner, without considering the explicit dependence on  $x$ . Notice that the new ingredient in this generalized definition of harmonic maps, i.e., the term  $G_{\mu\nu}(X, x)$  in the Lagrangian

density implies that we are taking into account the “interaction” between the base space  $M$  and the target space  $N$ . This interaction leads to an extra term in the motion equations, as can be seen in (5.3.1). It turns out that this interaction is the result of the effective presence of the gravitational field.

Notice that the limiting case of generalized linear harmonic maps is much more complicated than in the standard case. Indeed, for the motion equations (5.3.1) to become linear it is necessary that the conditions

$$\gamma^{ab}(\Gamma_{\nu\lambda}^{\mu} \partial_b X^{\lambda} + G^{\mu\lambda} \partial_b G_{\lambda\nu}) \partial_a X^{\nu} = 0, \quad (5.3.3)$$

be satisfied. One could search for a solution in which each term vanishes separately. The choice of a (pseudo-)Euclidean target metric  $G_{\mu\nu} = \eta_{\mu\nu}$ , which would imply  $\Gamma_{\nu\lambda}^{\mu} = 0$ , is not allowed, because it would contradict the assumption  $\partial_b G_{\mu\nu} \neq 0$ . Nevertheless, a flat background metric in curvilinear coordinates could be chosen such that the assumption  $G^{\mu\lambda} \partial_b G_{\mu\nu} = 0$  is fulfilled, but in this case  $\Gamma_{\nu\lambda}^{\mu} \neq 0$  and (5.3.3) cannot be satisfied. In the general case of a curved target metric, conditions (5.3.3) represent a system of  $m$  first order nonlinear partial differential equations for  $G_{\mu\nu}$ . Solutions to this system would represent linear generalized harmonic maps. The complexity of this system suggests that this special type of maps is not common.

As we mentioned before, the generalized action (5.3.2) includes an interaction between the base space  $N$  and the target space  $M$ , reflected on the fact that  $G_{\mu\nu}$  depends explicitly on the coordinates of the base space. Clearly, this interaction must affect the conservation laws of the physical systems we attempt to describe by means of generalized harmonic maps. To see this explicitly we calculate the covariant derivative of the generalized Lagrangian density

$$\mathcal{L} = \sqrt{|\gamma|} \gamma^{ab}(x) \partial_a X^{\mu} \partial_b X^{\nu} G_{\mu\nu}(X, x), \quad (5.3.4)$$

and replace in the result the corresponding motion equations (5.3.1). Then, the final result can be written as

$$\nabla_b \tilde{T}_a^b = -\frac{\partial \mathcal{L}}{\partial x^a} \quad (5.3.5)$$

where  $\tilde{T}_a^b$  represents the canonical energy-momentum tensor

$$\tilde{T}_a^b = \frac{\partial \mathcal{L}}{\partial(\partial_b X^\mu)} (\partial_a X^\mu) - \delta_a^b \mathcal{L} = 2\sqrt{\gamma} G_{\mu\nu} \left( \gamma^{bc} \partial_a X^\mu \partial_c X^\nu - \frac{1}{2} \delta_a^b \gamma^{cd} \partial_c X^\mu \partial_d X^\nu \right). \quad (5.3.6)$$

The standard conservation law is recovered only when the Lagrangian does not depend explicitly on the coordinates of the base space. Even if we choose a flat base space  $\gamma_{ab} = \eta_{ab}$ , the explicit dependence of the metric of the target space  $G_{\mu\nu}(X, x)$  on  $x$  generates a term that violates the standard conservation law. This term is due to the interaction between the base space and the target space which, consequently, is one of the main characteristics of the generalized harmonic maps introduced in this work.

An alternative and more general definition of the energy-momentum tensor is by means of the variation of the Lagrangian density with respect to the metric of the base space, i.e.

$$T_{ab} = \frac{\delta \mathcal{L}}{\delta \gamma^{ab}}. \quad (5.3.7)$$

A straightforward computation shows that for the action under consideration here we have that  $\tilde{T}_{ab} = 2T_{ab}$  so that the generalized conservation law (5.3.5) can be written as

$$\nabla_b T_a^b + \frac{1}{2} \frac{\partial \mathcal{L}}{\partial x^a} = 0. \quad (5.3.8)$$

For a given metric on the base space, this represents in general a system of  $m$  differential equations for the “fields”  $X^\mu$  which must be satisfied “on-shell”.

If the base space is 2-dimensional, we can use a reparametrization of  $x$  to choose a conformally flat metric, and the invariance of the Lagrangian density under arbitrary Weyl transformations to show that the energy-momentum tensor is traceless,  $T_a^a = 0$ .

In Section 5.1 we described stationary, axially symmetric, gravitational fields as a  $(4 \rightarrow 2)$ -nonlinear sigma model. There it was pointed out the convenience of having a 2-dimensional base space in analogy with string theory. Now we will show that this can be done by using the generalized harmonic maps defined above.

Consider a  $(2 \rightarrow 2)$ -generalized harmonic map. Let  $x^a = (\rho, z)$  be the coordinates on the base space  $M$ , and  $X^\mu = (f, \Omega)$  the coordinates on the target space  $N$ . In the base space we choose a flat metric and in the target

space a conformally flat metric, i.e.

$$\gamma_{ab} = \delta_{ab} \quad \text{and} \quad G_{\mu\nu} = \frac{\rho}{2f^2} \delta_{\mu\nu} \quad (a, b = 1, 2; \mu, \nu = 1, 2). \quad (5.3.9)$$

A straightforward computation shows that the generalized Lagrangian (5.3.4) coincides with the Lagrangian (5.2.4) for stationary axisymmetric fields, and that the equations of motion (5.3.1) generate the main field equations (4.1.3) and (4.1.4).

For the sake of completeness we calculate the components of the energy-momentum tensor  $T_{ab} = \delta\mathcal{L}/\delta\gamma^{ab}$ . Then

$$T_{\rho\rho} = -T_{zz} = \frac{\rho}{4f^2} \left[ (\partial_\rho f)^2 + (\partial_\rho \Omega)^2 - (\partial_z f)^2 - (\partial_z \Omega)^2 \right], \quad (5.3.10)$$

$$T_{\rho z} = \frac{\rho}{2f^2} (\partial_\rho f \partial_z f + \partial_\rho \Omega \partial_z \Omega). \quad (5.3.11)$$

This tensor is traceless due to the fact that the base space is 2-dimensional. It satisfies the generalized conservation law (5.3.8) on-shell:

$$\frac{dT_{\rho\rho}}{d\rho} + \frac{dT_{\rho z}}{dz} + \frac{1}{2} \frac{\partial \mathcal{L}}{\partial \rho} = 0, \quad (5.3.12)$$

$$\frac{dT_{\rho z}}{d\rho} - \frac{dT_{\rho\rho}}{dz} = 0. \quad (5.3.13)$$

Incidentally, the last equation coincides with the integrability condition for the metric function  $k$ , which is identically satisfied by virtue of the main field equations. In fact, as can be seen from Eqs.(4.1.5,4.1.6) and (5.3.10,5.3.11), the components of the energy-momentum tensor satisfy the relationships  $T_{\rho\rho} = \partial_\rho k$  and  $T_{\rho z} = \partial_z k$ , so that the conservation law (5.3.13) becomes an identity. Although we have eliminated from the starting Lagrangian (5.2.4) the variable  $k$  by applying a Legendre transformation on the Einstein-Hilbert Lagrangian (see [17] for details) for this type of gravitational fields, the formalism of generalized harmonic maps seems to retain the information about  $k$  at the level of the generalized conservation law.

The above results show that stationary axisymmetric spacetimes can be represented as a  $(2 \rightarrow 2)$ -generalized harmonic map with metrics given as in (5.3.9). It is also possible to interpret the generalized harmonic map given

above as a generalized string model. Although the metric of the base space  $M$  is Euclidean, we can apply a Wick rotation  $\tau = i\rho$  to obtain a Minkowski-like structure on  $M$ . Then,  $M$  represents the world-sheet of a bosonic string in which  $\tau$  measures the time and  $z$  is the parameter along the string. The string is “embedded” in the target space  $N$  whose metric is conformally flat and explicitly depends on the time parameter  $\tau$ . We will see in the next section that this embedding becomes more plausible when the target space is subject to a dimensional extension. In the present example, it is necessary to apply a Wick rotation in order to interpret the base space as a string world-sheet. This is due to the fact that both coordinates  $\rho$  and  $z$  are spatial coordinates. However, this can be avoided by considering other classes of gravitational fields with timelike Killing vector fields; examples will be given below.

The most studied solutions belonging to the class of stationary axisymmetric fields are the asymptotically flat solutions. Asymptotic flatness imposes conditions on the metric functions which in the cylindrical coordinates used here can be formulated in the form

$$\lim_{x^a \rightarrow \infty} f = 1 + O\left(\frac{1}{x^a}\right), \quad \lim_{x^a \rightarrow \infty} \omega = c_1 + O\left(\frac{1}{x^a}\right), \quad \lim_{x^a \rightarrow \infty} \Omega = O\left(\frac{1}{x^a}\right) \quad (5.3.14)$$

where  $c_1$  is an arbitrary real constant which can be set to zero by appropriately choosing the angular coordinate  $\varphi$ . If we choose the domain of the spatial coordinates as  $\rho \in [0, \infty)$  and  $z \in (-\infty, +\infty)$ , from the asymptotic flatness conditions it follows that the coordinates of the target space  $N$  satisfy the boundary conditions

$$\dot{X}^\mu(\rho, -\infty) = 0 = \dot{X}^\mu(\rho, \infty), \quad X'^\mu(\rho, -\infty) = 0 = X'^\mu(\rho, \infty) \quad (5.3.15)$$

where the dot stands for a derivative with respect to  $\rho$  and the prime represents derivation with respect to  $z$ . These relationships are known in string theory [16] as the Dirichlet and Neumann boundary conditions for open strings, respectively, with the extreme points situated at infinity. We thus conclude that if we assume  $\rho$  as a “time” parameter for stationary axisymmetric gravitational fields, an asymptotically flat solution corresponds to an open string with endpoints attached to  $D$ -branes situated at plus and minus infinity in the  $z$ -direction.

## 5.4 Dimensional extension

In order to further analyze the analogy between gravitational fields and bosonic string models, we perform an arbitrary dimensional extension of the target space  $N$ , and study the conditions under which this dimensional extension does not affect the field equations of the gravitational field. Consider an  $(m \rightarrow D)$ -generalized harmonic map. As before we denote by  $\{x^a\}$  the coordinates on  $M$ . Let  $\{X^\mu, X^\alpha\}$  with  $\mu = 1, 2$  and  $\alpha = 3, 4, \dots, D$  be the coordinates on  $N$ . The metric structure on  $M$  is again  $\gamma = \gamma(x)$ , whereas the metric on  $N$  can in general depend on all coordinates of  $M$  and  $N$ , i.e.  $G = G(X^\mu, X^\alpha, x^a)$ . The general structure of the corresponding field equations is as given in (5.3.1). They can be divided into one set of equations for  $X^\mu$  and one set of equations for  $X^\alpha$ . According to the results of the last section, the class of gravitational fields under consideration can be represented as a  $(2 \rightarrow 2)$ -generalized harmonic map so that we can assume that the main gravitational variables are contained in the coordinates  $X^\mu$  of the target space. Then, the gravitational sector of the target space will be contained in the components  $G_{\mu\nu}$  ( $\mu, \nu = 1, 2$ ) of the metric, whereas the components  $G_{\alpha\beta}$  ( $\alpha, \beta = 3, 4, \dots, D$ ) represent the sector of the dimensional extension.

Clearly, the set of differential equations for  $X^\mu$  also contains the variables  $X^\alpha$  and its derivatives  $\partial_a X^\alpha$ . For the gravitational field equations to remain unaffected by this dimensional extension we demand the vanishing of all the terms containing  $X^\alpha$  and its derivatives in the equations for  $X^\mu$ . It is easy to show that this can be achieved by imposing the conditions

$$G_{\mu\alpha} = 0, \quad \frac{\partial G_{\mu\nu}}{\partial X^\alpha} = 0, \quad \frac{\partial G_{\alpha\beta}}{\partial X^\mu} = 0. \quad (5.4.1)$$

That is to say that the gravitational sector must remain completely invariant under a dimensional extension, and the additional sector cannot depend on the gravitational variables, i.e.,  $G_{\alpha\beta} = G_{\alpha\beta}(X^\gamma, x^a)$ ,  $\gamma = 3, 4, \dots, D$ . Furthermore, the variables  $X^\alpha$  must satisfy the differential equations

$$\frac{1}{\sqrt{|\gamma|}} \partial_b \left( \sqrt{|\gamma|} \gamma^{ab} \partial_a X^\alpha \right) + \Gamma_{\beta\gamma}^\alpha \gamma^{ab} \partial_a X^\beta \partial_b X^\gamma + G^{\alpha\beta} \gamma^{ab} \partial_a X^\gamma \partial_b G_{\beta\gamma} = 0. \quad (5.4.2)$$

This shows that any given  $(2 \rightarrow 2)$ -generalized map can be extended, without affecting the field equations, to a  $(2 \rightarrow D)$ -generalized harmonic map.

It is worth mentioning that the fact that the target space  $N$  becomes split in two separate parts implies that the energy-momentum tensor  $T_{ab} = \delta\mathcal{L}/\delta\gamma^{ab}$  separates into one part belonging to the gravitational sector and a second one following from the dimensional extension, i.e.  $T_{ab} = T_{ab}(X^\mu, x) + T_{ab}(X^\alpha, x)$ . The generalized conservation law as given in (5.3.8) is satisfied by the sum of both parts.

Consider the example of stationary axisymmetric fields given the metrics (5.3.9). Taking into account the conditions (5.4.1), after a dimensional extension the metric of the target space becomes

$$G = \begin{pmatrix} \frac{\rho}{2f^2} & 0 & 0 & \cdots & 0 \\ 0 & \frac{\rho}{2f^2} & 0 & \cdots & 0 \\ 0 & 0 & G_{33}(X^\alpha, x) & \cdots & G_{3D}(X^\alpha, x) \\ \cdot & \cdot & \cdots & \cdots & \cdots \\ 0 & 0 & G_{D3}(X^\alpha, x) & \cdots & G_{DD}(X^\alpha, x) \end{pmatrix}. \quad (5.4.3)$$

Clearly, to avoid that this metric becomes degenerate we must demand that  $\det(G_{\alpha\beta}) \neq 0$ , a condition that can be satisfied in view of the arbitrariness of the components of the metric. With the extended metric, the Lagrangian density gets an additional term

$$\begin{aligned} \mathcal{L} = & \frac{\rho}{2f^2} \left[ (\partial_\rho f)^2 + (\partial_z f)^2 + (\partial_\rho \Omega)^2 + (\partial_z \Omega)^2 \right] \\ & + \left( \partial_\rho X^\alpha \partial_\rho X^\beta + \partial_z X^\alpha \partial_z X^\beta \right) G_{\alpha\beta}, \end{aligned} \quad (5.4.4)$$

which nevertheless does not affect the field equations for the gravitational variables  $f$  and  $\Omega$ . On the other hand, the new fields must be solutions of the extra field equations

$$\left( \partial_\rho^2 + \partial_z^2 \right) X^\alpha + \Gamma^\alpha_{\beta\gamma} \left( \partial_\rho X^\beta \partial_\rho X^\gamma + \partial_z X^\beta \partial_z X^\gamma \right) \quad (5.4.5)$$

$$+ G^{\alpha\gamma} \left( \partial_\rho X^\beta \partial_\rho G_{\beta\gamma} + \partial_z X^\beta \partial_z G_{\beta\gamma} \right) = 0. \quad (5.4.6)$$

An interesting special case of the dimensional extension is the one in which the extended sector is Minkowskian, i.e. for the choice  $G_{\alpha\beta} = \eta_{\alpha\beta}$  with additional fields  $X^\alpha$  given as arbitrary harmonic functions. This choice opens the possibility of introducing a “time” coordinate as one of the additional dimen-

sions, an issue that could be helpful when dealing with the interpretation of gravitational fields in this new representation.

The dimensional extension finds an interesting application in the case of static axisymmetric gravitational fields. As mentioned in Section 4.1, these fields are obtained from the general stationary fields in the limiting case  $\Omega = 0$  (or equivalently,  $\omega = 0$ ). If we consider the representation as an  $SL(2, R)/SO(2)$  nonlinear sigma model or as a  $(2 \rightarrow 2)$ -generalized harmonic map, we see immediately that the limit  $\Omega = 0$  is not allowed because the target space becomes 1-dimensional and the underlying metric is undefined. To avoid this degeneracy, we first apply a dimensional extension and only then calculate the limiting case  $\Omega = 0$ . In the most simple case of an extension with  $G_{\alpha\beta} = \delta_{\alpha\beta}$ , the resulting  $(2 \rightarrow 2)$ -generalized map is described by the metrics  $\gamma_{ab} = \delta_{ab}$  and

$$G = \begin{pmatrix} \frac{\rho}{2f^2} & 0 \\ 0 & 1 \end{pmatrix} \quad (5.4.7)$$

where the additional dimension is coordinatized by an arbitrary harmonic function which does not affect the field equations of the only remaining gravitational variable  $f$ . This scheme represents an alternative method for exploring static fields on nondegenerate target spaces. Clearly, this scheme can be applied to the case of gravitational fields possessing two hypersurface orthogonal Killing vector fields.

Our results show that a stationary axisymmetric field can be represented as a string “living” in a  $D$ -dimensional target space  $N$ . The string world-sheet is parametrized by the coordinates  $\rho$  and  $z$ . The gravitational sector of the target space depends explicitly on the metric functions  $f$  and  $\Omega$  and on the parameter  $\rho$  of the string world-sheet. The sector corresponding to the dimensional extension can be chosen as a  $(D - 2)$ -dimensional Minkowski space-time with time parameter  $\tau$ . Then, the string world-sheet is a 2-dimensional flat hypersurface which is “frozen” along the time  $\tau$ .

## 5.5 The general solution

If we take as seed metric the general static solution, the application of two HXK transformations generates a stationary solution with an infinite number of gravitoelectric and gravitomagnetic multipole moments. The HKX method is applied at the level of the Ernst potential from which the metric functions

can be calculated by using the definition of the Ernst potential  $E$  and the field equations for  $\gamma$ . The resulting expressions in the general case are quite cumbersome. We quote here only the special case in which only an arbitrary quadrupole parameter is present. In this case, the result can be written as

$$\begin{aligned} f &= \frac{R}{L} e^{-2qP_2Q_2}, \\ \omega &= -2a - 2\sigma \frac{\mathcal{M}}{R} e^{2qP_2Q_2}, \\ e^{2\gamma} &= \frac{1}{4} \left(1 + \frac{M}{\sigma}\right)^2 \frac{R}{x^2 - y^2} e^{2\hat{\gamma}}, \end{aligned} \quad (5.5.1)$$

where

$$\begin{aligned} R &= a_+ a_- + b_+ b_-, \quad L = a_+^2 + b_+^2, \\ \mathcal{M} &= \alpha x(1 - y^2)(e^{2q\delta_+} + e^{2q\delta_-})a_+ + y(x^2 - 1)(1 - \alpha^2 e^{2q(\delta_+ + \delta_-)})b_+, \\ \hat{\gamma} &= \frac{1}{2}(1 + q)^2 \ln \frac{x^2 - 1}{x^2 - y^2} + 2q(1 - P_2)Q_1 + q^2(1 - P_2) \left[ (1 + P_2)(Q_1^2 - Q_2^2) \right. \\ &\quad \left. + \frac{1}{2}(x^2 - 1)(2Q_2^2 - 3xQ_1Q_2 + 3Q_0Q_2 - Q_2') \right]. \end{aligned} \quad (5.5.2)$$

Here  $P_l(y)$  and  $Q_l(x)$  are Legendre polynomials of the first and second kind respectively. Furthermore

$$\begin{aligned} a_{\pm} &= x(1 - \alpha^2 e^{2q(\delta_+ + \delta_-)}) \pm (1 + \alpha^2 e^{2q(\delta_+ + \delta_-)}), \\ b_{\pm} &= \alpha y(e^{2q\delta_+} + e^{2q\delta_-}) \mp \alpha(e^{2q\delta_+} - e^{2q\delta_-}), \\ \delta_{\pm} &= \frac{1}{2} \ln \frac{(x \pm y)^2}{x^2 - 1} + \frac{3}{2}(1 - y^2 \mp xy) + \frac{3}{4}[x(1 - y^2) \mp y(x^2 - 1)] \ln \frac{x - 1}{x + 1}, \end{aligned}$$

the quantity  $\alpha$  being a constant

$$\alpha = \frac{\sigma - M}{a}, \quad \sigma = \sqrt{M^2 - a^2}. \quad (5.5.3)$$

The physical significance of the parameters entering this metric can be clarified by calculating the Geroch-Hansen [18, 19] multipole moments

$$M_{2k+1} = J_{2k} = 0, \quad k = 0, 1, 2, \dots \quad (5.5.4)$$

$$M_0 = M, \quad M_2 = -Ma^2 + \frac{2}{15}qM^3 \left(1 - \frac{a^2}{M^2}\right)^{3/2}, \dots \quad (5.5.5)$$

$$J_1 = Ma, \quad J_3 = -Ma^3 + \frac{4}{15}qM^3a \left(1 - \frac{a^2}{M^2}\right)^{3/2}, \dots \quad (5.5.6)$$

The vanishing of the odd gravitoelectric ( $M_n$ ) and even gravitomagnetic ( $J_n$ ) multipole moments is a consequence of the symmetry with respect to the equatorial plane. From the above expressions we see that  $M$  is the total mass of the body,  $a$  represents the specific angular momentum, and  $q$  is related to the deviation from spherical symmetry. All higher multipole moments can be shown to depend only on the parameters  $M$ ,  $a$ , and  $q$ .

We analyzed the geometric and physical properties of the above solution. The special cases contained in the general solution suggest that it can be used to describe the exterior asymptotically flat gravitational field of rotating body with arbitrary quadrupole moment. This is confirmed by the analysis of the motion of particles on the equatorial plane. The quadrupole moment turns out to drastically change the geometric structure of spacetime as well as the motion of particles, especially near the gravitational source.

We investigated in detail the properties of the Quevedo-Mashhoon (QM) spacetime which is a generalization of Kerr spacetime, including an arbitrary quadrupole. Our results show [20] that a deviation from spherical symmetry, corresponding to a non-zero electric quadrupole, completely changes the structure of spacetime. A similar behavior has been found in the case of the Erez-Rosen spacetime. In fact, a naked singularity appears that affects the ergosphere and introduces regions where closed timelike curves are allowed. Whereas in the Kerr spacetime the ergosphere corresponds to the boundary of a simply-connected region of spacetime, in the present case the ergosphere is distorted by the presence of the quadrupole and can even become transformed into non simply-connected regions. All these changes occur near the naked singularity which is situated at  $x = 1$ , a value that corresponds to the radial distance  $r = M + \sqrt{M^2 - a^2}$  in Boyer-Lindquist coordinates. In the limiting case  $a/M > 1$ , the multipole moments and the metric become complex, indicating that the physical description breaks down. Consequently, the extreme Kerr black hole represents the limit of applicability of the QM spacetime.

Since standard astrophysical objects satisfy the condition  $a/M < 1$ , we can conclude that the QM metric can be used to describe their exterior grav-

itational field. Two alternative situations are possible. If the characteristic radius of the body is greater than the critical distance  $M + \sqrt{M^2 - a^2}$ , i.e.  $x > 1$ , the exterior solution must be matched with an interior solution in order to describe the entire spacetime. If, however, the characteristic radius of the body is smaller than the critical distance  $M + \sqrt{M^2 - a^2}$ , the QM metric describes the field of a naked singularity.



# 6 Comparison of vacuum static quadrupolar metrics

## 6.1 Introduction

Most applications of Einstein's gravity theory follow from the investigation of exact solutions of the corresponding field equations. In the case of relativistic astrophysics, asymptotically flat solutions in empty space are of particular importance in order to describe the physical properties of the exterior field of compact objects [1]. From a physical point of view, it is sufficient in this case to limit ourselves to static and stationary solutions which are axially symmetric. In addition, it is appropriate to classify them in accordance with certain criteria which permits a comparison of their main properties. Using the analogy with Newtonian gravity, we propose to classify them in terms of their multipole moments.

The problem of defining invariant multipole moments in general relativity was first solved by Geroch and Hansen (GH) [27, 30], who proposed definitions for mass and spin multipoles of asymptotically flat spacetimes in vacuum. Moreover, Thorne, Simon and Beig defined relativistic multipole moments [41, 42] for non-stationary spacetimes. A proof of the equivalence between the GH moments and the Thorne moments for stationary systems was provided by Gürsel [28]. An elegant method to derive explicit expressions for the multipole moments of a given stationary and axially symmetric spacetime with asymptotic flatness was found by Fodor, Hoenselaers and Perjés (FHP) [26] using the Ernst formalism. This FHP method was generalized by Hoenselaers and Perjés [33]. Finally, Ryan found an alternative method for deriving the relativistic multipole moments [39] which has been intensively applied in relativistic astrophysics.

Although for the study of the gravitational field of relativistic compact objects, it is necessary to consider stationary solutions that take into account the rotation of the source, in this work, we will focus on the study of the static

case to explore in detail the physical properties of the solutions which then will be generalized to the case of stationary fields. From a physical point of view, the most important multipoles of a mass distribution are the monopole and the quadrupole; in this work, we will focus our analysis on mainly these two multipoles.

The first solution with only monopole moment was derived by Schwarzschild in 1916, just a couple of months after the publication of the theory of general relativity [40]. In 1917, Weyl found a class of static and axisymmetric solutions to the vacuum Einstein field equations [4]. The first static solution with quadrupole moment which includes the Schwarzschild metric as special case was found by Erez and Rosen in 1959 [22, 23]. This quadrupolar solution was generalized to include an infinite number of multipole moments by Quevedo in 1989 [37]. In 1966 and 1970, Zipoy and Voorhees found a transformation which allows us to generate new static solutions from known solutions [43, 44]. In particular, applying this transformation to the Schwarzschild metric, one obtains a new solution which, after a redefinition of the Zipoy-Voorhees parameter, was interpreted as the simplest static solution with generalizes the Schwarzschild metric and includes a quadrupole moment ( $q$ -metric) [38]. In 1985, Gutsunaev and Manko found an exact solution with monopole and quadrupole moments which was shown in [36] to have the same quadrupole as in the Erez-Rosen metric, but different contributions to higher relativistic multipole moments. In 1990, Manko [35] found a quadrupolar metric which can be interpreted as the non-linear combination of the Schwarzschild monopole solution with the quadrupolar term of the Weyl solution. In 1994, Hernández-Pastora and Martín [32] derived two exact solutions with different monopole-quadrupole structures.

To our knowledge, the above list includes all known static and asymptotically flat solutions of Einstein's equations in empty space. The main goal of the present work is to investigate the most important physical properties of these solutions. In particular, we will analyze the elementary flatness condition, curvature singularities, multipole moments structure and the relationships between them.

This paper is organized as follows. In Sec. 6.2, we present the general line element for static axisymmetric spacetimes and the corresponding vacuum field equations, and review the most general asymptotically flat solution in cylindrical coordinates discovered by Weyl. In Sec. 6.3, we present the solutions that contain the Schwarzschild spacetime as a particular case and an additional parameter which determines the quadrupole of the gravitational

source. Then, in Sec. 6.4, we investigate the conditions that the solutions must satisfy in order to be able to describe the exterior gravitational field of compact objects. Sec. 6.5 is devoted to the study of the multipole structure of the solutions. Finally, in Sec. 6.6, we discuss our results and present some initiatives for future works.

## 6.2 General properties of static and axisymmetric vacuum solutions

Although there exist in the literature many suitable coordinate systems, static axisymmetric gravitational fields are usually described in cylindrical coordinates  $(t, \rho, z, \varphi)$ , following the seminal work of Weyl. Stationarity implies that there exists a timelike Killing vector field with components  $\delta_t^\alpha$ , i.e.,  $t$  can be chosen as the time coordinate and the metric does not depend on time,  $\partial g_{\alpha\beta}/\partial t = 0$ . Axial symmetry, in addition, implies the existence of a spacelike Killing vector field with components  $\delta_\varphi^\alpha$ , which commutes with the timelike Killing vector. The coordinates can then be chosen such that  $\partial g_{\alpha\beta}/\partial \varphi = 0$ , and the axis of symmetry corresponds to  $\rho = 0$ . Furthermore, if we assume that the timelike Killing vector is hypersurface-orthogonal, the spacetime is static, i.e., it is invariant with respect to the transformation  $\varphi \rightarrow -\varphi$ .

Furthermore, using the properties of staticity and axial symmetry, together with the vacuum field equations, for a general metric of the form  $g_{\alpha\beta} = g_{\alpha\beta}(\rho, z)$ , it is possible to show that the most general line element for this type of gravitational fields can be written in the Weyl-Lewis-Papapetrou form as [4, 5, 6, 1]

$$ds^2 = e^{2\psi} dt^2 - e^{-2\psi} \left[ e^{2\gamma} (d\rho^2 + dz^2) + \rho^2 d\varphi^2 \right], \quad (6.2.1)$$

where  $\psi$  and  $\gamma$  are functions of  $\rho$  and  $z$  only. The vacuum field equations can be reduced to the following set of independent differential equations

$$\psi_{\rho\rho} + \frac{1}{\rho}\psi_\rho + \psi_{zz} = 0, \quad (6.2.2)$$

$$\gamma_\rho = \rho \left( \psi_\rho^2 - \psi_z^2 \right), \quad \gamma_z = 2\rho\psi_\rho\psi_z, \quad (6.2.3)$$

where  $\psi_\rho = \partial\psi/\partial\rho$ , etc. We see that the main field equation (6.2.2) corresponds to the linear Laplace equation for the metric function  $\psi$ . Furthermore,

the solution for the function  $\gamma$  can be obtained by quadratures once the function  $\psi$  is known.

The general solution of Laplace's equation is known and, if we demand additionally asymptotic flatness, we obtain the Weyl solution [4, 1]

$$\psi = \sum_{n=0}^{\infty} \frac{a_n}{(\rho^2 + z^2)^{\frac{n+1}{2}}} P_n(\cos \theta), \quad \cos \theta = \frac{z}{\sqrt{\rho^2 + z^2}}, \quad (6.2.4)$$

where  $a_n$  ( $n = 0, 1, \dots$ ) are arbitrary real constants, and  $P_n(\cos \theta)$  represents the Legendre polynomials of degree  $n$ . The expression for the metric function  $\gamma$  can be obtained from the two first-order differential equations (6.2.3). Then

$$\gamma = - \sum_{n,m=0}^{\infty} \frac{a_n a_m (n+1)(m+1)}{(n+m+2)(\rho^2 + z^2)^{\frac{n+m+2}{2}}} (P_n P_m - P_{n+1} P_{m+1}). \quad (6.2.5)$$

Since this is the most general static, axisymmetric, asymptotically flat vacuum solution, it must contain all known solutions of this class. In particular, one of the most interesting special solutions, which is Schwarzschild's spherically symmetric black hole spacetime, must be included as a special case. To see this, we must choose the constants  $a_n$  in such a way that the infinite sum (6.2.4) converges to the Schwarzschild solution in cylindrical coordinates. A straightforward computation shows that

$$a_{2n} = -\frac{m^{2n+1}}{2n+1}, \quad a_{2n+1} = 0, \quad (6.2.6)$$

where  $m$  is the mass parameter [31]. Clearly, this representation is not appropriate to handle the Schwarzschild metric.

It turns out that to investigate the properties of solutions with multipole moments, it is convenient to use prolate spheroidal coordinates  $(t, x, y, \varphi)$  in which the line element can be written as

$$ds^2 = e^{2\psi} dt^2 - \sigma^2 e^{-2\psi} \left[ e^{2\gamma} (x^2 - y^2) \left( \frac{dx^2}{x^2 - 1} + \frac{dy^2}{1 - y^2} \right) + (x^2 - 1)(1 - y^2) d\varphi^2 \right] \quad (6.2.7)$$

where

$$x = \frac{r_+ + r_-}{2\sigma}, \quad (x^2 \geq 1), \quad y = \frac{r_+ - r_-}{2\sigma}, \quad (y^2 \leq 1) \quad (6.2.8)$$

$$r_{\pm}^2 = \rho^2 + (z \pm \sigma)^2, \quad \sigma = \text{const.}, \quad (6.2.9)$$

and the metric functions  $\psi$ , and  $\gamma$  depend on  $x$  and  $y$ , only. In this coordinate system, the field equations become

$$[(x^2 - 1)\psi_x]_x + [(1 - y^2)\psi_y]_y = 0, \quad (6.2.10)$$

$$\gamma_x = \left( \frac{1 - y^2}{x^2 - y^2} \right) \left[ x(x^2 - 1)\psi_x^2 - x(1 - y^2)\psi_y^2 - 2y(x^2 - 1)\psi_x\psi_y \right] \quad (6.2.11)$$

$$\gamma_y = \left( \frac{x^2 - 1}{x^2 - y^2} \right) \left[ y(x^2 - 1)\psi_x^2 - y(1 - y^2)\psi_y^2 + 2x(1 - y^2)\psi_x\psi_y \right].$$

The simplest physically meaningful solution to the above system of differential equations is the Schwarzschild solution

$$\psi_s = \frac{1}{2} \ln \left( \frac{x - 1}{x + 1} \right), \quad \gamma_s = \frac{1}{2} \ln \left( \frac{x^2 - 1}{x^2 - y^2} \right), \quad (6.2.12)$$

which takes the standard form in spherical coordinates with  $x = r/m - 1$ ,  $y = \cos \theta$ , and  $\sigma = m$ . In principle, there could be an infinite number of exact solutions to the above equations. Not all of them, however, can be physically meaningful, in particular, if we demand that they should describe the exterior field of realistic compact objects. To this end, it is necessary that the solutions satisfy the conditions of asymptotic flatness, elementary flatness and regularity.

Asymptotic flatness means that at spatial infinity, the solution reduces to the Minkowski metric, indicating that the gravitational field far away from the source is practically negligible. This is a consequence of the long-range property of the gravitational interaction. In the case of the static metric in prolate spheroidal coordinates 6.2.7, this condition implies that

$$\lim_{x \rightarrow \infty} \psi = \text{const.}, \quad \lim_{x \rightarrow \infty} \gamma = \text{const.}, \quad (6.2.13)$$

where the constants can be set equal to zero by a suitable rescaling of the coordinates.

Elementary flatness is necessary in order to guarantee that near the rotation axis the geometry is Lorentzian, i.e., there are no conical singularities on the axis [1]. This condition can be expressed in an invariant manner by using the spacelike Killing vector field  $\eta^\alpha = \delta_\varphi^\alpha$  as

$$\lim_{\rho \rightarrow 0} \frac{(\eta^\alpha \eta_\alpha)_{,\beta} (\eta^\alpha \eta_\alpha)_{,\beta}}{4(\eta^\alpha \eta_\alpha)} = 1. \quad (6.2.14)$$

A direct computation by using the general line element in prolate spheroidal coordinates shows that the elementary flatness condition is equivalent to demanding that

$$\lim_{y \rightarrow \pm 1} \gamma = 0, \quad (6.2.15)$$

independently of the value of the spatial coordinate  $x$ .

Finally, the regularity condition implies that the solution must be free of curvature singularities outside a region located near the origin of coordinates so that it can be covered by an interior solution. Curvature singularities can be detected by analyzing the behavior of curvature invariants. In general, the Riemann curvature tensor in four dimensions possess 14 independent invariants. In the case of vacuum spacetimes, however, the Riemann tensor coincides with the Weyl tensor that has only four invariants which can be expressed as [21]

$$\begin{aligned} K &= I_1 = R_{\alpha\beta\gamma\delta} R^{\alpha\beta\gamma\delta}, & I_2 &= *R_{\alpha\beta\gamma\delta} R^{\alpha\beta\gamma\delta}, \\ I_3 &= R_{\alpha\beta\gamma\delta} R^{\gamma\delta\lambda\tau} R_{\lambda\tau}^{\alpha\beta}, & I_4 &= *R_{\alpha\beta\gamma\delta} R^{\gamma\delta\lambda\tau} R_{\lambda\tau}^{\alpha\beta}, \end{aligned} \quad (6.2.16)$$

where the dual is defined as

$$*R_{\alpha\beta\gamma\delta} = \frac{1}{2} \epsilon_{\alpha\beta\lambda\tau} R^{\lambda\tau}_{\gamma\delta}, \quad (6.2.17)$$

with  $\epsilon_{\alpha\beta\lambda\tau}$  being the Levi-Civita symbol. The quadratic invariants  $K = I_1$  and  $I_2$  are usually known as the Kretschmann and the Chern-Pontryagin scalars, respectively. If anyone of the four invariants happens to diverge at some particular place, it is said that there exists a curvature singularity at that place.

In the next section, we will investigate the properties of several exact solu-

tions with monopole and quadrupole moment. In particular, we will find out if they satisfy all the conditions to be physically relevant in the sense that they can be used to describe the exterior gravitational field of compact objects.

### 6.3 Static vacuum metrics with quadrupole

As mentioned in the last section, the Weyl metric can be considered as the most general static and axisymmetric solution which contains an infinite number of parameters, representing all the multipole moments. Therefore, a particular choice of parameters could represent a solution with only mass and quadrupole. However, such a form of a metric with an infinite number of parameters is not very suitable to be applied in the case of realistic sources like compact astrophysical objects. For this reason, we consider now metrics which include only two independent parameters that can be interpreted as mass and quadrupole.

In 1959, Erez and Rosen [23] presented a solution which generalizes the Schwarzschild metric and contains an additional parameter  $q$ . In this case, the function  $\psi$  can be expressed as

$$\psi_{ER} = \frac{1}{2} \ln \left( \frac{x-1}{x+1} \right) + \frac{1}{2} q (3y^2 - 1) \left[ \frac{1}{4} (3x^2 - 1) \ln \left( \frac{x-1}{x+1} \right) + \frac{3}{2} x \right]. \quad (6.3.1)$$

The corresponding function  $\gamma_{ER}$  can be expressed in a compact form as follows:

$$\begin{aligned} \gamma_{ER} = & \frac{1}{2} (q+1)^2 \ln \left( \frac{x^2-1}{x^2-y^2} \right) \\ & - \frac{3}{2} q (1-y^2) \left[ \frac{3}{32} q (x^2-1) (9x^2y^2 - x^2 - y^2 + 1) \ln^2 \left( \frac{x-1}{x+1} \right) \right. \\ & + \frac{1}{8} x (27qx^2y^2 - 3qx^2 - 21qy^2 + 5q + 8) \ln \left( \frac{x-1}{x+1} \right) \\ & \left. + \frac{1}{8} (27qx^2y^2 - 3qx^2 - 12qy^2 + 4q + 16) \right]. \quad (6.3.2) \end{aligned}$$

This solution was obtained by using the method of separation of variables for the function  $\psi$ . An explicit generalization which contains higher multipole moments was presented in 1989 in [37] by using the same method.

In 1984, Gutsunayev and Manko [29] found a new static solution for the function  $\psi$  which is given by

$$\psi_{GM} = \frac{1}{2} \ln \left( \frac{x-1}{x+1} \right) + q \frac{x}{(x^2-y^2)^3} (x^2 - 3x^2y^2 + 3y^2 - y^4), \quad (6.3.3)$$

and the function  $\gamma_{GM}$  is given by

$$\begin{aligned} \gamma_{GM} = & \frac{1}{2} \ln \left( \frac{x^2-1}{x^2-y^2} \right) \\ & + \frac{1}{2} q \frac{1-y^2}{(x^2-y^2)^4} \left( 3(-5y^2+1)(x^2-y^2)^2 \right. \\ & + 8y^2(-5y^2+3)(x^2-y^2) + 24y^4(-y^2+1) \left. \right) \\ & + \frac{1}{8} q^2 \frac{(1-y^2)}{(x^2-y^2)^8} \left( -12(25y^4-14y^2+1)(x^2-y^2)^5 \right. \\ & + 3(-675y^6+697y^4-153y^2+3)(x^2-y^2)^4 \\ & + 32y^2(-171y^6+259y^4-105y^2+9)(x^2-y^2)^3 \\ & + 32y^4(-225y^6+451y^4-271y^2+45)(x^2-y^2)^2 \\ & + 2304y^6(-2y^6+5y^4-4y^2+1)(x^2-y^2) \\ & \left. + 1152y^8(-y^6+3y^4-3y^2+1) \right). \end{aligned} \quad (6.3.4)$$

This solution was found by applying a particular differential operator to the Schwarzschild metric. This method was shown to be based upon the property that in Cartesian coordinates the derivatives of a harmonic function are also harmonic functions [36]. The metric function  $\gamma$  takes the form

In 1990, Manko [35] found a different static solution in the form

$$\psi_M = \frac{1}{2} \ln \left( \frac{x-1}{x+1} \right) + q \frac{3x^2y^2 - x^2 - y^2 + 1}{2(x^2 + y^2 - 1)^{5/2}}, \quad (6.3.5)$$

which leads to a particular function  $\gamma_M$

$$\begin{aligned}\gamma_M &= \frac{1}{2} \ln \left( \frac{x^2 - 1}{x^2 - y^2} \right) \\ &+ \frac{qx(2x^4 - 5x^2 + 5x^2y^2 + 3 - 3y^2)}{(x^2 + y^2 - 1)^{5/2}} - 2q \\ &+ \frac{3q^2}{8(x^2 + y^2 - 1)^5} \left( \frac{x^2y^2(5x^2y^2 - 3x^2 - 3y^2 + 3)^2}{x^2 + y^2 - 1} \right. \\ &\left. - (3x^2y^2 - x^2 - y^2 + 1)^2 \right)\end{aligned}\quad (6.3.6)$$

The first term of this solution corresponds to the Schwarzschild metric, whereas the second term coincides with the quadrupolar term of the general Weyl solution in prolate spheroidal coordinates.

Furthermore, in 1994, Hernández-Pastora and Martín [32] derived two different exact solutions which can be written as

$$\begin{aligned}\psi_{HM1} &= \frac{1}{2} \ln \left( \frac{x-1}{x+1} \right) - \frac{5}{8}q \left[ \frac{1}{4} \left( (3x^2 - 1)(3y^2 - 1) - 4 \right) \ln \left( \frac{x-1}{x+1} \right) \right. \\ &\left. + \frac{2x}{(x^2 - y^2)} - \frac{3}{2}x(3y^2 - 1) \right]\end{aligned}\quad (6.3.7)$$

and

$$\begin{aligned}\psi_{HM2} &= \psi_{HM1} - \frac{5}{32}q^2 \left[ \left( 33 + 90P_2(x)P_2(y) - \frac{153}{2}P_4(x)P_4(y) \right) \ln \left( \frac{x-1}{x+1} \right) \right. \\ &- 135xP_2(y) - \frac{153}{24}x(55 - 105x^2)P_4(y) \\ &\left. - \frac{x}{x^2 - y^2} \left( 33 - \frac{5}{(x^2 - y^2)^2} (3x^2y^2 + y^4 - x^2 - 3y^2) \right) \right],\end{aligned}\quad (6.3.8)$$

where

$$P_2(y) = \frac{1}{2}(3y^2 - 1), \quad (6.3.9)$$

$$P_4(y) = \frac{1}{8}(35y^4 - 30y^2 + 3). \quad (6.3.10)$$

The corresponding functions  $\gamma_{HM1}$  and  $\gamma_{HM2}$  have a quite complicated struc-

ture which we will not present here.

Finally, in 1966 and 1970 Zipoy [44] and Voorhees [43], respectively, found a particular symmetry of the vacuum field equations, and derived a transformation which can be used to generate new solutions from known solutions. In the case of the Schwarzschild metric, the new solution can be expressed simply as

$$\psi_{zV} = \frac{1}{2}\delta \ln \left( \frac{x-1}{x+1} \right), \quad \gamma_{zV} = \frac{1}{2}\delta^2 \ln \left( \frac{x^2-1}{x^2-y^2} \right), \quad (6.3.11)$$

where  $\delta$  is an arbitrary real constant. This solution is also known as the  $\delta$ -metric of the  $\gamma$ -metric for notational reasons [34]. Later on, in 2011, this metric was reinterpreted as a quadrupolar metric and renamed as the  $q$ -metric [38] which in spherical coordinates can be transformed into the simple form

$$ds^2 = \left(1 - \frac{2m}{r}\right)^{1+q} dt^2 - \left(1 - \frac{2m}{r}\right)^{-q} \times \left[ \left(1 + \frac{m^2 \sin^2 \theta}{r^2 - 2mr}\right)^{-q(2+q)} \left( \frac{dr^2}{1 - 2m/r} + r^2 d\theta^2 \right) + r^2 \sin^2 \theta d\varphi^2 \right]. \quad (6.3.12)$$

It is easy to see that all the above solutions represent a generalization of the Schwarzschild metric which is obtained in the limiting case  $q \rightarrow 0$ . To our knowledge, the solutions presented above are the only exact solutions that generalize the Schwarzschild monopole solution and satisfy the conditions expected from a metric that describes a realistic gravitational field.

## 6.4 Physical conditions

All the solutions presented in the last section are asymptotically flat because at spatial infinity they behave as

$$\psi_0 = \lim_{x \rightarrow \infty} \psi = 0, \quad \gamma_0 = \lim_{x \rightarrow \infty} \gamma = 0, \quad (6.4.1)$$

which determine the Minkowski metric, independently of the value of  $y$ . Notice, moreover, that this condition is satisfied for all finite values of the in-

dependent parameters  $m$  and  $q$ . This means that for any finite values of the monopole and quadrupole moments, the solutions presented in the last section are asymptotically Minkowski.

As mentioned above, the condition that no conical singularities exist on the symmetry axis (6.2.14) in prolate spheroidal coordinates becomes

$$\lim_{y \rightarrow \pm 1} \gamma = 0. \quad (6.4.2)$$

An inspection of the  $\gamma$  function for the Erez-Rosen, Gutsunayev-Manko and Manko solutions and the  $q$ -metric, mentioned in the last section, shows that this condition is always satisfied, independently of the value of  $x$ , indicating that all of them are elementary flat. In the case of the Hernández-Martín solutions, however, a direct computation shows that they are elementary flat only for positive values of the coordinate  $x$ . In spherical coordinates, this means that the HM solutions are well-defined only outside the radius  $r = 2m$ . A geometric and physical analysis inside the horizon  $r = 2m$  is possible only by considering the presence of conical singularities along the symmetry axis.

We now analyze the regularity condition by using first the Kretschmann scalar  $K = R_{\alpha\beta\gamma\delta}R^{\alpha\beta\gamma\delta}$ . First, we consider the Schwarzschild metric (6.2.12) for which we obtain

$$K_s = \frac{48}{m^4(x+1)^6}. \quad (6.4.3)$$

This expression is singular only for  $x = -1$  ( $r = 0$ ), indicating the well-known fact that the Schwarzschild spacetime is singular only at the origin of coordinates.

Another example of a solution that can be investigated analytically is the  $q$ -metric. In this case, all the calculations can be performed explicitly and the resulting Kretschmann scalar reads

$$K_q = \frac{48}{\sigma^4} (q+1)^2 \frac{p(x, y; q)}{(x+1)^{2(q^2+3q+3)} (x-1)^{2(q^2+q+1)} (x^2-y^2)^{-2q^2-4q+1}}, \quad (6.4.4)$$

where

$$\begin{aligned}
 p(x, y; q) &= (x - 1)^2(x^2 - y^2) - 2q(x - 1)^2(x + y^2) & (6.4.5) \\
 &+ q^2 \left[ (2 - y^2)x^2 - 3(1 - y^2)x + \frac{1}{2}(4 - 7y^2) \right] \\
 &- q^3 \left( x - \frac{4}{3} \right) (1 - y^2) + \frac{1}{3}q^4(1 - y^2).
 \end{aligned}$$

First, we see that for all values of  $q$  there is always a singularity at  $x = -1$ . Moreover, we have two possible divergences at  $x = 1$  and  $x = \pm y$ . These divergent factors can only be canceled by the function  $p$ , but it does not vanish for  $x = 1$  or  $x = \pm y$  for arbitrary values of  $q$ , except for  $q = -2$ . In this case, one has  $p(x, y; -2) = (x + 1)^2(x^2 - y^2)$  so that

$$K_{q=-2} = \frac{48}{\sigma^4(x - 1)^6}, \quad (6.4.6)$$

which diverges for  $x = 1$ . For other values of the parameter  $q$ , the Kretschmann scalar of the  $q$ -metric diverges at  $x = \pm 1$  and  $x = \pm y$ , as far as the exponents of the corresponding factors are negative. The exponents of the factors  $x + 1$  and  $x - 1$  are negative definite, but the exponent of the factor  $x^2 - y^2$  vanishes for  $q = -1 + \sqrt{3}/2$  and  $q = -1 - \sqrt{3}/2$ .

Consequently, the Kretschmann scalar of the  $q$ -metric diverges at  $x = -1$  for  $q \neq -2$ , at  $x = 1$  for  $q \neq 0$  and at  $x = \pm y$  for  $q \in (-1 - \sqrt{3}/2, -1 + \sqrt{3}/2)$  restricted to  $q \neq 0$  and  $q \neq -2$ . An additional restriction to the value of the parameter  $q$  is imposed by assuming  $\sigma > 0$  and requiring its mass monopole to be positive. We will see in the next section that this physical condition implies that  $q > -1$ , leading to the conclusion that the singularity at  $x = -1$  is always present.

The investigation of the remaining quadrupolar solutions is much more complicated. The results of our analysis are summarized in Table 6.1, where we include the Schwarzschild solution for comparison, and use spherical coordinates with  $x = r/m - 1$  and  $y = \cos \theta$ . The boldfaced radii represent singularities that are present, independently of the value of the parameters  $m, q$  and the coordinate  $\theta$ . The remaining radii represent singularities which are not always present, but depend on the value of  $q$  or the coordinate  $\theta$ . We see that only the  $q$ -metric is characterized by a completely singular horizon at  $r = 2m$ , representing the outermost singularity, which is the only one

Static metric	Naked singularities
Schwarzschild	$r = 0$
$q$ -metric	$r = 0, m(1 \pm \cos \theta), 2m$
Erez-Rosen	$r = 0, m(1 \pm \cos \theta), 2m$
Gutsunayev-Manko	$r = 0, m(1 \pm \cos \theta), 2m$
Manko	$r = 0, m(1 \pm \cos \theta), 2m$
Hernández-Martí 1 and 2	$r = 0, m(1 \pm \cos \theta), 2m$

**Table 6.1:** Singularities of spacetimes with monopole and quadrupole moments. Boldfaced values are naked singularities which exist for all values of the parameters  $m, q$  and  $\theta$ . Other singularities exist only for particular values of these parameters.

that can be observed by an exterior observer. In the remaining cases, the Schwarzschild horizon remains partially regular, implying that for certain values of  $q$ , it is possible to observe the singularity located at the origin of coordinates.

Finally, we mention that the analysis of the remaining three curvature invariants does not lead to additional singularities.

## 6.5 Multipole moments

Using the original definition formulated by Geroch [27], the calculation of multipole moments is quite laborious. Fodor, Hoenselaers and Perjés [26] found a relation between the Ernst potential [24, 25] and the multipole moments which facilitates the computation. In the case of static axisymmetric spacetimes, the Ernst potential is defined as

$$\zeta(x, y) = \frac{1 - e^{2\psi}}{1 + e^{2\psi}}. \quad (6.5.1)$$

The idea is that the multipole moments can be obtained explicitly from the values of the Ernst potential on the axis by using the following procedure. On the axis of symmetry  $y = 1$ , we can introduce the inverse of the Weyl coordinate  $z$  as

$$\tilde{z} = \frac{1}{z} = \frac{1}{mx}, \quad \text{with } \sigma = m. \quad (6.5.2)$$

If we now introduce the inverse potential as

$$\tilde{\xi}(\tilde{z}, 1) = \frac{1}{\tilde{z}} \xi(\tilde{z}, 1), \quad (6.5.3)$$

the multipole moments can be calculated as

$$\mathcal{M}_n = m_n + d_n, \quad m_n = \frac{1}{n!} \left. \frac{d^n \tilde{\xi}(\tilde{z}, 1)}{d\tilde{z}^n} \right|_{\tilde{z}=0}, \quad (6.5.4)$$

where the additional terms  $d_n$  must be determined from the original Geroch definition. The main point now is that the first term  $m_n$  is completely determined by the  $n$ -th derivative of the inverse Ernst potential  $\tilde{\xi}$ , whereas the second term  $d_n$  depends on the derivatives of order less than  $n$ , so that the moment  $\mathcal{M}_n$  can be calculated explicitly once all the derivatives of order  $n$  or less are known.

In this manner, it is easy to show that for the Schwarzschild spacetime the multipole moments are given as

$$\mathcal{M}_0 = m, \quad \mathcal{M}_k = 0, \quad (k \geq 1), \quad (6.5.5)$$

a result which is in accordance with the physical interpretation of the Schwarzschild metric obtained by using other methods.

For the Erez-Rosen metric, we obtain

$$\begin{aligned} \mathcal{M}_0 &= m \\ \mathcal{M}_2 &= Q \\ \mathcal{M}_4 &= -\frac{2}{7} Q m^2 \\ \mathcal{M}_6 &= -\frac{8}{231} Q m^4 (1 + 3q) \\ \mathcal{M}_8 &= -\frac{8}{3003} Q m^6 \left( 2 - \frac{74}{15} q + \frac{84}{45} q^2 \right) \\ \mathcal{M}_{10} &= \frac{32}{3927} Q m^8 \left( -\frac{28}{247} + \frac{37}{57} q + \frac{1124}{741} q^2 \right), \end{aligned}$$

where  $Q = 2qm^3/15$ .

For the Gutsunayev-Manko metric, we obtain

$$\begin{aligned}
 \mathcal{M}_0 &= m \\
 \mathcal{M}_2 &= Q \\
 \mathcal{M}_4 &= \frac{6}{7}Qm^2 \\
 \mathcal{M}_6 &= \frac{8}{231}Qm^4(14 - 45q) \\
 \mathcal{M}_8 &= \frac{8}{3003}Qm^6(84 - 1282q - 420q^2) \\
 \mathcal{M}_{10} &= \frac{32}{3927}Qm^8\left(\frac{2772}{247} - \frac{1343804}{2717}q - \frac{50}{1463}q^2\right),
 \end{aligned}$$

where  $Q = 2qm^3$ .

For the Manko solution, we obtain

$$\begin{aligned}
 \mathcal{M}_0 &= m \\
 \mathcal{M}_2 &= Q = -m^3q \\
 \mathcal{M}_4 &= -\frac{8}{7}Qm^2 \\
 \mathcal{M}_6 &= \frac{1}{231}Qm^4(180q + 133) \\
 \mathcal{M}_8 &= -\frac{2}{3003}Qm^6(420q^2 + 2182q + 357) \\
 \mathcal{M}_{10} &= \frac{1}{969969}Qm^8(1379100q^2 + 1277710q + 85701).
 \end{aligned}$$

For the first Hernández-Martín metric, we obtain

$$\begin{aligned}
 \mathcal{M}_0 &= m \\
 \mathcal{M}_2 &= Q \\
 \mathcal{M}_4 &= 0 \\
 \mathcal{M}_6 &= -\frac{60}{77}Qm^4 \\
 \mathcal{M}_8 &= -\frac{4}{3003}qQm^6(265 + 210q) \\
 \mathcal{M}_{10} &= \frac{4}{3927}qQm^8\left(-\frac{104370}{714} + \frac{769125}{1729}q\right),
 \end{aligned}$$

and for the second Hernández-Martín solution

$$\begin{aligned}
 \mathcal{M}_0 &= m \\
 \mathcal{M}_2 &= Q \\
 \mathcal{M}_4 &= 0 \\
 \mathcal{M}_6 &= 0 \\
 \mathcal{M}_8 &= -\frac{40}{143}q^2Qm^6 \\
 \mathcal{M}_{10} &= -\frac{42140}{46189}q^2Qm^8,
 \end{aligned}$$

where  $Q = qm^3$ .

Finally, for the  $q$ -metric we get

$$\begin{aligned}
 \mathcal{M}_0 &= \delta m \\
 \mathcal{M}_2 &= \frac{1}{3}\delta m^3(1 - \delta^2) \\
 \mathcal{M}_4 &= \delta m^5 \left( \frac{19}{105}\delta^4 - \frac{8}{21}\delta^2 + \frac{1}{5} \right) \\
 \mathcal{M}_6 &= \delta m^7 \left( -\frac{389}{3465}\delta^6 + \frac{23}{63}\delta^4 - \frac{457}{1155}\delta^2 + \frac{1}{7} \right) \\
 \mathcal{M}_8 &= \delta m^9 \left( \frac{257}{3465}\delta^8 - \frac{44312}{135135}\delta^6 + \frac{73522}{135135}\delta^4 - \frac{54248}{135135}\delta^2 + \frac{1}{9} \right) \\
 \mathcal{M}_{10} &= \delta m^{11} \left( -\frac{443699}{8729721}\delta^{10} + \frac{17389}{61047}\delta^8 - \frac{27905594}{43648605}\delta^6 + \frac{6270226}{8729721}\delta^4 \right. \\
 &\quad \left. - \frac{5876077}{14549535}\delta^2 + \frac{1}{11} \right),
 \end{aligned}$$

where  $\delta = 1 + q$ .

A comparison of these results show that all the above solutions are equivalent up to the quadrupole moment. Indeed, a simple redefinition of the parameter  $q$  which enters all the metrics leads to equivalent values for the monopole and quadrupole moments. We see, however, that differences appear between all the solutions at the level of higher moments. The particularity of the first and second Hernández-Martín solutions is that by choosing the form of the metric  $\psi_{HM}$  appropriately, the multipoles  $\mathcal{M}_4$  and  $\mathcal{M}_6$  can be made to vanish identically. This means that by following the same procedure,

it is possible to generate a solution with only monopole and quadrupole moments. In all the remaining solutions, contributions of higher multipoles are always present.

We conclude that from the point of view of the monopole-quadrupole structure all the solutions presented in Sec. 6.3 are physically equivalent.

## 6.6 Remarks

In this work, we analyzed all the exact solutions of Einstein's vacuum field equations which contain the Schwarzschild solution as a particular case and, in addition, possess an arbitrary parameter which determines the quadrupole of the gravitational source. In particular, we studied the Erez-Rosen, Gut-sunayev-Manko, Manko, Hernández-Pastora solutions and the  $q$ -metric, obtained from the Schwarzschild by applying a Zipoy-Voorhees transformation.

First, we established that all the above solutions are asymptotically and elementary flat. This means that at infinity the gravitational field strength is negligible, and the rotation axis is free of conical singularities, respectively. We performed also a detailed analysis of the Kretschmann scalar to determine the curvature singularity structure of these spacetimes. We found that in general there are three types of naked singularities which are located at the origin of coordinates  $r = 0$ , between the origin and the Schwarzschild horizon  $r = m(1 \pm \cos \theta)$  and on the horizon  $r = 2m$ , where  $m$  is the mass of the gravitational source. The main difference is that only in the case of the  $q$ -metric, the outermost singularity located at  $r = 2m$  exists for all values of the parameters  $m$  and  $q$  and the coordinate  $\theta$ . For all the remaining metrics, the second and third singularities exist only for certain specific values of  $q$  or  $\theta$ . This means that in principle it is possible to observe the interior singularities located at  $r = 0$  and  $r = m(1 \pm \cos \theta)$ , which is not possible in the case of a spacetime described by the  $q$ -metric. Suppose that we want to use an interior solution to "cover" the naked singularities generated by the quadrupole. In the case of the  $q$ -metric, the surface of the interior mass distribution can be located anywhere outside the outermost singularity situated at  $r = 2m$ . In the case of all the remaining exterior metrics, the surface of the interior distribution can have even a zero radius for certain values of the quadrupole parameter.

The study of the multipole moments of all the solutions shows that by choosing the quadrupole parameter appropriately all of them are character-

ized by the same mass and quadrupole, although differences can appear at the level of higher multipoles. This means that all the solutions can be used to describe the exterior gravitational field of a distorted mass distribution with quadrupole moment.

Our results show that all the solutions analyzed in this work are equivalent from the physical point of view in the sense that they satisfy all the conditions that are necessary to describe the exterior gravitational field of realistic compact objects. Nevertheless, from a practical point of view the  $q$ -metric presents certain advantages over the remaining metrics. Indeed, the mathematical structure of this metric is very simple which facilitates its study. For instance, when searching for interior solutions with quadrupole that could be matched with an exterior quadrupolar metric, one certainly would try first the  $q$ -metric because of its simplicity.

To completely describe the gravitational field of realistic compact objects with quadrupole, it is necessary to take the rotation into account. Moreover, a suitable interior solution is also necessary in order to describe the entire spacetime, as required in general relativity. Due to the mathematical complexity of the inner field equations and the matching conditions, it would be easier to start with the simplest possible case which can be handled analytically. Our results show that the  $q$ -metric is the best candidate for this task. We expect to explore this problem in future works.

\*\*\*\*\*

# 7 Observers in Kerr spacetimes: the ergoregion on the equatorial plane

## 7.1 Introduction

The physics of black holes (**BHs**) is probably one of the most complex and still controversial aspects of Einstein's geometric theory of gravitation. Many processes of High Energy Astrophysics are supposed to involve singularities and their formation from a stellar progenitor collapse or from the merging of a binary **BH** system. The interaction of these sources with the matter environment, which can lead to accretion and jets emission, is the basis for many observed phenomena. As a consequence of this interaction, the singularity properties, determined generally by the values of their intrinsic spin, mass or electric charge parameters, might be modified, leading to considerable changes of the singularity itself. In this work, we concentrate our analysis on the ergoregion in the naked singularity (**NS**) and **BH** regimes of the axisymmetric and stationary Kerr solution. We are concerned also about the implications of any spin-mass ratio oscillation between the **BH** and the **NS** regimes from the viewpoint of stationary observers and their frequencies, assuming the invariance of the system symmetries (axial symmetry and time independence). One of the goals of this work is to explore the existence of spin transitions in very weak naked singularities [46], which are characterized by a spin parameter  $a/M \approx 1$ . If the collapse of a stellar object or the merging of several stellar or **BH** attractors lead to the formation of a naked singularity, then a total or partial destruction of the horizon may occur which should be accompanied by oscillations of the spin-to-mass ratio. Naked singularities can also appear in non-isolated **BH** configurations as the result of their interaction with the surrounding matter, i. e., in some transient process of the evolution of an interacting black hole. Indeed, the interaction can

lead to modifications of characteristic **BH** parameters, for instance, through a spin-up or spin-down process which can also alter the spacetime symmetries. The details of such spin transitions, leading possibly to the destruction of the horizon, and their consequences are still an open problem.

In this work, keeping the Kerr spacetime symmetries unchanged, we focus on the variation of the dimensionless spin parameter in the region within the static limit on the equatorial plane of the attractor, this being the plane of symmetry of the Kerr solution. This special plane of the axisymmetric geometry has many interesting properties; for instance, constants of motion emerge due to the symmetry under reflection with respect to this plane; the geometry has some peculiarities that make it immediately comparable with the limiting static Schwarzschild solution, in particular, the location of the outer ergoregion boundary is independent of the spin value, and coincides with the location of the Schwarzschild horizon. There is also a clear astrophysical interest in the exploration of such a plane, as the large majority of accretion disks are considered to be located on the equatorial plane of their attractors.

From a methodological viewpoint, our analysis represents a comparative study of stationary and static observers in Kerr spacetimes for any range of the spin parameter. The findings in this work highlight major differences between the behavior of these observers in **BH** and **NS** geometries. These issues are clearly related to the most general and widely discussed problem of defining **BHs**, their event horizon and their intrinsic thermodynamic properties [47, 48, 49, 50, 51, 52]. Further, it seems compelling to clarify the role of the static limit and of the ergoregion in some of the well-analyzed astrophysical processes such as the singularity formation, through the gravitational collapse of a stellar “progenitor” or the merging of two **BHs**. Similarly, it is interesting to analyze the role of the frame-dragging effect in driving the accretion processes. In fact, the ergosphere plays an important role in the energetics of rotating black holes.

The dynamics inside the ergoregion is relevant in Astrophysics for possible observational effects, since in this region the Hawking radiation can be analyzed and the Penrose energy extraction process occurs [57, 53, 54, 55, 56]<sup>1</sup>.

---

<sup>1</sup>The Hawking process is essentially due to the vacuum fluctuation happening in the regions close to the **BH** horizon; it is not related to the properties of the ergoregion itself. The Hawking radiation is the (spontaneous) emission of thermal radiation which is created in the vacuum regions surrounding a **BH**, and leads to a decrease of the mass. Connected in many ways to the Unruh effects, it generally leads to the production of pairs

For the actual state of the Penrose process, see [59]. Another interesting effect connected directly to the ergoregion is discussed in [60]. The mechanism, by which energy from compact spinning objects is extracted, is of great astrophysical interest and the effects occurring inside the ergoregion of black holes are essential for understanding the central engine mechanism of these processes [61, 62]. Accreting matter can even get out, giving rise, for example, to jets of matter or radiation [61, 63] originated inside the ergoregion. Another possibility is the extraction of energy from a rotating black hole through the Blandford-Znajek mechanism (see, for instance, [64, 65, 66, 67, 68, 69, 70, 71, 72, 73]). An interesting alternative scenario for the role of the Blandford-Znajek process in the acceleration of jets is presented in [74]. Further discussions on the Penrose and Blandford-Znajek processes may be found in [75, 76]. In general, using orbits entering the ergosphere, energy can be extracted from a Kerr black hole or a naked singularity. On the other hand, naked singularity solutions have been studied in different contexts in [77, 78, 79, 80, 81, 82, 83, 84, 85, 86, 87, 88]. Kerr naked singularities as particle accelerators are considered in [89]– see also [90, 91]. More generally, Kerr naked singularities can be relevant in connection to superspinars, as discussed in [90]. The stability of Kerr superspinars has been analyzed quite recently in [92], assenting the importance of boundary conditions in dealing with perturbations of **NSs**.

An interesting perspective exploring duality between elementary particles and black holes, pursuing quantum black holes as the link between microphysics and macrophysics, can be found in [93, 94, 95, 96]– see also [97]. A general discussion on the similarities between characteristic parameter values of **BHs** and **NSs**, in comparison with particle like objects, is addressed also in [99, 98, 100, 101]. Quantum evaporation of **NSs** was analyzed in [102], radiation in [103], and gravitational radiation in [104, 105, 106].

Creation and stability of naked singularities are still intensively debated [107, 108, 109, 110, 111, 112]. A discussion on the ergoregion stability can be found in [113, 114]. However, under quite general conditions on the progenitor, these analysis do not exclude the possibility that considering instability

---

of particles, one escaping to infinity while the other is trapped by the **BH** horizon. On the other hand, the Penrose energy extraction, or its wave-analogue of super-radiance, is related essentially to a classical (i.e. non quantum) phenomenon occurring in the ergoregion,  $]r_+, r_e^+[$ , due to the frame-dragging of the spinning spacetime. In this way, energy can be extracted from the source, lowering its angular momentum. For a study of the Hawking radiation in Kerr and Kerr-Newman spacetimes see also [58]

processes a naked singularity can be produced as the result of a gravitational collapse. These studies, based upon a numerical integration of the corresponding field equations, often consider the stability of the progenitor models and investigate the gravitational collapse of differentially rotating neutron stars in full general relativity [115]. Black hole formation is then associated with the formation of trapped surfaces. As a consequence of this, a singularity without trapped surfaces, as the result of a numerical integration, is usually considered as a proof of its naked singularity nature. However, the non existence of trapped surfaces after or during the gravitational collapse is not in general a proof of the existence of a naked singularity. As shown in [116], in fact, it is possible to choose a very particular slicing of spacetime during the formation of a spherically symmetric black hole where no trapped surfaces exist (see also [117]). Eventually, the process of gravitational collapse towards the formation of **BHs** (and therefore, more generally, the issues concerning the formation or not of a horizon and hence of **NSs**) is still, in spite of several studies, an open problem. There are transition periods of transient dynamics, possibly involving topological deformations of the spacetime, in which we know the past and future asymptotic regions of the spacetime, but it is still in fact largely unclear what happens during that process. The problem is wide and involves many factors as, especially in non-isolated systems, the role of matter and symmetries during collapse. Another major process that leads to black hole formation is the merging of two (or more) black holes, recently detected for the first time in the gravitational waves sector [118]. See also [119, 120] for the first observation of the probable formation of a **BH** from the coalescence of two neutron stars. An interesting and detailed analysis of Kerr and Kerr-Newman naked singularities in the broader context of braneworld Kerr-Newman (**B-KN**) spacetimes can be found in [121], where a new kind of instability, called mining instability, of some **B-KN** naked singularity spacetimes was found. In there, the exploration of the “causality violation region” is also faced. This is the region where the angular coordinate becomes timelike, leading eventually to closed timelike curves. Details on the relation between this region and the Kerr ergoregion can be found in the aforementioned reference.

In [99, 98, 101, 100, 46, 122], we focused on the study of axisymmetric gravitational fields, exploring different aspects of spacetimes with **NSs** and **BHs**. The results of this analysis show a clear difference between naked singularities and black holes from the point of view of the stability properties of cir-

cular orbits<sup>2</sup>. This fact would have significant consequences for the extended matter surrounding the central source and, hence, in all processes associated with energy extraction. Indeed, imagine an accretion disk made of test particles which are moving along circular orbits on the equatorial plane of a Kerr spacetime. It turns out that in the case of a black hole the accretion disk is continuous whereas in the case of a naked singularity it is discontinuous. This means that we can determine the values of intrinsic physical parameters of the central attractor by analyzing the geometric and topological properties of the corresponding Keplerian accretion disk. In addition, these disconnected regions, in the case of a naked singularities, are a consequence of the repulsive gravity properties found also in many other black hole solutions and in some extensions or modifications of Einstein's theory. The effects of repulsive gravity in the case of the Kerr geometry were considered in [126] and [127]. Analogies between the effects of repulsive gravity and the presence of a cosmological constant was shown also to occur in regular black hole spacetimes or in strong gravity objects without horizons [128, 129].

Several studies have already shown that it is necessary to distinguish between weak ( $a/M \approx 1$ ) and strong naked singularities ( $a/M \gg 1$ ). It is also possible to introduce a similar classification for black holes; however, we prove here that only in the case of naked singularities there are obvious fundamental distinctions between these classes which are not present among the different black hole classes. Our focus is on strong **BHs**, and weak and very weak **NSs**. This analysis confirms the distinction between strong and weak **NSs** and **BHs**, characterized by peculiar limiting values for the spin parameters. Nevertheless, the existence and meaning of such limits is still largely unclear, and more investigation is due. However, there are indications about the existence of such limits in different geometries, where weak and strong singularities could appear. In [46, 99, 98, 100, 101], it was established that the motion of test particles on the equatorial plane of black hole spacetimes can be used to derive information about the structure of the central source of gravitation; moreover, typical effects of repulsive gravity were observed in the naked singularity ergoregion (see also [130, 131, 132, 78]). In addition, it was pointed out that there exists a dramatic difference between

---

<sup>2</sup>Test particle motion can be used to determine the topological properties of general relativistic spacetimes [123, 124, 125]. Moreover, we proved that in certain **NS** geometries different regions of stable timelike circular orbits are separated from each other by empty regions; this means that an accretion disk made of test particles will show a particular ring-like structure with specific topological properties.

black holes and naked singularities with respect to the zero and negative energy states in circular orbits (stable circular geodesics with negative energy were for the first time discussed in [133]). The static limit would act indeed as a semi-permeable membrane separating the spacetime region, filled with negative energy particles, from the external one, filled with positive energy particles, gathered from infinity or expelled from the ergoregion with impoverishment of the source energy. The membrane is selective because it acts so as to filter the material in transit between the inner region and outside the static limit. This membrane wraps and selectively isolates the horizon in Kerr black holes and the singularity in superspinning solutions, partially isolating it from the outer region by letting selectively rotating infalling or outgoing matter to cross the static limit. As mentioned above, the ergoregion is involved in the **BH** spin-up and spin-down processes leading to a radical change of the dynamical structure of the region closest to the source and, therefore, potentially could give rise to detectable effects. It is possible that, during the evolutionary phases of the rotating object interacting with the orbiting matter, there can be some evolutionary stages of spin adjustment, for example, in the proximity of the extreme value ( $a \lesssim M$ ) where the speculated spin-down of the **BH** can occur preventing the formation of a naked singularity with  $a \gtrsim M$  (see also [111, 134, 135, 136, 137, 138, 139, 140, 141, 109, 142]). The study of extended matter configurations in the Kerr ergoregion is faced for example in [143, 46]. In [143, 144, 146, 145, 147], a model of multi-accretion disks, so called ringed accretion disks, both corotating and counterrotating on the equatorial plane of a Kerr **BH**, has been proposed, and a model for such ringed accretion disks was developed. Matter can eventually be captured by the accretion disk, increasing or removing part of its energy and angular momentum, therefore prompting a shift of its spin [148, 110, 133, 149, 150, 151]. A further remarkable aspect of this region is that the outer boundary on the equatorial plane of the central singularity is invariant for every spin change, and coincides with the radius of the horizon of the static case. In the limit of zero rotation, the outer ergosurface coalesces with the event horizon. The extension of this region increases with the spin-to-mass ratio, but the outer limit is invariant. Although on the equatorial plane the ergoregion is invariant with respect to any transformation involving a change in the source spin (but not with respect to a change in the mass  $M$ ), the dynamical structure of the ergoregion is not invariant with respect to a change in the spin-to-mass ratio. Nevertheless, concerning the invariance of this region with respect to spin shifts it has been argued, for example in [152], that the ergoregion can-

not indeed disappear as a consequence of a change in spin, because it may be filled by negative energy matter provided by the emergence of a Penrose process<sup>3</sup> [57]. The presence of negative energy particles, a distinctive feature of the ergoregion of any spinning source in any range of the spin value, has special properties when it comes to the circular motion in weakly rotating naked singularities. The presence of this special matter in an “antigravity” sphere, possibly filled with negative energy formed according to the Penrose process, and bounded by orbits with zero angular momentum, is expected to play an important role in the source evolution. In this work, we clarify and deepen those results, formulate in detail those considerations, analyze the static limit, and perform a detailed study of this region from the point of view of stationary observers. In this regards, we mention also the interesting and recent results published in [153] and [154].

In detail, this article is organized as follows: in Sec. 7.2 we discuss the main properties of the Kerr solution and the features of the ergoregion in the equatorial plane of the Kerr spacetimes. Concepts and notation used throughout this work are also introduced. Stationary observers in **BH** and **NS** geometries are introduced in Sec. 7.3. Then, in Sec. 7.4, we investigate the case of zero angular momentum observers and find all the spacetime configurations in which they can exist. Finally, in Sec. 7.5, we discuss our results.

## 7.2 Ergoregion properties in the Kerr spacetime

The Kerr metric is an axisymmetric, stationary (nonstatic), asymptotically flat exact solution of Einstein’s equations in vacuum. In spheroidal-like Boyer–Lindquist (BL) coordinates, the line element can be written as

$$ds^2 = -dt^2 + \frac{\rho^2}{\Delta} dr^2 + \rho^2 d\theta^2 + (r^2 + a^2) \sin^2 \theta d\phi^2 + \frac{2M}{\rho^2} r (dt - a \sin^2 \theta d\phi)^2, \quad (7.2.1)$$

$$\Delta \equiv r^2 - 2Mr + a^2, \quad \text{and} \quad \rho^2 \equiv r^2 + a^2 \cos^2 \theta. \quad (7.2.2)$$

The parameter  $M \geq 0$  is interpreted as the mass parameter, while the rotation parameter  $a \equiv J/M \geq 0$  (*spin*) is the *specific* angular momentum, and

---

<sup>3</sup>We note that the wave analog of the Penrose process is the superradiant scattering.

$J$  is the *total* angular momentum of the gravitational source. The spherically symmetric (static) Schwarzschild solution is a limiting case for  $a = 0$ .

A Kerr black hole (**BH**) geometry is defined by the range of the spin-mass ratio  $a/M \in ]0, 1[$ , the extreme black hole case corresponds to  $a = M$ , whereas a super-spinner Kerr compact object or a naked singularity (**NS**) geometry occurs when  $a/M > 1$ .

The Kerr solution has several symmetry properties. The Kerr metric tensor (7.2.1) is invariant under the application of any two different transformations:  $\mathcal{P}_{\mathbf{Q}} : \mathbf{Q} \rightarrow -\mathbf{Q}$ , where  $\mathbf{Q}$  is one of the coordinates  $(t, \phi)$  or the metric parameter  $a$  while a single transformation leads to a spacetime with an opposite rotation with respect to the unchanged metric. The metric element is independent of the coordinate  $t$  and the angular coordinate  $\phi$ . The solution is stationary due to the presence of the Killing field  $\xi_t = \partial_t$  and the geometry is axisymmetric as shown by the presence of the rotational Killing field  $\xi_\phi = \partial_\phi$ .

An observer orbiting, with uniform angular velocity, along the curves  $r = \text{constant}$  and  $\theta = \text{constant}$  will not see the spacetime changing during its motion. As a consequence of this, the covariant components  $p_\phi$  and  $p_t$  of the particle four-momentum are conserved along the geodesics<sup>4</sup> and we can introduce the constants of motion

$$\mathcal{E} \equiv -g_{\alpha\beta} \xi_t^\alpha p^\beta, \quad \mathcal{L} \equiv g_{\alpha\beta} \xi_\phi^\alpha p^\beta. \quad (7.2.3)$$

The constant of motion (along geodesics)  $\mathcal{L}$  is interpreted as the angular momentum of the particle as measured by an observer at infinity, and we may interpret  $\mathcal{E}$ , for timelike geodesics, as the total energy of a test particle coming from radial infinity, as measured by a static observer located at infinity.

As a consequence of the metric tensor symmetry under reflection with respect to the equatorial hyperplane  $\theta = \pi/2$ , the equatorial (circular) trajectories are confined in the equatorial geodesic plane. Several remarkable surfaces characterize these geometries: For black hole and extreme black hole

---

<sup>4</sup>We adopt the geometrical units  $c = 1 = G$  and the signature  $(-, +, +, +)$ , Greek indices run in  $\{0, 1, 2, 3\}$ . The four-velocity satisfy  $u^\alpha u_\alpha = -1$ . The radius  $r$  has units of mass  $[M]$ , and the angular momentum units of  $[M]^2$ , the velocities  $[u^t] = [u^r] = 1$  and  $[u^\phi] = [u^\theta] = [M]^{-1}$  with  $[u^\phi/u^t] = [M]^{-1}$  and  $[u_\phi/u_t] = [M]$ . For the sake of convenience, we always consider a dimensionless energy and effective potential  $[V_{eff}] = 1$  and an angular momentum per unit of mass  $[L]/[M] = [M]$ .

spacetimes the radii

$$r_{\pm} \equiv M \pm \sqrt{M^2 - a^2} : g^{rr} = 0 \quad (7.2.4)$$

are the event outer and inner (Killing) horizons<sup>5</sup>, whereas

$$r_{\epsilon}^{\pm} \equiv M \pm \sqrt{M^2 - a^2 \cos^2 \theta} : g_{tt} = 0 \quad (7.2.5)$$

are the outer and inner *ergosurfaces*, respectively<sup>6</sup>, with  $r_{\epsilon}^{-} \leq r_{-} \leq r_{+} \leq r_{\epsilon}^{+}$ . In an extreme **BH** geometry, the horizons coincide,  $r_{-} = r_{+} = M$ , and the relation  $r_{\epsilon}^{\pm} = r_{\pm}$  is valid on the rotational axis (i.e., when  $\cos^2 \theta = 1$ ).

In this work, we will deal particularly with the geometric properties of the *ergoregion*  $\Sigma_{\epsilon}^{+} : ]r_{+}, r_{\epsilon}^{+}]$ ; in this region, we have that  $g_{tt} > 0$  on the *equatorial plane* ( $\theta = \pi/2$ ) and also  $r_{\epsilon}^{+}|_{\pi/2} = r_{+}|_{a=0} = 2M$  and  $r_{\epsilon}^{-} = 0$ . The outer boundary  $r_{\epsilon}^{+}$  is known as the *static* (or also *stationary*) limit [155]; it is a *timelike* surface except on the axis of the Kerr source where it matches the outer horizon and becomes null-like. On the equatorial plane of symmetry,  $\rho = r$  and the spacetime singularity is located at  $r = 0$ . In the naked singularity case, where the singularity at  $\rho = 0$  is not covered by a horizon, the region  $\Sigma_{\epsilon}^{+}$  has a toroidal topology centered on the axis with the inner circle located on the singularity. On the equatorial plane, as  $a \rightarrow 0$  the geometry “smoothly” resembles the spherical symmetric case,  $r_{+} \equiv r_{\epsilon}^{+}|_{\pi/2}$ , and the

<sup>5</sup>A Killing horizon is a *null* surface,  $S_0$ , whose *null* generators coincide with the orbits of an one-parameter group of isometries (i. e., there is a Killing field  $\mathcal{L}$  which is normal to  $S_0$ ). Therefore, it is a lightlike hypersurface (generated by the flow of a Killing vector) on which the norm of a Killing vector goes to zero. In static **BH** spacetimes, the event, apparent, and Killing horizons with respect to the Killing field  $\xi_t$  coincide. In the Schwarzschild spacetime, therefore,  $r = 2M$  is the Killing horizon with respect to the Killing vector  $\partial_t$ . The event horizons of a spinning **BH** are Killing horizons with respect to the Killing field  $\mathcal{L}_h = \partial_t + \omega_h \partial_{\phi}$ , where  $\omega_h$  is defined as the angular velocity of the horizon. In this article we shall extensively discuss this special vector in the case of **NS** geometries. We note here that the surface gravity of a **BH** may be defined as the rate at which the norm of the Killing vector vanishes from the outside. The surface gravity,  $\mathcal{S}\mathcal{G}_{Kerr} = (r_{+} - r_{-})/2(r_{+}^2 + a^2)$ , is a conformal invariant of the metric, but it rescales with the conformal Killing vector. Therefore, it is not the same on all generators (but obviously it is constant along one specific generator because of the symmetries).

<sup>6</sup>In the Kerr solution, the Killing vector  $\partial_t$ , representing time translations at infinity, becomes null at the outer boundary of the ergoregion,  $r_{\epsilon}^{+}$ , which is however a timelike surface; therefore,  $r_{\epsilon}^{+}$  is *not* a Killing horizon. More precisely, on the ergosurfaces the time translational Killing vector becomes null.

frequency of the signals emitted by an infalling particle in motion towards  $r = 2M$ , as seen by an observer at infinity, goes to zero.

In general, for  $a \neq 0$  and  $r \in \Sigma_\epsilon^+$ , the metric component  $g_{tt}$  changes its sign and vanishes for  $r = r_\epsilon^+$  (and  $\cos^2 \theta \in ]0, 1[$ ). In the ergoregion, the Killing vector  $\zeta_t^\alpha = (1, 0, 0, 0)$  becomes spacelike, i.e.,  $g_{\alpha\beta} \zeta_t^\alpha \zeta_t^\beta = g_{tt} > 0$ . As the quantity  $\mathcal{E}$ , introduced in Eq. (7.2.3), is associated to the Killing field  $\zeta_t = \partial_t$ , then the particle energy can be also negative inside  $\Sigma_\epsilon^+$ . For stationary spacetimes ( $a \neq 0$ ) in  $\Sigma_\epsilon^+$ , the motion with  $\dot{\phi} = \text{const}$  is *not* possible and all particles are forced to rotate with the source, i.e.,  $\dot{\phi}a > 0$ . This fact implies in particular that an observer with four-velocity proportional to  $\zeta_t^\alpha$  so that  $\dot{\theta} = \dot{r} = \dot{\phi} = 0$ , (the dot denotes the derivative with respect to the proper time  $\tau$  along the trajectory), cannot exist inside the ergoregion. Therefore, for any infalling matter (timelike or photonlike) approaching the horizon  $r_+$  in the region  $\Sigma_\epsilon^+$ , it holds that  $t \rightarrow \infty$  and  $\phi \rightarrow \infty$ , implying that the world-lines around the horizon, as long as  $a \neq 0$ , are subjected to an infinite twisting. On the other hand, trajectories with  $r = \text{const}$  and  $\dot{r} > 0$  (particles crossing the static limit and escaping outside in the region  $r \geq r_\epsilon^+$ ) are possible.

Concerning the frequency of a signal emitted by a source in motion along the boundary of the ergoregion  $r_\epsilon^+$ , it is clear that the proper time of the source particle is not null<sup>7</sup>. Then, for an observer at infinity, the particle will reach and penetrate the surface  $r = r_\epsilon^+$ , in general, in a finite time  $t$ . For this reason, the ergoregion boundary is *not* a surface of infinite redshift, except for the axis of rotation where the ergoregion coincides with the event horizon [156, 46]. This means that an observer at infinity will see a non-zero emission frequency. In the spherical symmetric case ( $a = 0$ ), however, as  $g_{t\phi} = 0$  the proper time interval  $d\tau = \sqrt{|g_{tt}|}dt$  goes to zero as one approaches  $r = r_+ = r_\epsilon^+$ . For a timelike particle with positive energy (as measured by an observer at infinity), it is possible to cross the static limit and to escape towards infinity. In Sec. 7.3, we introduce stationary observers in **BH** and **NS** geometries. We find the explicit expression for the angular velocity of stationary observers, and perform a detailed analysis of its behavior in terms of the radial distance to the source and of the angular momentum of the gravity source. We find all the conditions that must be satisfied for a light-surface to exist.

---

<sup>7</sup>However, since  $g_{tt}(r_\epsilon^\pm) = 0$ , it is also known as an infinity redshift surface; see, for example, [155].

## 7.3 Stationary observers and light surfaces

We start our analysis by considering *stationary observers* which are defined as observers whose tangent vector is a spacetime Killing vector; their four-velocity is therefore a linear combination of the two Killing vectors  $\xi_\phi$  and  $\xi_t$ , i.e., the coordinates  $r$  and  $\theta$  are constants along the worldline of a stationary observer [157]. As a consequence of this property, a stationary observer does not see the spacetime changing along its trajectory. It is convenient to introduce the (uniform) *angular velocity*  $\omega$  as

$$d\phi/dt = u^\phi/u^t \equiv \omega, \quad \text{or} \quad u^\alpha = \gamma(\xi_t^\alpha + \omega\xi_\phi^\alpha), \quad (7.3.1)$$

which is a dimensionless quantity. Here,  $\gamma$  is a normalization factor

$$\gamma^{-2} \equiv -\kappa(\omega^2 g_{\phi\phi} + 2\omega g_{t\phi} + g_{tt}), \quad (7.3.2)$$

where  $g_{\alpha\beta}u^\alpha u^\beta = -\kappa$ . The particular case  $\omega = 0$  defines *static observers*; these observers cannot exist in the ergoregion.

The angular velocity of a timelike stationary observer ( $\kappa = +1$ ) is defined within the interval

$$\omega \in ]\omega_-, \omega_+[ \quad \text{where} \quad \omega_\pm \equiv \omega_Z \pm \sqrt{\omega_Z^2 - \omega_*^2}, \quad (7.3.3)$$

$$\omega_*^2 \equiv \frac{g_{tt}}{g_{\phi\phi}} = \frac{g^{tt}}{g^{\phi\phi}}, \quad \omega_Z \equiv -\frac{g_{\phi t}}{g_{\phi\phi}},$$

as illustrated in Figs. 7.1 and 7.2-*right*, where the frequencies  $\omega_\pm$  are plotted for fixed values of  $r/M$  and as functions of the spacetime spin  $a/M$  and radius  $r/M$ , respectively. In particular, the combination

$$\mathcal{L}_\pm \equiv \xi_t + \omega_\pm \xi_\phi \quad (7.3.4)$$

defines null curves,  $g_{\alpha\beta}\mathcal{L}_\pm^\alpha \mathcal{L}_\pm^\beta = 0$ , and, therefore, as we shall see in detail below, the frequencies  $\omega_\pm$  are limiting angular velocities for physical observers, defining a family of null curves, rotating with the velocity  $\omega_\pm$  around the axis of symmetry. The Killing vectors  $\mathcal{L}_\pm$  are also generators of Killing event horizons. The Killing vector  $\xi_t + \omega\xi_\phi$  becomes null at  $r = r_+$ . At the horizon  $\omega_+ = \omega_-$  and, consequently, stationary observers cannot exist inside this surface.

### 7.3.1 The frequencies $\omega_{\pm}$

We are concerned here with the orbits  $r = \text{const}$  and  $\omega = \text{const}$ , which are eligible for stationary observers. This analysis enlightens the differences between **NS** and **BH** spacetimes. Inside the ergoregion, the quantity in parenthesis in the r.h.s. of Eq. (7.3.2) is well defined for any source. However, it becomes null for photon-like particles and the rotational frequencies  $\omega_{\pm}$ . On the equatorial plane, the frequencies  $\omega_{\pm}$  are given as

$$\omega_{\pm} \equiv \frac{2aM^2 \pm M\sqrt{r^2\Delta}}{r^3 + a^2(2M + r)} \quad (7.3.5)$$

$$\text{with } \omega_{\pm}(r_+) = \omega_Z(r_+) = \omega_h \equiv \frac{a}{2r_+} \equiv \frac{M}{2\omega_0 r_+},$$

$$\text{and } \lim_{r \rightarrow \infty} \omega_{\pm} = 0, \quad \lim_{r \rightarrow 0} \omega_{\pm} = \omega_0 \equiv \frac{M}{a}.$$

Moreover, for the case of very strong naked singularities  $a \gg M$ , we obtain that  $\omega_{\pm} \rightarrow 0$ .

The above quantities are closely related to the main black hole characteristics, and determine also the main features that distinguish **NS** solutions from **BH** solutions. The constant  $\omega_h$  plays a crucial role for the characterization of black holes, including their thermodynamic properties. It also determines the uniform (rigid) angular velocity on the horizon, representing the fact that the black hole rotates rigidly. This quantity enters directly into the definition of the **BH** surface gravity and, consequently, into the formulation of the rigidity theorem and into the expressions for the Killing vector (7.3.1). More precisely, the Kerr **BH** surface gravity is defined as  $\kappa = \kappa_s - \gamma_a$ , where  $\kappa_s \equiv 1/4M$  is the Schwarzschild surface gravity, while  $\gamma_a = M\omega_h^2$  (the effective spring constant, according to [158]) is the contribution due to the additional component of the **BH** intrinsic spin;  $\omega_h$  is therefore the angular velocity (in units of  $1/M$ ) on the *event horizon*. The (strong) rigidity theorem connects then the event horizon with a Killing horizon stating that, under suitable conditions, the event horizon of a stationary (asymptotically flat solution with matter satisfying suitable hyperbolic equations) **BH** is a Killing horizon<sup>8</sup>.

---

<sup>8</sup> Assuming the cosmic censorship validity, the gravitational collapse should lead to **BH** configurations. The surface area of the **BH** event horizon is non-decreasing with time (which is the content of the second law of black hole thermodynamics). The **BH** event horizon of this stationary solution is a Killing horizon with constant surface gravity (ze-

The constant limit  $\omega_0 \equiv M/a$  plays an important role because it corresponds to the asymptotic limit for very small values of  $r$  and  $R \equiv r/a$ . Note that, on the equatorial plane,  $g_{\alpha\beta}\mathcal{L}_0^\alpha\mathcal{L}_0^\beta = R^2$ , where  $\mathcal{L}_0 \equiv \mathcal{L}_\pm|_{\omega_0}$ . The asymptotic behavior of these frequencies may be deeper investigated by considering the power series expansion for the spin parameter and the radius determined by the expression

$$\text{for } r \rightarrow \infty : \omega_\pm = \pm \frac{M}{r} \left( 1 - \frac{M}{r} \right) + o[r^{-3}], \quad (7.3.6)$$

which shows a clear decreasing as the gravitational field diminishes. For large values of the rotational parameter, we obtain

$$\begin{aligned} \omega_\pm &= \frac{M}{a} \frac{2M \pm r}{2M + r} + \\ &\frac{M}{a^3} \frac{r^2}{(2M + r)^2} \left( \mp 2M^2 - 2Mr \mp \frac{1}{2}r^2 \right) + o[a^{-5}], \end{aligned} \quad (7.3.7)$$

so that for extreme large values of the source rotation, the frequencies vanish and no stationary observers exist, thought differently for the limiting frequencies  $\omega_\pm$  (see Figs. 7.2). It is therefore convenient to introduce the dimensionless radius  $R \equiv r/a$ , for which we obtain the limit

$$R \rightarrow 0 : \quad \omega_+ = \frac{M}{a} - \frac{MR^2}{2a} - \frac{M^2R^3}{4a^2} + o[R^3]; \quad (7.3.8)$$

$$\begin{aligned} \omega_- &= \frac{M}{a} - R + \frac{(M^2 + a^2)R^2}{2Ma} - \\ &\frac{(a^4 + 4M^2a^2 - M^4)R^3}{4a^2M^2} + o[R^3]; \end{aligned} \quad (7.3.9)$$

$$R \rightarrow \infty : \quad \omega_\pm = \frac{(\mp M^2 + 4Ma \mp a^2)M}{2a^3R^3} \mp \frac{M^2}{a^2R^2} \pm \frac{M}{aR} + o[R^{-3}]. \quad (7.3.10)$$

Equations (7.3.7), (7.3.8) and (7.3.9) show the particularly different behavior of  $\omega_\pm$  with respect to the asymptote  $\omega_0$ . The behavior of the frequencies for fixed values of the radial coordinate  $r$  and varying values of the specific

---

roth law) [159, 160, 161, 162].

rotational parameter  $a/M$  is illustrated in Fig. 7.1. We see that the region of allowed values for the frequencies is larger for naked singularities than for black holes. In fact, for certain values of the radial coordinate  $r$ , stationary observers can exist only in the field of naked singularities. This is a clear indication of the observational differences between black holes and naked singularities. The allowed values for the frequencies are bounded by the

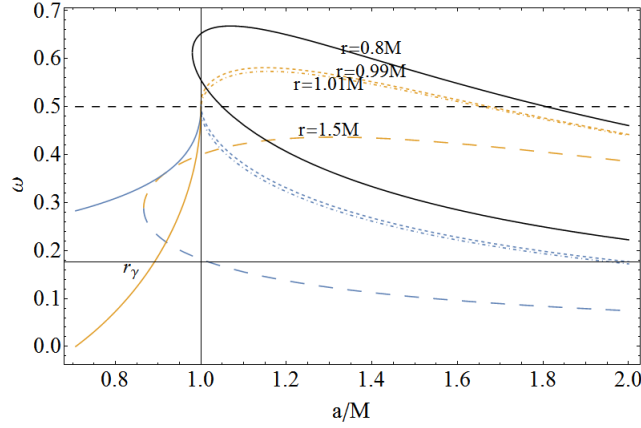


**Figure 7.1:** Plot of the limit frequencies  $\omega_{\pm}$  for fixed values of  $r/M$ . Frequencies  $\omega_{\pm}$ , on  $r = r_{\gamma} \in \Sigma_{\epsilon}^{+}$ , photon circular orbit in the BHs ergoregion are also plotted—see Table 7.1 and [46].

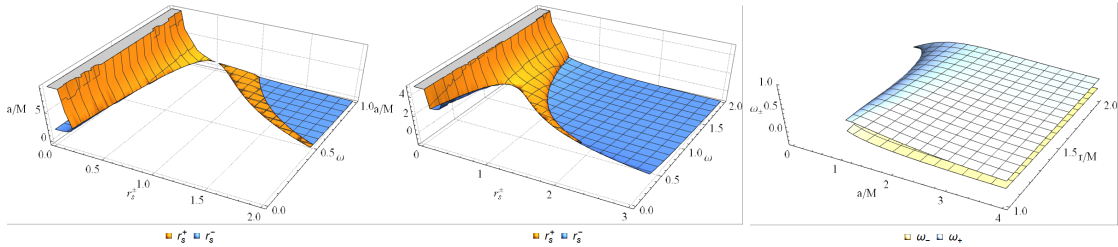


**Figure 7.2:** Left and central panels: Plot of the limit radii  $r_s^{\pm}$  as functions of the spacetime spin  $a/M$  and frequencies  $\omega$ —see also Figs. 7.4. Right panel: Plot of the limit frequencies  $\omega_{\pm}$  as functions of the spacetime spin  $a/M$  and radius  $r/M$ —see also Fig. 7.5.

limiting value  $\omega_0 = M/a$ ; for a broader discussion on the role of the dimen-

sionless spin parameter  $a/M$  in Kerr geometries, see also [143]<sup>9</sup> Moreover, for a given value of  $\omega_{\pm}$ , the corresponding radius is located at a certain distance from the source, depending on the value of the rotational parameter  $a$ . The following configuration of frequencies, radii and spin determines the location structure of stationary observers:

$$\omega_+ \in ]0, \omega_0[, \text{ for } a \in ]0, M[ \text{ in } r \in ]0, r_-] \cup [r_+, +\infty[ \quad (7.3.11)$$

and for  $a \geq M$  in  $r > 0$

$$\omega_- \in ]0, \omega_0[ \text{ for } a \in ]0, M[ \text{ in } r \in ]0, r_-] \cup [r_+, r_{\epsilon}^+[ \quad (7.3.12)$$

and for  $a \geq M$  in  $r \in ]0, r_{\epsilon}^+[$ .

Thus, we see that in the interval  $]0, M/a[$  observers can exist with frequencies  $\omega_{\pm}$ ; moreover, the frequency  $\omega_-$  is allowed in  $r \in \Sigma_{\epsilon}^+$ , while observers with  $\omega_- < 0$  can exist in  $r > r_{\epsilon}^+$ . Moreover, it is possible to show that, in **BH** geometries, the condition  $\omega_{\pm} \not\geq 1/2$  must be satisfied outside the outer horizon ( $r > r_+$ ). The particular value  $\omega_{\pm} = \omega_h = 1/2$  is therefore the limiting angular velocity in the case of an extreme black hole, i.e., for  $a = M$  so that  $r = r_+ = r_- = M$  in Eq.(7.3.5). The behavior of the special frequency  $\omega_{\pm} = 1/2$  is depicted in Fig. 7.3 and in Figs. 7.4, 7.2, 7.5, and 7.6, where other relevant frequencies are also plotted.

Eqs (7.3.11) enlighten some important properties of the light surfaces (frequencies  $\omega_{\pm}$ ) and of stationary observers, associated with frequencies  $\omega \in ]\omega_-, \omega_+[$  in the regime of strong singularities. Eqs(7.3.11) also enlighten the dependence of the frequencies on the dimensionless spin  $a/M$  and radius  $R = r/a$ . It is clear that when the frequency interval  $]\omega_-, \omega_+[$  shrinks, depending on the singularity spin  $a/M$  or the distance from the source  $r/M$ , the range of possible frequencies for stationary observers reduces. This occurs in general when  $\omega_+ \approx \omega_-$ . According to Eqs (7.3.11), the frequencies  $\omega_{\pm}$  are bounded from above by the limiting frequencies  $\omega_0 = M/a$  and from

<sup>9</sup>For simplicity we use here dimensionless quantities. We introduce the rotational version of the Killing vectors  $\zeta_t$  and  $\zeta_{\phi}$ , i.e., the canonical vector fields  $\tilde{V} \equiv (r^2 + a^2)\partial_t + a\partial_{\phi}$  and  $\tilde{W} \equiv \partial_{\phi} + a\sigma^2\partial_t$ . Then, the contraction of the geodesic four-velocity with  $\tilde{W}$  leads to the (non-conserved) quantity  $\mathcal{L} - \mathcal{E}a\sigma^2$ , which is a function of the conserved quantities  $(\mathcal{E}, \mathcal{L})$ , the spacetime parameter  $a$  and the polar coordinate  $\theta$ ; on the equatorial plane, it then reduces to  $\mathcal{L} - \mathcal{E}a$ . When we consider the principal null congruence  $\gamma_{\pm} \equiv \pm\partial_r + \Delta^{-1}\tilde{V}$ , the angular momentum  $\mathcal{L} = a\sigma^2$ , that is,  $\bar{\ell} = 1$  (and  $\mathcal{E} = +1$ , in proper units), every principal null geodesic is then characterized by  $\bar{\ell} = 1$ . On the horizon, it is  $\mathcal{L} = \mathcal{E} = 0$  [163, 143]

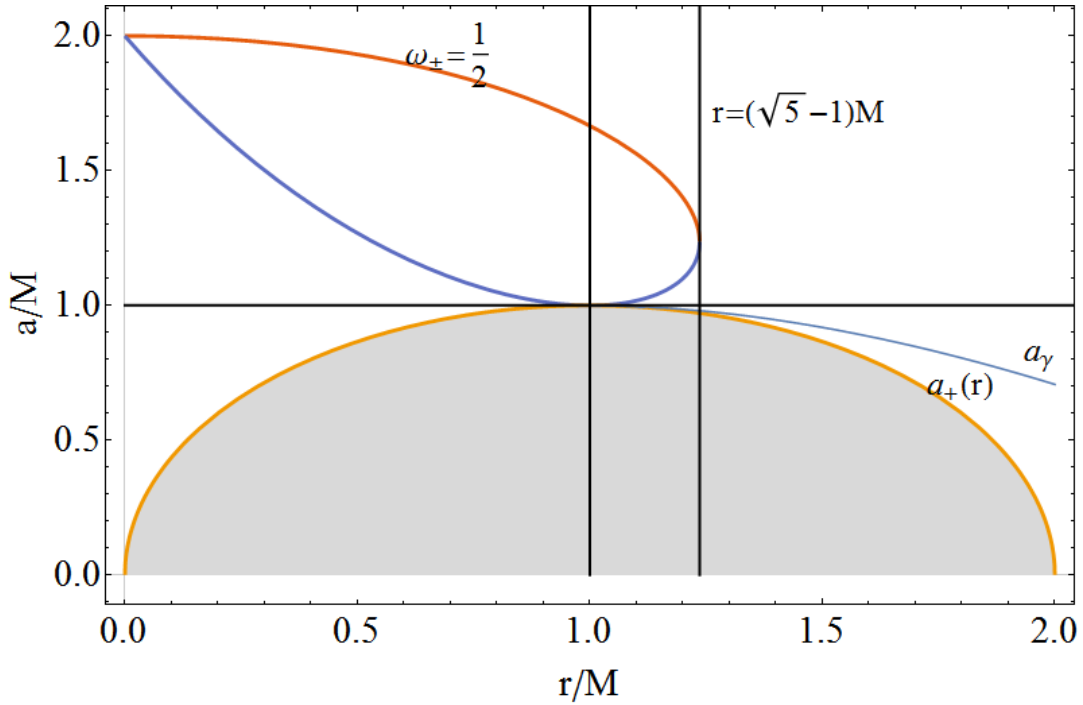


**Figure 7.3:** Plot of the limiting frequency  $\omega_{\pm} = 1/2$ . The spin  $a_+(r) \equiv \sqrt{r(2M - r)}$ , solution of  $r = r_+$ , and  $a_{\gamma}$ , solution of  $r = r_{\gamma}$  where  $r_{\gamma} \in \Sigma_{\epsilon}^+$  is the photon orbit in the ergoregion in a Kerr BH, are also plotted.

below by the null value  $\omega_{\pm} = 0$ . Thus, at fixed radius  $r$ , for very strong naked singularities  $a/M \gg 1$ , we have that  $\omega_0 \approx 0$  and the range of possible frequencies for stationary observers becomes smaller. This effect will be discussed more deeply in Sec. 7.3.2, where we shall focus specifically on the frequency  $\omega_0$ . On the other hand, considering the limits (7.3.5), together with Eqs (7.3.6)– (7.3.10), we find that the range of possible frequencies shrinks also in the following situations: when moving outwardly with respect to the singularity (at fixed  $a$ ), very close to the source, approaching the horizon  $r_h$  according to Eq. (7.3.5), or also for very large or very small  $R = r/a$ . The last case points out again the importance of the scaled radius  $r/a$ .

Essentially, stationary observers can be near the singularity only at a particular frequency. The greater is the NS dimensionless spin, the lower is the limiting frequency  $\omega_{\pm}$ , with the extreme limit at  $\omega_+ = \omega_-$ . In other words, the frequency range,  $]\omega_-, \omega_+[$ , for stationary observers vanishes as the value

$r = 0$  is approached. The singularity at  $r = 0$  in the **NS** regime is actually related to the characteristic constant frequency  $\omega = \omega_0$  in the same way as in **BH**-geometries the outer horizon  $r = r_+$  is related to the constant frequency  $\omega_h$  (cf. Eq. (7.3.5)). Consequently, a **NS** solution must be characterized by the frequency  $\omega_0$  and a **BH** solution by the frequency  $\omega_h$ . Therefore, the frequency  $\omega_0$  may be seen actually as the **NS** counterpart of the **BH** horizon angular frequency  $\omega_h$  (see Fig. 7.4). For  $r > r_+$ , it holds that  $\omega_+ > \omega_-$ .

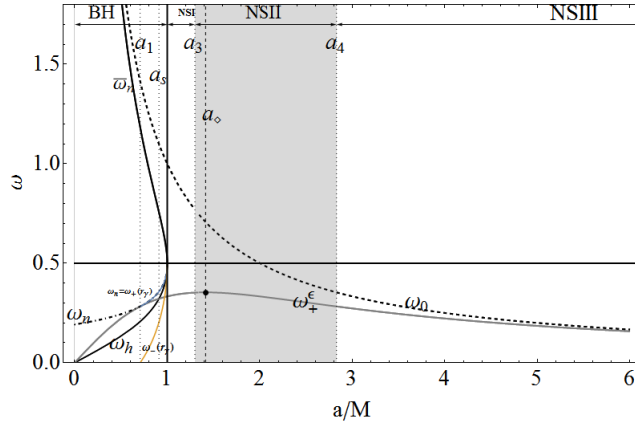


**Figure 7.4:** Stationary observers: The angular velocities  $\omega_+^\epsilon$  (gray curve),  $\omega_h$  (black curve),  $\omega_n$  (dot-dashed curve),  $\omega_0$  (dashed curve),  $\bar{\omega}_n > \omega_n > \omega_h$  (black thick curve). Here  $\bar{\omega}_n = \omega_n = \omega_h = 1/2$  at  $a = M$ ,  $\omega_+^\epsilon = \omega_h = 0.321797$  at  $a = a_s$ , and  $\omega_+^\epsilon = \omega_n = 0.282843$  at  $a = a_1$ . The maximum of  $\omega_+^\epsilon$ , at  $a = a_\diamond = \sqrt{2}M$  (dashed line) where  $a_\diamond : r_e = r_\epsilon^+$ —see Eq. (7.4.4), is marked with a point. See also Fig. 7.2. The angular velocities  $\omega_\pm$  on the **BH** photon orbit  $r_\gamma \in \Sigma_\epsilon^+$  are also plotted. Note that  $\omega_n$  it is an extension of  $\omega_+(r_\gamma)$  for  $a < a_1$ —see Table 7.2.

Then, in general, for **BHs** and **NSs** in the static limit  $r_\epsilon^+ = 2M$ , we obtain that

$$\omega_+^\epsilon \equiv \omega_+(r_\epsilon^+) = \frac{aM}{2M^2 + a^2} \quad \text{with} \quad \omega_-(r_\epsilon^+) = 0. \quad (7.3.13)$$

Moreover,  $\omega_- < 0$  for  $r > r_\epsilon^+$ , and  $\omega_- > 0$  inside the ergoregion  $\Sigma_\epsilon^+$ , while  $\omega_+ > 0$  everywhere.

In general, any frequency value should be contained within the range  $\omega_+ -$

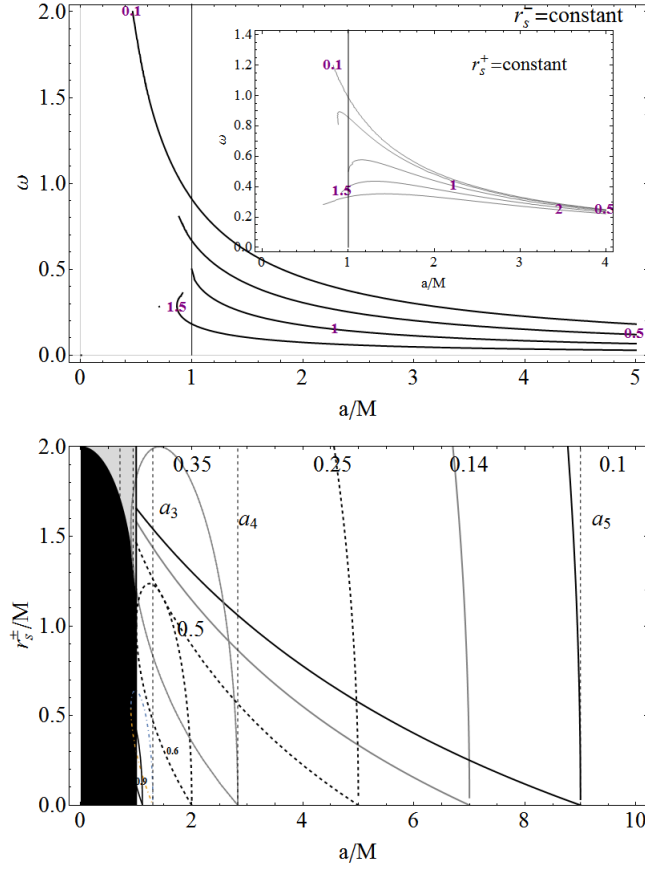


**Figure 7.5:** Upper panel: Plot of the curves  $r_s^- = \text{constant}$  and  $r_s^+ = \text{constant}$  (inside panel) in the plane  $(\omega, a/M)$ . The numbers denote the constant radii  $r_s^\pm / M$  (light cylinders). Bottom panel: The radii  $r_s^\pm$  versus the spin  $a/M$ , for different values of the velocity  $\omega$  (numbers close to the curves), the gray region is  $a \in [0, M]$  (BH-spacetime). The black region corresponds to  $r < r_+$ . The dashed lines denote  $a_1 < a_2 < a_3 < a_4$ . The angular momentum and the velocity  $(a, \omega)$  for  $r_s^\pm(a, \omega) = 0$  are related by  $\omega = M/a$ . See also Figs. 7.2.

$\omega_-$ ; therefore, it is convenient to define the *frequency interval*

$$\Delta\omega_\pm \equiv \omega_+ - \omega_- = 2\sqrt{\omega_Z^2 - \omega_*^2}, \quad (7.3.14)$$

which is a function of the radial distance from the source and of the attractor

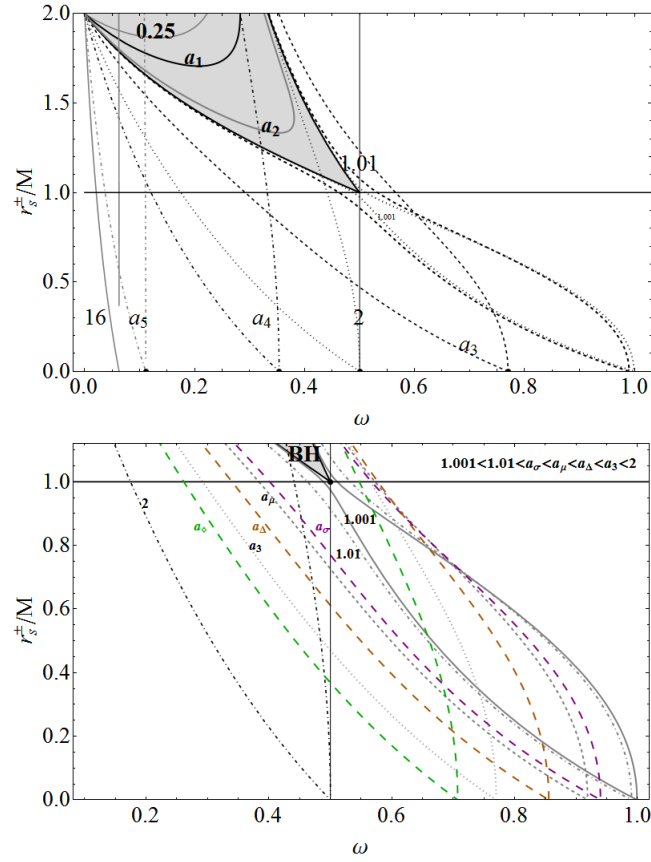


**Figure 7.6:** The radii  $r_s^\pm$  versus the frequency  $\omega$  for different values of the spin  $a/M$  (numbers close to the curves). The gray region is the only region allowed for the case of **BH** spacetimes. The surfaces  $\hat{r}_\pm$  at  $a = M$  (extreme-**BH**-case) are shown in black-thick.

spin. Figs. 7.7 show the frequency interval  $\Delta\omega_\pm$  as a function of  $r/M$  and  $a/M$ .

An analysis of this quantity makes it possible to derive some key features about the eligible frequencies. For convenience, we present in Table 7.1 some special values of the spin-mass ratio, which we will consider in the following analysis. We summarize the obtained results in the following way:

Firstly, for any **NS** source with  $a > a_\Delta \equiv 1.16905M$ , the interval  $\Delta\omega_\pm$  increases as the observer (on the equatorial plane) moves inside the ergoregion  $\Sigma_\epsilon^+$  towards the static limit.

**Table 7.1:** Classes of **BH** and **NS** geometries according to their specific spins. The radii  $(r_{\gamma}^-, r_{mso}^-)$  correspond to the photon circular orbit (or also last circular orbit) and the marginally stable circular orbit, respectively, for corrotating orbits in **BH** geometries. The **NS** case is characterized by the zero angular momentum radii  $(\mathcal{L}(\hat{r}_{\pm}) = 0)$  and the radius of the marginally stable circular orbit  $r_{mso}^{(NS)-} \in \Sigma_{\epsilon}^+$ . The explicit expressions for these radii can be found in [99, 98, 101, 100, 122]

---

**Black hole classes:**

**BHI** :  $[0, a_1[$ ;   **BHII** :  $[a_1, a_2[$ ,   **BHIII** :  $[a_2, M]$

$$a_1/M \equiv 1/\sqrt{2} \approx 0.707107 : r_{\gamma}^-(a_1) = r_{\epsilon}^+,$$

$$a_2/M \equiv 2\sqrt{2}/3 \approx 0.942809 : r_{mso}^-(a_2) = r_{\epsilon}^+$$

---

**Naked singularity classes:**

**NSI** :  $]M, a_3]$ ,   **NSII** :  $]a_3, a_4]$ ,   **NSIII** :  $]a_4, +\infty]$

$$a_3/M \equiv 3\sqrt{3}/4 \approx 1.29904 : \hat{r}_+(a_3) = \hat{r}_-(a_3),$$

$$a_4/M \equiv 2\sqrt{2} \approx 2.82843 : r_{mso}^{(NS)-}(a_4) = r_{\epsilon}^+$$


---

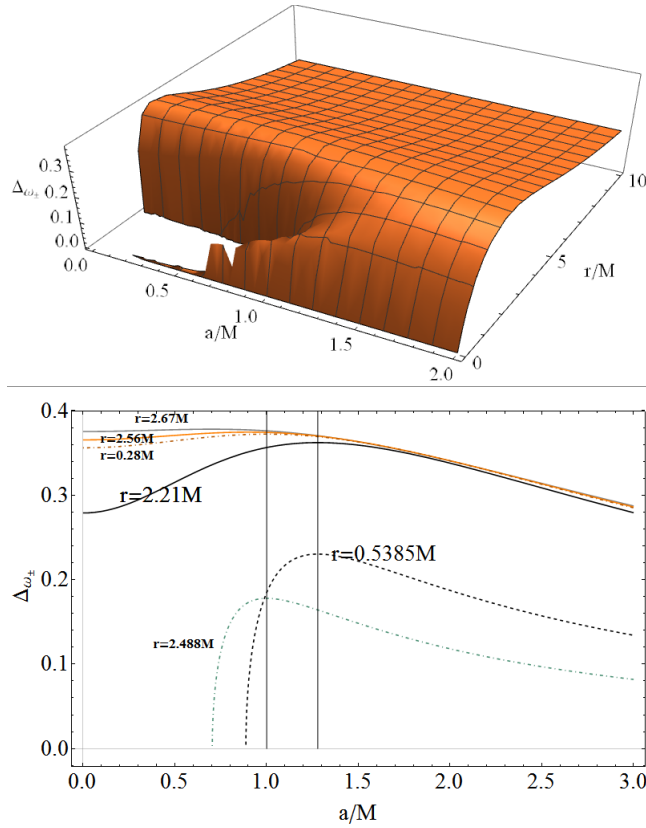


**Figure 7.7:** Upper panel: Plot of the frequency interval  $\Delta\omega_{\pm} = \omega_{+} - \omega_{-}$  as a function of the radius  $r/M$  and the **BH** and **NS** spin  $a/M$ . The extrema  $r_{\Delta}^{\pm}$  and  $r_{\blacksquare}^{\pm}$  are solutions of  $\partial_r \Delta\omega_{\pm} = 0$  and  $\partial_a \Delta\omega_{\pm} = 0$ , respectively. Lower panel: The frequency interval  $\Delta\omega_{\pm} = \omega_{+} - \omega_{-}$  as a function of  $a/M$  for selected values of the orbit radius  $r/M$ ; the maximum points are for the radii  $r_{\Delta}^{\pm}$  or  $r_{\blacksquare}^{\pm}$ —see Figs. 7.8.

Secondly, in the case of **NS** geometries with  $a \in ]M, a_{\Delta}[$ , i.e., belonging partially to the class of **NSI** spacetimes, the situation is very articulated. There is a region of maximum and a minimum frequencies, as the observer moves from the source towards the static limit. This phenomenon involves an orbital range partially located within the interval  $] \hat{r}_{-}, \hat{r}_{+}[$ , which is characterized by the presence of counterrotating circular orbits with negative orbital angular momentum  $\mathcal{L} = -\mathcal{L}_{-}$  (cf. Fig. 7.8, where the radii  $\hat{r}_{\pm}$  are plotted.).

For the maximum spin,  $a = a_{\Delta}$ , we obtain  $\omega^{+} = \omega^{-}$  on the radius  $r \equiv$

$r_{\Delta}^{\pm}(a_{\Delta}) = 0.811587M$  and, therefore, the range of possible frequencies for stationary observers vanishes. The points  $r_{\Delta}^{\pm}(a)$  represent the extrema of the interval  $\Delta_{\omega^{\pm}}$ , i.e., the solutions of the equation  $\partial_r \Delta_{\omega^{\pm}} = 0$  – Fig. 7.8. This property is present *only* in the case of **NS** geometries. In fact, there are the two critical orbits  $r_{\Delta}^{+} > r_{\Delta}^{-}$  and  $r = r_{\Delta}^{\pm}(a_{\Delta})$ , which are the boundaries of a closed region, whose extension reaches a maximum in the case of the extreme Kerr geometry  $a = M$ , and is zero for  $a = a_{\Delta}$ . For  $r \in ]r_{\Delta}^{-}, r_{\Delta}^{+}[$ , the separation parameter  $\Delta_{\omega^{\pm}}$  decreases with the orbital distance, then on the inner radius  $r_{\Delta}^{-}$  it reaches a maximum value, whereas on the outer radius  $r_{\Delta}^{+}$  it reaches a minimum. In the outer regions, at  $r > r_{\Delta}^{+}$ , the separation parameter increases with the distance from the source. This feature constitutes therefore a major difference in the the behavior of stationary observers within and outside the ergoregion of a naked singularity spacetime. However, a deeper analysis of the equatorial plane, outside the static limit, shows the existence of a second region for light surfaces in the **NS** case.

On the other hand, the angular velocity  $\omega_{-}$  decreases with the orbit in the Kerr spacetime. The maximum frequency  $\omega_{+}$  also decreases in the **NS** spacetimes. In the **BH** cases, the angular velocity is always increasing for sources of the class **BHI**, while for the other sources there is a maximum for the velocity  $\omega_{+}$  at  $r = r_{\gamma}^{-}$ , which is the circular orbit of a photon or null-like particle corotating with the source. Such a kind of orbit, contained in  $\Sigma_{\epsilon}^{+}$ , is a feature of the **BHII-III** spacetimes [46], this is also know as marginally or last circular orbit as no circular particle motion is possible in the region  $r < r_{\gamma}^{-}$ . We close this section with a brief discussion on the variation of the frequency interval  $\Delta_{\omega^{\pm}}$ , following a spin transition with  $a > 0$ . In the case of a singularity spin-transition, there are two extreme radii for the frequency interval

$$r_{\blacksquare}^{+} \equiv \eta \cos \left[ \frac{1}{3} \arccos \left( -\frac{8a^2}{\eta^3} \right) \right], \quad (7.3.15)$$

$$r_{\blacksquare}^{-} \equiv \eta \sin \left[ \frac{1}{3} \arcsin \left( \frac{8a^2}{\eta^3} \right) \right], \quad \eta \equiv \frac{2\sqrt{8M^2 - a^2}}{\sqrt{3}},$$

$$\text{or alternatively } a = \sqrt{-\frac{r(r^2 - 8M^2)}{r + 2M}} \quad \text{for } r \in ]0, 2\sqrt{2}M[ ,$$

where  $r_{\blacksquare}^{\pm} : \partial_a \Delta_{\omega^{\pm}}|_{r_{\blacksquare}^{\pm}} = 0$  are maximum points– see Figs. 7.8 and 7.7.

### 7.3.2 Light surfaces

In this section, we briefly study the conditions for the existence of *light surfaces* and their morphology. The condition (7.3.3), for the definition of a stationary observer, can be restated in terms of the solutions  $r_s^\pm$ , considering  $\omega$  as a fixed parameter. Therefore, we now consider the solutions  $r_s^\pm$  of the equation for the light surfaces defined in Eq. (7.3.4) in terms of the Killing null generator  $\mathcal{L}_\pm$ , as functions of the frequency  $\omega$ . We obtain

$$\frac{r_s^-}{M} \equiv \frac{2\beta_1 \sin\left(\frac{1}{3} \arcsin \beta_0\right)}{\sqrt{3}}, \quad \frac{r_s^+}{M} \equiv \frac{2\beta_1 \cos\left(\frac{1}{3} \arccos(-\beta_0)\right)}{\sqrt{3}}$$

where  $\beta_1 \equiv \sqrt{\frac{1}{\omega^2} - \frac{1}{\omega_0^2}}$ ,  $\beta_0 \equiv \frac{3\sqrt{3}\beta_1\omega^2}{\left(\frac{\omega}{\omega_0} + 1\right)^2}$ , (7.3.16)

where  $\omega_0 \equiv M/a$  (cf. Eq. (7.3.5) and Fig. 7.2). For  $\omega = 1/2$ , in the limiting case of  $a = M$ , we have that  $\omega_n = \bar{\omega}_n = \omega_h = 1/2$  and  $r_s^\pm = M$ —see Figs. 7.4, 7.6 and 7.2<sup>10</sup>. Thus, there are solutions  $r_s^+ = r_s^- = 0$  for  $a \in ]0, M[$  if  $\omega \in (\omega_n, \bar{\omega}_n)$  where (for simplicity we use a dimensionless spin  $a \rightarrow a/M$ )

$$\bar{\omega}_n \equiv \frac{9 - a^2 + 6\sqrt{9 - 5a^2} \cos\left[\frac{1}{3} \arccos \alpha\right]}{a(a^2 + 27)} \quad (7.3.17)$$

$$\omega_n \equiv \frac{9 - a^2 - 6\sqrt{9 - 5a^2} \sin\left[\frac{1}{3} \arcsin \alpha\right]}{a(a^2 + 27)} \quad (7.3.18)$$

$$\alpha \equiv \frac{a^4 - 36a^2 + 27}{(9 - 5a^2)^{3/2}} \quad (7.3.19)$$

The situation is summarized in Table 7.2. We see that  $\omega_n = \omega_+^\epsilon$  for  $a = a_1$ ,

<sup>10</sup>More precisely, it is  $r_s^+ = r_s^- = 0$  for  $a > 0$  and  $\omega = \omega_0$ . Also,  $r_s^+ = r_s^- > r_+$  for  $a = 0$  and  $\omega = \pm \frac{1}{3\sqrt{3}}$ . In the extreme Kerr spacetime geometry, we have that  $r_s^+ = r_s^- > 0$  for  $a = M$ ,  $\omega = 1/2$  for  $r = M$ , and  $\omega = -1/7$  for  $r = 4M$ . For a Kerr geometry, where  $a/M \in ]0, 1[$ , it is  $r_s^+ = r_s^- > r_+$  for  $\omega = \omega_n$  or  $\bar{\omega}_n$  (one positive and one negative value solution), while in the naked singularity case where  $a > M$ , the condition  $r_s^+ = r_s^- > 0$  is valid only for one negative frequency – see Figs. 7.5 and 7.6.

**Table 7.2:** Existence of stationary observers in **BH** and **NS** spacetimes, respectively. The spin/mass ratio  $a/M$ , angular frequencies  $\omega$  and orbital ranges  $r$  are listed. See also Fig. 7.4.

Black holes:			Naked singularities:		
$a \in ]0, a_1]$	$\omega \in ]0, \omega_+^\epsilon[$	$r \in ]r_s^-, r_\epsilon^+]$	$a > M$	$\omega \in ]0, \omega_+^\epsilon[$	$r \in ]r_s^-, r_\epsilon^+]$
$a \in ]a_1, M]$	$\omega \in ]0, \omega_+^\epsilon[$	$r \in ]r_s^-, r_\epsilon^+]$		$\omega = \omega_+^\epsilon$	$r \in ]r_s^-, r_\epsilon^+]$
	$\omega = \omega_+^\epsilon$	$r \in ]r_s^-, r_\epsilon^+]$		$]\omega_+^\epsilon, \omega_0[$	$r \in ]r_s^-, r_s^+]$
	$\omega \in ]\omega_+^\epsilon, \omega_n[$	$r \in ]r_s^-, r_s^+]$			

$\omega_n = \bar{\omega}_n = \omega_h = 1/2$  at<sup>11</sup>  $a = M$ ,  $\omega_+^\epsilon = \omega_h$  at  $a = a_s \equiv \sqrt{2(\sqrt{2}-1)}M \approx 0.91017M$  and  $a = 0$  (the static solution). Moreover, we have that  $\omega_0 > \bar{\omega}_n > \omega_n > \omega_+^\epsilon$  and  $\omega_n > \omega_h$  for **BH**-sources, where  $\omega_h > \omega_+^\epsilon$  for  $a \in ]a_s, M]$ . In the **NS** case, there are no crossing points for the radii  $r_s^\pm$  and  $\omega_0 > \omega_+^\epsilon$  (see Fig. 7.4). The shrinking of the frequency interval  $]\omega_-, \omega_+[$  is also shown in Figs. 7.6, 7.9 and 7.10, where the radii  $r_s^\pm$  are also plotted as functions of the frequencies.

Figures 7.4, 7.5, and 7.6 contain all the information about the differences between black holes with  $a < M$ , and the case of naked singularities with  $a > M$ . We summarize the situation in the following statements:

**Naked singularities spacetimes:** For  $a > M$ , the solutions for the equation of the light surfaces in the limiting case  $\omega = 0$  (static observer) are located at  $r = r_\epsilon^+$ . While for any frequency within the range  $\omega \in ]0, \omega_+^\epsilon[$  there is one solution  $r_s^-$ , for larger frequencies in the range  $\omega \in [\omega_+^\epsilon, \omega_0[$  there are two solutions  $r_s^\pm$ . In the ergoregion  $\Sigma_\epsilon^+$  of a naked singularity, there exists a limit  $\omega_0 \equiv M/a$  for the angular frequency.

**Extreme black hole spacetime:** For  $a = M$ , we obtain the following set of solutions ( $\omega = 0, r = r_\epsilon^+$ ), ( $\omega \in ]0, 1/3[, r = r_s^-$ ), and ( $\omega \in [1/3, 1/2[, r = r_s^\pm$ ).

**Black hole spacetimes:** We consider first the class **BHI** with  $a \in ]0, a_1]$ . In the limit  $\omega = 0$ , there exists a solution for the light surface with  $r = r_\epsilon^+$ . More generally, the solutions are constrained by the following set of

<sup>11</sup>For a closer look at the role of this special frequency we note that  $\bar{\omega}_n = \omega_n = \omega_h = 1/2$  at  $a = M$  and, clearly,  $\omega_0 = 1/2$  for  $a = 2M$ . We refer then to Figs. 7.3, 7.4, 7.5, 7.6, and 7.9.

conditions:

$$\mathfrak{C}_1 : \quad \omega \in ]0, \omega_+^\epsilon] \cup \omega \neq \omega_h \quad \text{with solution } r = r_s^-. \quad (7.3.20)$$

$$\mathfrak{C}_2 : \quad \omega \in [\omega_+^\epsilon, \omega_n[ \quad \text{with solution } r = r_s^\pm, \quad (7.3.21)$$

$$\omega = \omega_n, \quad \text{with solution } r = r_s^-. \quad (7.3.22)$$

Then, we consider **BH** spacetimes with spin  $a \in ]a_1, a_s[$ , where  $a_s \equiv \sqrt{2(\sqrt{2}-1)}M < a_2$ . These spacetimes include a part of **BHII**-sources and the condition  $\mathfrak{C}_1$  applies.

For spacetimes with rotation  $a = a_s$ , the conditions  $\mathfrak{C}_1$  and  $\mathfrak{C}_2$  apply. Then, in the special case  $\omega_+^\epsilon = \omega_h$  or  $\omega = \omega_+^\epsilon$ , there is a solution with  $r = r_s^+$ .

Finally, for spacetimes with  $a \in ]a_s, M[$ , which belong to the class of **BHII** and **BHIII** sources, the condition  $\mathfrak{C}_1$  holds, whereas the condition  $\mathfrak{C}_2$  applies for frequencies within the interval  $\omega_h < \omega_n$ . Finally, in the special case  $\omega = \omega_h$ , there is one solution at  $r = r_s^+$ , and for  $\omega = \omega_n$  we have the solution  $r = r_s^-$ .

A summary and comparison of these two cases is proposed also in Figs. 7.5 and 7.6, where the surfaces  $r_s^\pm$  are studied as functions of  $a/M$  and  $\omega$ . It is evident that the extreme solution  $a/M = 1$  is a limiting case of both surfaces  $r_s^\pm$ , varying both in terms of the spin and the angular velocity  $\omega$ . Thus, the difference between the regions where stationary observers can exist in the **BH** case (gray regions in Figs. 7.6) and in the **NS** case are clearly delineated. In **BH** spacetimes, the surfaces  $r_s^\pm$  are confined within a restricted radial and frequency range. On the other hand, in the naked singularity case, the orbits and the frequency range is larger than in the black hole case. Moreover, the surfaces  $r_s^\pm$  can be closed in the case of **NS** spacetimes, inside the ergoregion, for sufficiently low values of the spin parameter, namely  $a \in ]M, a_4]$ . Furthermore, in any Kerr spacetime, there is a light surface at  $r_s^\pm = r_\epsilon^+$  with  $\omega = M/a_4$ . In Sec. 7.4, we complete this analysis by investigating the special case of zero angular momentum observers, and we find all the spacetime configurations in which they can exist.

## 7.4 Zero angular momentum observers

This section is dedicated to the study of Zero Angular Momentum Observers (ZAMOs) which are defined by the condition

$$\mathcal{L} \equiv u_\alpha \tilde{\zeta}_{(\phi)}^\alpha = g_{\alpha\beta} \tilde{\zeta}_{(\phi)}^\alpha p^\beta = g_{t\phi} \dot{t} + g_{\phi\phi} \dot{\phi} = 0. \quad (7.4.1)$$

In terms of the particle's four-velocity, the condition  $\mathcal{L} = 0$  is equivalent to  $d\phi/dt = -g_{\phi t}/g_{\phi\phi} \equiv \omega_Z = (\omega_+ + \omega_-)/2$ , where the quantity  $\omega_Z$  is the ZAMOs angular velocity introduced in Eq. (7.3.3), and the frequency of arbitrary stationary observers is written in terms of  $\omega_Z$  [46]. The sign of  $\omega_Z$  is in concordance with the source rotation. The ZAMOs angular velocity is a function of the spacetime spin (see Figs. 7.11 and 7.12, where constant ZAMOs frequency profiles are shown). In the plane  $\theta = \pi/2$ , we find explicitly

$$\omega_Z|_{(\theta=\pi/2)} = \frac{2aM^2}{r^3 + a^2(r + 2M)}. \quad (7.4.2)$$

As discussed in [101, 100, 46], ZAMOs along circular orbits with radii  $\hat{r}_\pm$  are possible only in the case of “slowly rotating” naked singularity spacetimes of class **NSI**. This is a characteristic of naked singularities which is interpreted generically as a repulsive effect exerted by the singularity [99, 98, 101, 100, 122]. On the other hand,  $\omega_Z^2 = \omega_*^2$  for  $r = r_\pm$ , while  $\omega_Z^2 > \omega_*^2$  in the region  $r > r_+$  for **BH** spacetimes, and in the region  $r > 0$  for **NS** spacetimes (see also Fig. 7.12).

### ZAMOs angular velocity and orbital regions

The ZAMOs angular velocity  $\omega_Z$  is always positive for  $a > 0$ , and vanishes only in the limiting case  $a = 0$ . This means that the ZAMOs rotate in the same direction as the source (dragging of inertial frames).

As can be seen from Eq.(7.4.2), the frequency  $\omega_Z$  for a fixed mass and  $a \neq 0$  is strictly decreasing as the radius  $r/M$  increases.

For the **NS** regime it is interesting to investigate the variation of **ZAMO** frequency  $\omega_Z$  on the orbits  $\hat{r}^\pm$ . These special radii of the **NS** geometries do not remain constant under a spin-transition of the central singularity. We shall consider this aspect focusing on the curves  $\hat{r}^\pm(a)$  of the plane  $r - a$  as illustrated in Fig. 7.8. This will enable us to evaluate simultaneously the frequency variation on these special orbits, following a spin variation of the naked singularity in the rage of definition of  $\hat{r}^\pm$ , and to evaluate the com-

bined effects of a variation in the orbital distance from the singularity and a change of spin. A similar analysis will be done, from a different point of view, also for stationary observers.

In  $\Sigma_\epsilon^\pm$ , the velocity  $\omega_Z = \hat{\omega}^-$  (in **NSs**) always *decreases* with the orbital radii  $\hat{r}^-$ , i.e.  $\partial_{\hat{r}^-}\hat{\omega}^- < 0$ , when the spin increases, i.e.  $\partial_a\hat{r}^- > 0$  (see Figs. 7.8 and 7.12). As  $\hat{r}^+$  monotonically decreases with the spin during a **NS** spin-up process (see Fig. 7.8), the frequency  $\hat{\omega}^+ = \omega_Z(\hat{r}^+)$  decreases in the spin-range  $a \in [M, a_\omega[$ , and increases in the range  $]a_\omega, a_3]$ ; therefore, the special value  $a_\omega = 1.1987M$  is a minimum point of the ZAMOs frequency  $\hat{\omega}_Z^+$ —see Fig. 7.12. *Viceversa*, as  $\hat{r}^-$  increases after a **NS** spin-up, the corresponding ZAMOs frequency  $\hat{\omega}^- = \omega_Z(\hat{r}^-)$  decreases as the observer moves along the curve  $\hat{r}^-(a)$ . Thus, we can say that, if the **NS** spin increases, the frequency  $\hat{\omega}^+$  decreases, approaching, but never reaching, the singularity, i. e.,  $\partial_a\hat{r}^+ < 0$  for  $a \in [M, a_\omega[$ . *Viceversa*, increasing the **NSs** spin in spacetimes with  $a \in ]a_\omega, a_3[$ , the frequency  $\hat{\omega}^+$  increases again and the orbit  $\hat{r}^+$  moves towards the central singularity. On the other hand, the frequency  $\hat{\omega}^-$  monotonically decreases with the naked singularity spin, i.e.  $\partial_a\hat{r}^- > 0$ ; therefore, for a fixed **NS** spin, the frequency interval decreases, i.e.  $\hat{\omega}^- > \hat{\omega}^+$ . In fact, the velocity  $\omega_Z$  is strictly *decreasing* with the radius  $r$  in the **BH** and **NS** regimes with  $a \neq 0$  (i.e.  $\partial_r\omega_Z < 0$ ). Moreover, in general  $\omega_Z$  increases as the observer approaches the black hole at fixed spin, and it decreases as the observer moves far away from the center of rotation.

In the static limit, we have that  $\omega_Z(r_\epsilon^+) = \omega_+^\epsilon/2$ . In fact, the asymptotic behavior of the frequency is determined by the relations

$$\lim_{r \rightarrow r_+} \omega_Z = \lim_{r \rightarrow r_+} \omega_\pm = \omega_h, \quad \lim_{r \rightarrow +\infty} \omega_Z = 0, \quad \lim_{r \rightarrow 0} \omega_Z = \omega_0. \quad (7.4.3)$$

**Change in the intrinsic spin** The angular velocity of the ZAMOs inside  $\Sigma_\epsilon^+$  varies according to the source spin. This might be especially important in a possible process of spin-up or spin-down as a result of the interaction, for example, with the surrounding matter. In [46], this phenomenon and its implications were investigated, considering different regions close to the singularity. For a fixed orbital radius  $r$ , the ZAMOs angular velocity strongly depends on the value of the spacetime spin-mass ratio. In particular, depending on the value of the ratio  $a/M$ , there can exist a radius of maximum frequency  $r_e$  given by

$$r_e \equiv \frac{\sqrt[3]{3a^2 + Y^2}}{3^{2/3}Y}, \quad Y \equiv \sqrt[3]{9Ma^2 + \sqrt{3}\sqrt{a^4(27M^2 - a^2)}} \quad (7.4.4)$$

that are solutions of the equation  $\partial_a \omega_Z|_{\pi/2} = 0$  at which the frequency is denoted by  $\omega_e \equiv \omega_Z(r_e)$  (see Figs. 7.11 and 7.12). A detailed analysis of the expression for the radius  $r_e$  shows that it can exist in spacetimes that belong to the class **BHII** with spin  $a = a_s$ , where  $r_e(a_s) = r_+(a_s)$ , and to the classes **BHIII**, **NSI**, and **NSII** with the limiting value  $a = a_\diamond = \sqrt{2}M$ , where  $a_\diamond : r_e = r_e^+$  (see Figs. 7.11 and 7.2). Spacetimes with spin  $a_s$  belong to the class **BHII**, as defined in Table 7.2, and have been analyzed in the context of stationary observers in Sec. 7.3.2 and Sec. 7.3.1 (Figs. 7.4, 7.11, 7.12 and 7.13 show the behavior of several quantities related to ZAMOs in relation to other frequencies.). In this particular case, we have that

$$\omega_+^e = \omega_h = 0.321797 \quad \text{and} \quad r_e(a_s) = r_+(a_s). \quad (7.4.5)$$

We focus our attention on ergoregion  $\Sigma_\epsilon^+$ , bounded from above by the radius  $r_\epsilon^+$  and from below by  $r = 0$  and  $r = r_+$  for **NSs** and **BHs**, respectively. We consider the role of the radius  $r_e$ , as the maximum point of the ZAMO frequency, as a function of the source spin-mass ratio. Thus, for black holes with  $a \in [0, a_s]$ , the frequency  $\omega_Z$  increases with  $a/M$  always inside the ergoregion; this holds for any orbit inside  $\Sigma_\epsilon^+$  (i.e. for a fixed value  $\bar{r} \in \Sigma_\epsilon^+$ , if a **BH** spin-up shift occurs in the range  $[0, a_s]$ , the function  $\omega_Z(\bar{r}, a)$  increases with  $\bar{r}$ ). For spins  $a \in ]a_s, M]$ , instead, the frequency  $\omega_Z$  grows with the spin only for  $\bar{r} \in ]r_e, r_\epsilon^+[$ ; on the contrary, for radii located close to the horizon,  $\bar{r} \in ]r_+, r_e]$ ,  $\omega_Z(\bar{r}, a)$  decreases following a spin up in the range  $\in ]a_s, M]$  (i.e.  $\partial_a r_+ < 0$  and  $\partial_a r_e > 0$ ).

In the case of **NS**-spacetimes, the frequency  $\omega_Z(\bar{r}, a)$  is an increasing function of the dimensionless spin in the **NS** spin range  $]M, a_\diamond[$  and on the orbit  $\bar{r} \in ]r_e, r_\epsilon^+[$ . Moreover, the frequency  $\omega_Z(\bar{r}, a)$  decreases with the spin in the range of values  $a \in ]M, a_\diamond[$  and on  $\bar{r} \in ]0, r_e]$ . This situation is distinctly different for **NS** with  $a > a_\diamond$ , for which in the ergoregion an increase of the spin corresponds to a decrease of  $\omega_Z$ . This is an important distinction between different **NS** regimes.

We note that  $r_e(a_s) = r_+(a_s)$  for the spin  $a_s = \sqrt{2}(\sqrt{2} - 1)M$  (see Fig. 7.11).

Moreover, in NSII naked singularity spacetimes with spin  $a_\diamond = \sqrt{2}M$ :  $r_e = r_e^+$ , we obtain that  $\omega_Z^\varepsilon = \omega_e$ —Fig. 7.12. Remarkably, the spin  $a_\diamond$  is the maximum point of the frequency  $\omega_Z^\varepsilon(a_\diamond) = \omega_e(a_\diamond) \equiv \omega_Z^{\varepsilon-Max} = 0.176777$  and also the maximum point of the frequency  $\omega_+^\varepsilon$  (see Fig. 7.2). In other words, in naked singularity spacetimes with  $a = a_\diamond$ , where  $r_e = r_e^+$ , the ZAMOs frequency at the ergosurface  $\omega_Z^\varepsilon$  reaches a maximum value which is equal to  $\omega_e$ , defined through the radius in Eq. (7.4.4); moreover, the frequency  $\omega_+^\varepsilon$  reaches its maximum value at the ergosurface.

### ZAMOs energy

The circular motion of test particles can be described easily by using the effective potential approach [164]. The exact form of such an effective potential in the Kerr spacetime is well known in the literature (see, for example, [101, 100]). The effective potential function  $\mathcal{V}_{eff}^+$  represents the value of  $\mathcal{E}/\mu$  that makes  $r$  into a turning point ( $\mathcal{V}_{eff} = \mathcal{E}/\mu$ ),  $\mu$  being the particle mass; in other words, it is the value of  $\mathcal{E}/\mu$  (in the case of photons,  $\mu$  shall depend on an affine parameter and the impact parameter  $\ell \equiv \mathcal{L}/\mathcal{E}$  is relevant for the analysis of trajectories) at which the (radial) kinetic energy of the particle vanishes. This can easily be obtained from the geodesic equations with the appropriate constraints or through the normalization conditions of the four-velocities, taking into account the constraints and the constants of motion [164]. Here we consider specifically an effective potential associated to the ZAMOs. In general, the effective potential for a particle on a circular orbit can *always* be written in terms of the frequencies  $\omega_Z$  and  $\omega_*$  introduced in Eq. (7.3.3), by using the quantities  $\omega_Z$  and  $\omega_*$  and the conserved particle angular momentum  $\mathcal{L}$  of Eq. (7.2.3). This can be shown as follows.

First, we consider the normalization condition for a particle with momentum  $p^\alpha = \mu u^\alpha$ , mass  $\mu$  and four-velocity  $u^\alpha$  so that  $g_{\alpha\beta}u^\alpha u^\beta = -\kappa$ , where  $\kappa = 0, -1, 1$  for null, spacelike and timelike curves, respectively (for photon orbits the mass  $\mu$  must be changed with a different parameter related to the affine curve parametrization; for a discussion on this point see, for example, [164]). Then, we can introduce the quantities  $\mathcal{M} \equiv \{\Lambda \equiv u^r, \Sigma \equiv u^t, \Phi \equiv u^\phi, \Theta \equiv u^\theta\}$ . Using  $\mathcal{M}$  in Eq. (7.2.3), we obtain

$$\mathcal{E} = -(g_{tt}\Sigma + g_{\phi t}\Phi), \quad \mathcal{L} = (g_{\phi\phi}\Phi + g_{\phi t}\Sigma), \quad (7.4.6)$$

$$\Sigma = \frac{\mathcal{E}g_{\phi\phi} + g_{\phi t}\mathcal{L}}{g_{\phi t}^2 - g_{tt}g_{\phi\phi}}, \quad \Phi = \frac{\mathcal{E}g_{\phi t} + g_{tt}\mathcal{L}}{-g_{\phi t}^2 + g_{tt}g_{\phi\phi}}, \quad (7.4.7)$$

expressing the components  $u^t$  and  $u^\phi$  in terms of the constants of motion. The normalization condition can be solved for  $\mathcal{E}$  to obtain the following *two* solutions,

$$\mathcal{E}_\pm = \frac{-g_{\phi t}\mathcal{L} \pm \sqrt{(g_{\phi t}^2 - g_{tt}g_{\phi\phi}) [\mathcal{L}^2 + g_{\phi\phi}(g_{\theta\theta}\Theta^2 + g_{rr}\Lambda^2 + \kappa)]}{g_{\phi\phi}}. \quad (7.4.8)$$

Considering now the angular frequency  $\omega$  and the specific angular momentum  $\ell \equiv \mathcal{L}/\mathcal{E}$ , or photon impact parameter, we get

$$\omega \equiv \frac{\Phi}{\Sigma} = -\frac{\mathcal{E}g_{\phi t} + g_{tt}\mathcal{L}}{\mathcal{E}g_{\phi\phi} + g_{\phi t}\mathcal{L}} = -\frac{g_{t\phi} + g_{tt}\ell}{g_{\phi\phi} + g_{t\phi}\ell}, \quad (7.4.9)$$

$$\ell \equiv \frac{\mathcal{L}}{\mathcal{E}} = -\frac{\Phi + g_{\phi t}\Sigma}{g_{tt}\Sigma + g_{\phi t}\Phi} = -\frac{g_{t\phi} + g_{\phi\phi}\omega}{g_{tt} + g_{t\phi}\omega}, \quad (7.4.10)$$

which shows explicitly the relation between the angular frequency  $\omega$  of circular orbits, the constants of motion  $\mathcal{L}$  and  $\mathcal{E}$  and the photon impact parameter  $\ell$ . The ZAMO case corresponds to  $\mathcal{L} = 0$ , and is considered in Sec. 7.4.

Equation (7.4.8) leads to the definition of the effective potential  $V_{eff}^\kappa(a; \mathcal{L}, r) \equiv \mathcal{E}_\pm/\mu|_{\Lambda=0}$  on the equatorial plane. Circular motion is defined by the constraint  $\Lambda = 0$ , and  $\Theta = 0$  determines the equatorial hyperplane  $\theta = \pi/2$ . Then, explicitly,

$$V_{eff}(\ell) = \pm \sqrt{\frac{\kappa(g_{\phi t}^2 - g_{tt}g_{\phi\phi})}{g_{\phi\phi} + 2\ell g_{\phi t} + \ell^2 g_{tt}}}, \quad (7.4.11)$$

$$V_{eff}^\pm(\mathcal{L}) = \frac{-g_{\phi t}\mathcal{L} \pm \sqrt{(g_{\phi t}^2 - g_{tt}g_{\phi\phi}) (\mathcal{L}^2 + \kappa g_{\phi\phi})}}{g_{\phi\phi}} \quad (7.4.12)$$

$$= \mathcal{L}\omega_Z \pm \sqrt{(\kappa g_{\phi\phi} + \mathcal{L}^2) (\omega_Z^2 - \omega_*^2)} \quad (7.4.13)$$

$$= \frac{1}{2} \left( \mathcal{L} (\omega_- + \omega_+) \pm \sqrt{(\omega_- - \omega_+)^2 (g_{\phi\phi}\kappa + \mathcal{L}^2)} \right). \quad (7.4.14)$$

In the case of light-like particle,  $\kappa = 0$ , we have that  $\mathcal{E}_\pm = \mathcal{L}\omega_\pm$  and, for  $a \geq a_1$ ,  $\omega_\gamma \equiv |\mathcal{E}_+/\mathcal{L}_-(\mathcal{E}_+)|_{r_\gamma^-} = |\omega_+|_{r_\gamma^-}$ ,  $r_\gamma^-$  is the photon (corotating) orbit in the ergoregion. The frequency  $\omega_-$  corresponds to the case of energy  $\mathcal{E}_-$

with appropriately defined angular momentum on  $r_\gamma^-$ . The functions  $V_{eff}(\mathcal{L})$  and  $V_{eff}(\ell)$  in Eqs. (7.4.11) are related by the transformation  $\mathcal{L} = \mathcal{L}(\ell)$  or  $\ell = \ell(\mathcal{L})$ :

$$\mathcal{L}(\ell) = \sqrt{\ell^2 V_{eff}(\ell)^2} = \sqrt{\frac{(g_{\phi t}^2 - g_{tt}g_{\phi\phi})\kappa\ell^2}{g_{\phi\phi} + \ell(2g_{\phi t} + g_{tt}\ell)}}. \quad (7.4.15)$$

We can write now the effective potential  $V_{eff}^\pm(a; \mathcal{L}, r)$  in Eq.(7.4.8) for timelike particles in terms of the angular momentum  $\ell$ , using Eq. (7.4.9), as

$$u_t^2 = V_{eff}^\pm(a; \ell, r)^2 = \kappa \frac{g_{\phi t}^2 - g_{tt}g_{\phi\phi}}{g_{\phi\phi} + 2\ell g_{\phi t} + \ell^2 g_{tt}} \quad (7.4.16)$$

$$= \kappa \frac{\mathcal{E}^2 (g_{\phi t}^2 - g_{tt}g_{\phi\phi})}{\mathcal{E}^2 g_{\phi\phi} + 2\mathcal{E}g_{\phi t}\mathcal{L}(\ell) + g_{tt}\mathcal{L}(\ell)^2}. \quad (7.4.17)$$

Note that the limiting frequencies  $\omega_\pm(r; a)$ , which determine the light surfaces  $r_s^\pm(\omega; a)$ , are defined from the normalization condition for light-like surfaces; in this sense, they are related to the photon circular motion on the equatorial plane  $u^r = u^\theta = 0$ , i. e., they contain but do not coincide with geodesic circular orbits, which are a particular case. In order to describe motion, it is necessary to specify the dynamics, that is, to consider the normalization condition together with the equations of motion. For the case of an equation in which the effective potential  $V_{eff}^\pm$  appears with the conditions  $\kappa = 0$  and  $\Lambda = \Theta = 0$  (circular motion on the equatorial plane), it is necessary to choose an appropriate parametrization – see, for example, [164, 88].

In fact, the above rearranging of the terms is useful to determine immediately the potential in which a ZAMO observer moves, assuming  $\mathcal{L} = 0$ , and to compare with different orbits where  $\mathcal{L} \neq 0$  (clearly in this case the effective potential will be a function of  $r$  and  $a$ , through  $\omega_*$ ,  $\omega_Z$  and  $g_{\phi\phi}$  which depend on the parameter  $\mathcal{L}$ ). Here we consider for the ZAMO  $V_{eff}|_Z = \tilde{\kappa}g_{\phi\phi}[\omega_*^2 - \omega_Z^2]$  where  $\tilde{\kappa}$  is a factor related to the normalization condition of the ZAMO four-velocity ( $\tilde{\kappa} = -1$  for timelike ZAMOs, where  $u^\phi = -\omega_Z u^t$  and  $u^t = -\epsilon\mathcal{E}/g_{\phi\phi}[\omega_*^2 - \omega_Z^2]$ ,  $\epsilon = 1$  according to Eq. (7.2.3); in the ergoregion  $V_{eff}|_Z^2 > 0$ , but  $V_{eff}|_Z^2 = 0$  for  $r = 0$  and  $r = r_+$ ). The orbits  $\hat{r}_\pm$  are critical points of the effective potential, i. e.,  $\hat{r}_\pm : \partial_r V_{eff}|_Z^2 = 0$ .

<sup>12</sup>. The energy of the ZAMOs is always positive for both **BH** and **NS** spacetimes, and it grows with the source spin; in fact, solutions for  $V_{eff}|_Z = 0$  are not possible because this would correspond to the case of a null angular momentum with null energy. The energy on the orbits  $\hat{r}_\pm$  where  $\mathcal{L} = 0$  is always positive. In **BH** geometries, the potential  $\mathcal{V}_{eff}^0$  at  $\mathcal{L} = 0$ , increases with the distance from the source and has no critical points as a function of  $r/M$ . The most interesting case is then for the slow naked singularity spacetimes of the first class, **NSI** with  $a \in ]M, a_1]$ , where there is a closed and connected orbital region of circular orbits with  $r \in ]\hat{r}_-, \hat{r}_+[$ . The radii  $\hat{r}_\pm$  are ZAMOs orbits, and in this region the potential decreases with the orbital radius. However, in the outer region  $r \in ]r_+, \hat{r}_- [ \cup ]\hat{r}_+, 2M[$ , the potential increases with the radius. This implies that the radii  $\hat{r}_\pm$  are possible circular ZAMOs orbits. In fact,  $\hat{r}_-$  is an *unstable* orbit and  $\hat{r}_+$  is a *stable* orbit. Thus, in any geometry of this set, there is a stable orbit for the ZAMOs with angular velocity  $\hat{\omega}_Z^\pm \equiv \omega_Z(\hat{r}_\pm)$  different from zero, where  $\hat{\omega}_Z^- < \hat{\omega}_Z^+$  (see Fig. 7.12).

In [46], we investigated the orbital nature of the static limit. Here, in Fig. 7.13, the velocity  $\omega_Z$  and the ratio  $\mathcal{R}^\epsilon \equiv \mathcal{E}_-^\epsilon / \mathcal{L}_-^\epsilon$  (that is, the inverse of the specific angular momentum defined as  $u_\phi / u_t$ ) are considered as functions of the source spin at the static limit. We explore the relation between the ZAMOs and the stationary observers, where  $\omega_Z = (\omega_+ + \omega_-) / 2$ , for **NSI** sources at the static limit. A maximum value,  $\mathcal{R}^\epsilon = 0.853553M$ , is reached at  $a = 2M \in$  **NSII**. Also, a maximum value  $\omega_Z^{\epsilon-Max} = 0.176777$  exists for the ZAMOs angular velocity at  $a = a_\diamond \in$  **NSII**. This ratio is always greater than the angular momentum of the ZAMOs at the static limit.

In **BH** spacetimes, the angular velocity for stationary observers is limited by the value  $\omega_h$  which occurs for the radius  $r_+$ . We can evaluate the deviation of this velocity in a neighborhood of the radius  $r_+$ , since the four-velocity of the observers rotating with  $\omega$  (where  $u^a \equiv \xi_t + \omega \xi_\phi$ ) must be timelike outside the horizon and therefore it has to be  $\mathcal{R} = \mathcal{E} / \mathcal{L} > \omega_h$  in that range (the event horizon of a Kerr black hole rotates with angular velocity  $\omega_h$  [45]). This limit cannot be extended to the case of naked singularities. However, one can set similarly the threshold  $\mathcal{E} > \omega_a \mathcal{L}$  in the case of circular orbits, where the frequency limit is restricted to the values  $\omega_a \in [1, a_\mu^{-1}M[$  as  $\omega_a \in [\omega_0(a = M), \omega_0(a_\mu)[$ .

---

<sup>12</sup>The function  $V_{eff}|_Z \equiv \mathcal{V}_{eff}(\omega_Z, r)|_{\mathcal{L}=0}$  resembles the effective potential for the motion of a neutral particle in the Reissner-Norström spacetime [122].

## 7.5 Remarks

In this work, we carried out a detailed analysis of the physical properties of stationary observers moving in the ergoregion along equatorial circular orbits in the gravitational field of a spinning source, described by the stationary and axisymmetric Kerr metric. We derived the explicit value of the angular velocity of stationary observers and analyzed all possible regions where circular motion is allowed, depending on the radius and the rotational Kerr parameter. We found that in general the region of allowed values for the frequencies is larger for naked singularities than for black holes. In fact, for certain values of the radius  $r$ , stationary observers can exist only in the field of naked singularities. We interpret this result as a clear indication of the observational differences between black holes and naked singularities. Given the frequency and the orbit radius of a stationary observer, it is always possible to determine the value of the rotational parameter of the gravitational source. Our results show that in fact the probability of existence of a stationary observer is greater in the case of naked singularities than in the case of black holes. Moreover, it is possible to introduce a classification of rotating sources by using their rotational parameter which, in turn, determines the properties of stationary observers. Black holes and naked singularities turn out to be split each into three different classes in which stationary observers with different properties can exist. In particular, we point out the existence of weak (**NSI**) and strong (**NSIII**) naked singularities, corresponding to spin values close to or distant from the limiting case of an extreme black hole, respectively.

Light surfaces are also a common feature of rotating gravitational configurations. We derived the explicit value of the radius for light surfaces on the equatorial plane of the Kerr spacetime. In the case of black holes, light surfaces are confined within a restricted radial and frequency range. On the contrary, in the naked singularity case, the orbits and the frequency ranges are larger than for black holes. Again, we conclude that light surfaces can be found more often in naked singularities. The observation and measurement of the physical parameters of a particular light surface is sufficient to determine the main rotational properties of the spinning gravitational source. We believe that the study of light surfaces (defining the “throat” discussed in Sec. 7.3) has important applications regarding the possibility of directly observing a black hole in the immediate vicinity of an event horizon (within the region defined by the static limit), as this seems to be possible in the immediate future through, for example, the already active Event Horizon Telescope

(EHT) projects<sup>13</sup>.

We also analyzed the conditions under which a ZAMO can exist in a Kerr spacetime. In particular, we computed the orbital regions and the energy of ZAMOs. The frequency of the ZAMOs is always positive, i.e., they rotate in the same direction of the spinning source as a consequence of the dragging of inertial frames. The energy is also always positive. The most interesting case is that of slowly rotating naked singularities (**NSI**) where there exists a closed and disconnected orbital region. This particular property could, in principle, be used to detect naked singularities of this class. We derived the particular radius at which the frequency of the ZAMOs is maximal, showing that the measurement of this radius could be used to determine whether the spinning source is a black hole or a naked singularity and its class, according to the classification scheme formulated here. To be more specific, from Table 7.2 we infer that the existence of stationary observers in black hole spacetimes is limited from above by the frequency  $\omega_+^e$ , which is the highest frequency on the static limit, implying the frequency lower bound  $\omega = 0$  – see also Fig. 7.4. In this figure, we also show the maximum frequency,  $\omega_e^+$ , at the static limit for a naked singularity with  $a = a_\diamond = \sqrt{2}M \in \mathbf{NSII}$ . This spin plays an important role for the variation of the ZAMOs frequency in **NSs** in terms of the singularity dimensionless spin – see Fig. 7.12 and Fig. 7.13. On the other hand, for strong **BHs**, with  $a > a_1$ , the frequency is bounded from below by  $\omega = \omega_e^+$  and from above by  $\omega_n$ , as the radial upper bound is  $r_s^+$ . A similar situation occurs for **NSs**, provided that  $\omega_n$  is replaced with the limiting frequency  $\omega_0$ . The special role of the **BH** spin  $a_1$  is related to the presence of the photon circular orbit in the **BH** ergoregion, which is absent in **NS** geometries; consequently, as seen in Table 7.2, there is no distinction between the naked singularities classes. However, the analysis of the frequencies in Fig. 7.4 shows differently that there are indeed distinguishing features in the corresponding ergoregions. In the case of naked singularities, the frequency range of stationary observers has as a boundary the outer light-surface,  $r = r_s^+$ , then it narrows as the spin increases, and finally vanishes near the static limit.

The frequency of the orbits on the static limit, in fact, converges to the limit  $\omega_0 = M/a$ , which is an important frequency threshold for the **NS** regime. The presence of a maximum for the special **NS** geometry with  $a = a_\diamond$  on the static limit is symptomatic for the nature of this source – see Figs. 7.4, 7.6 and 7.13. The study of the surfaces  $r_s^\pm$  on the plane  $(r, \omega)$ , for different values

---

<sup>13</sup> <http://www.eventhorizontelescope.org/>

of the spin-mass ratio, shows a clear difference between the allowed regions in naked singularities and black holes (gray region in Fig. 7.6). There is an open “throat” between the spin values  $a \lesssim M$  (strong BHs) and  $a \gtrsim M$  (very weak NSs), with an opening of the cusp (at  $r = 0$  in these special coordinates) for the frequency  $\omega = 0.5$ . We note a change in the situation for spins in  $a/M \in ]1, 1.0001]$ ; this region is in fact extremely sensitive to a change of the source spin; the throat of  $r_s^\pm$  has, in this special spin range, a saddle point around  $(r = M, \omega = 1/2)$  between  $[a_\mu, a_3]$ , which is not present in stronger singularities. The spins in this range are related to the negative state energy and the radii  $r_v^\pm$ , where the orbital energy is  $\mathcal{E} = 0$  – Fig. 7.8. Particularly, we point out the spin  $a = a_\sigma = 1.064306M$ , where  $r_v^- = r_\Delta^- = 0.5107M$ , for which at  $r_\Delta^\pm$  there is a critical point of the frequency amplitude  $\Delta\omega^\pm$ . In BH geometries, the frequencies increase with the spin and with the decrease of the radius towards the horizon. The curves  $r_s^\pm$  continue to increase with the presence of a transition throat at  $r = M$  that increases, stretching and widening. This throat represents a “transition region” between BH and super-spinning sources from the viewpoint of stationary observers. The regions outlined here play a distinct role in the collapse processes with possible spin oscillations and different behaviors for weak, very weak, and strong naked singularities. As the spin increases, the frequencies of NSs observes move to lower values, widening the throat. This trend, however, changes with the spin, enlightening some special thresholds.

This analysis shows firstly the importance of the limiting frequency  $\omega_0 = M/a$ , determining the main properties of both frequencies  $\omega_\pm$  and the radii  $r_s^\pm$ ; it is also relevant in relation to ZAMOs dynamics in NS geometries. In this way, we may see  $\omega_0$  as an extension of the frequency  $\omega_h$  at the horizon for BH solutions—Fig. 7.4. In the NS regime, all the curves  $r_s^\pm$  converge to the same “focal point”  $r = 0$ , regardless of the type of naked singularity, but as  $\omega_h$  is the limiting frequency at the BH horizon, each source is characterized by only one  $\omega_0 \neq 0$  frequency. The greater is the spin, the lower is the frequency  $\omega_\pm$  at fixed radius, and particularly in the neighborhood of the singularity ring, according to the limiting value  $\omega_0$ . The frequency range at fixed  $r/M$  narrows for higher dimensionless NS spin  $a/M$ . This feature distinguishes between strong, weak and very weak naked singularities. From Figs. 7.6 it is clear also that the throat of the light-surfaces  $r_s^\pm$ , in the plane  $r - \omega$ , for different spins  $a/M$  closes for  $a \approx M$ , which is a spin transition region that includes the extreme Kerr solution. This region has been enlarged

in Fig. 7.6-bottom. Figures 7.9 and 7.10 show from a different perspective the transition between the **BH** region, gray region in Figs. 7.6, and the **NS** region for different spins. Any spin oscillation in that region generates a tunnel in the light-surface<sup>14</sup>. The transition region is around  $\omega_{\pm} \approx 1/2$ , which is a special value related to the spin  $a = 2M$  of strong naked singularities—see Figs. 7.3 and 7.2. In this region, as in the neighborhood of the ring singularity ( $r = 0$ ), the orbital range reaches relatively small values<sup>15</sup>. This shows the existence of limitations for a spin transition in the parameter region of very weak naked singularities, pointed out also in [99, 98, 122, 100, 101].

On the other hand, in the strong **NSs** regimes, a spin threshold emerges at  $a = 2M$  and  $a = M$  (see Figs. 7.3, 7.4 and 7.6). In Fig. 7.13, we analyze the properties at the static limit  $r_{\epsilon}^{+}$ . The maximum value of  $\mathcal{E}_{-}/\mathcal{L}_{-}$  is then reached in the ergoregion of the **NSII** class<sup>16</sup>. Around  $a = a_3$  the throat width becomes more or less constant. The situation is different for  $a > a_3$  and  $a > 2M$  and then for  $a_4$ , where the frequencies range narrows, and near  $r = r_{\epsilon}^{+}$  becomes restricted to a small range of a few mass units in the limit of large spin  $a/M$ . In strong and very strong **NSs**, the wide region is inaccessible for stationary observers, whereas it is accessible in the **BH** case. This significantly separates strong and weak **NSs**, and distinguish them from the **BH** case. Interestingly, the saddle point around  $r = M$ , which narrows the throat of frequencies even in the case of **NS** geometries for  $a \in ]M, a_{\sigma}[$ , could perhaps be viewed as a trace of the presence of  $r_{+}$ , which is absent for  $a > M$ . For  $a = a_{\sigma}$ , where the saddle point disappears, the shape of the  $r_{\epsilon}^{\pm}$  tube is dif-

---

<sup>14</sup>Since any simulation of stellar collapse returns to the **BH** regime, there must be some (retroactive) mechanism that closes the observer tunnel, as even light does not run away in the forbidden region at  $r < M$ . Moreover, hypothetical super-luminary matter would violate the bonding of the tunnel wall.

<sup>15</sup>It is worth to mention that predicted quantum effects close to the singularities could play a major role in this region. However, we recall that the extreme limit  $a = M$  in this model is never faced, as we continue to see the spacetime for all **NSs** using a Boyer-Lindquist frame. It is well known that approaching the horizon at  $a = M$ , the radial coordinate velocity appears as never penetrating the black hole, spiraling as  $t$  goes to infinity. This is the consequence of a coordinate singularity which can be avoided by using Kerr coordinates or Eddington-Finkelstein coordinates.

<sup>16</sup>The throat depth in the region would lead to an immediate change of the observers properties and it is reasonable to ask if this may imply an activation instead of a “positive feedback” phenomenon. We recall that in this scenario, we are not considering a change of symmetries which would have an essential role. Then it is important to emphasize that in these hypothetical spin transitions, the external boundary of the ergoregion remains unchanged, but not the frequency at the static limit.

ferent. This, on the other hand, would suggest that the existence of the flex in the case of very weak **NSs** would prevent a further increasing of the spin. This does not hold for a transition to stronger **NSs**,  $a \geq a_\sigma$ , where no saddle point is present—Fig. 7.8-bottom. Obviously, the consequences of the hypothetical transition processes should also take into account the transient phase times. Very weak naked singularities show a “rippled-structure” in the frequency profiles of  $\omega$  with respect to  $r/M$  and  $a/M$ , as appears in Figs. 7.2, 7.6, 7.9, and 7.10. The significance of this structure is still to be fully investigated, but it may be seen perhaps as a fingerprint-remnant of the **BH** horizon. This may open an interesting perspective for the study of **NS** geometries.

An interesting application of our results would be related to the characterization of the optical phenomena in the Kerr naked singularity and black hole geometries, such as the **BH** raytracing and the determination of the **BH** silhouette (shadow). The light escape cones are a key element for such phenomena. Light escape cones of local observers (intended as sources) determine the portion of radiation emitted by a source that could escape to infinity and the one which is trapped. This is related to the study of the radial motion of photons because the boundary of the escape cones is given by directional angles associated to unstable spherical photon orbits. Light escape cones can be identified in locally non-rotating frames, in frames associated to circular geodesic motion and in radially free-falling observers [165, 166, 88, 167, 168]. We want to point out, however, that light escape cones do not define the properties of the light-cone causal structure, and are not directly related to stationary observers; they rather depend on the photon orbits. A thorough-out analysis of the photon circular motion in the region of the ergoregion can be found in [46]. In Figs. 7.1, 7.3, 7.4 and 7.12, we show the photon orbit  $r_\gamma$  and the limiting frequencies crossing this radius; this enlightens the relation with the frequency  $\omega_n$ . A more detailed discussion on the relation between angular frequencies  $\omega_\pm$  and the photon orbit in  $\Sigma_e^+$  in **BH** spacetimes was presented above. We consider there in more detail the relation between the quantities  $\omega_Z$ ,  $\omega_*$ , the constants of motion  $\mathcal{L}$  and  $\mathcal{E}$  and the effective potential, briefly addressed also in Sec. 7.4.

In general, we see that it is possible to detect black holes and naked singularities by analyzing the physical properties (orbital radius and frequency) of stationary observers and ZAMOs. Moreover, the main physical properties (mass and angular momentum) of the spinning gravitational source can be determined by measuring the parameters of stationary observers. This is certainly important for astrophysical purposes since the detection and analysis

of compact astrophysical objects is one of the most important issues of modern relativistic astrophysics. In addition, the results presented in this work are relevant especially for investigating non-isolated singularities, the energy extraction processes, according to Penrose mechanism, and the gravitational collapse processes which lead to the formation of black holes.

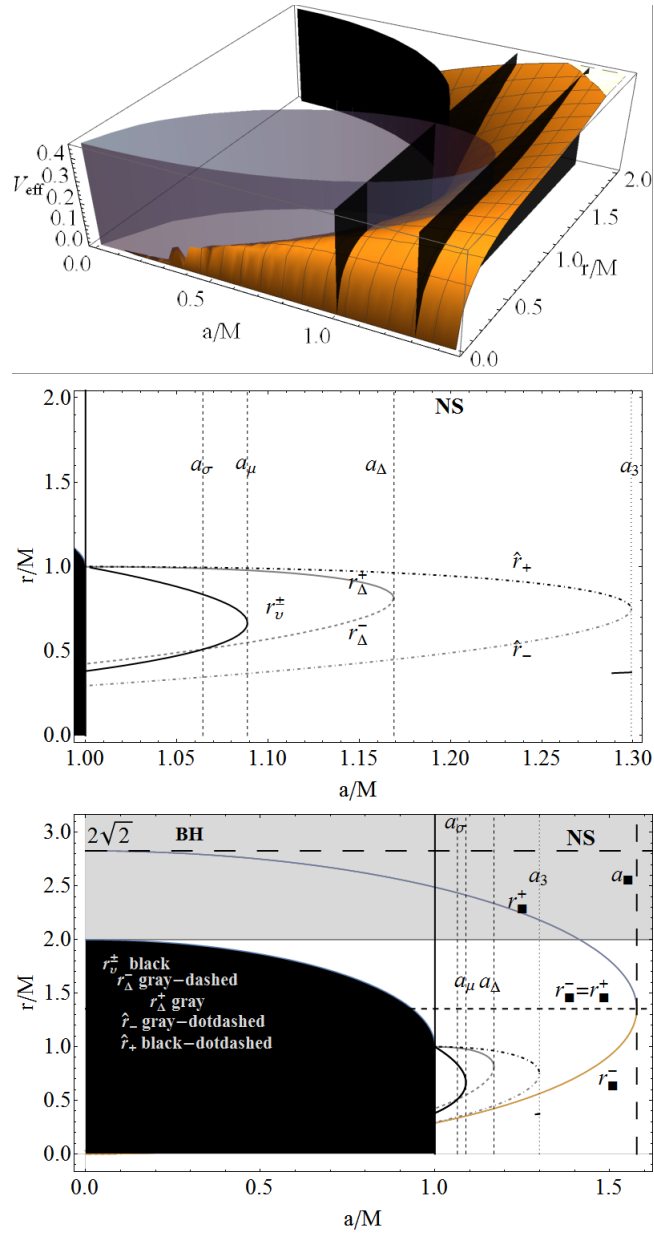


**Figure 7.8:** Upper panel: The effective potential  $V_{\text{eff}}|_Z$  for the ZAMOS  $\mathcal{L} = 0$ , for **BH** and **NS** sources as a function of the source spin  $a/M$  and the radius  $r/M$ . Black planes represent the spin values  $a = M$ , extreme Kerr **BH**, and  $a_3 \equiv 3\sqrt{3}/4M$ , a **NS** geometry, where  $\hat{r}_- = \hat{r}_+$ . The orbits  $\hat{r}_- \leq \hat{r}_+$ , gray surfaces, are for  $a < M$  (**BH**-case) inside the horizon ( $r < r_+$ ). The inner black surface is the horizon  $r_+$ . Central panel: The radius  $r(a)$ , solution of  $\partial_r \Delta \omega_\pm = 0$ . The radius  $r_v^\pm$ , where the orbital energy  $\mathcal{E} = 0$ , and the orbits  $\hat{r}_\pm$ , for which  $\mathcal{L} = 0$ , are also plotted. Dashed lines represent the spins  $a_\sigma \equiv 1.064306M$ ,  $a_\mu \equiv 4\sqrt{2}/3/3M \approx 1.08866M$ ,  $a_\Delta = 1.16905M$  and  $a_3 = 3\sqrt{3}/4M$ . The black region corresponds to  $r < r_+$ . Bottom panel: The radii  $r_\square^\pm : \partial_a \Delta \omega_\pm = 0$  are plotted as functions of  $a/M$ —see also Figs. 7.7.

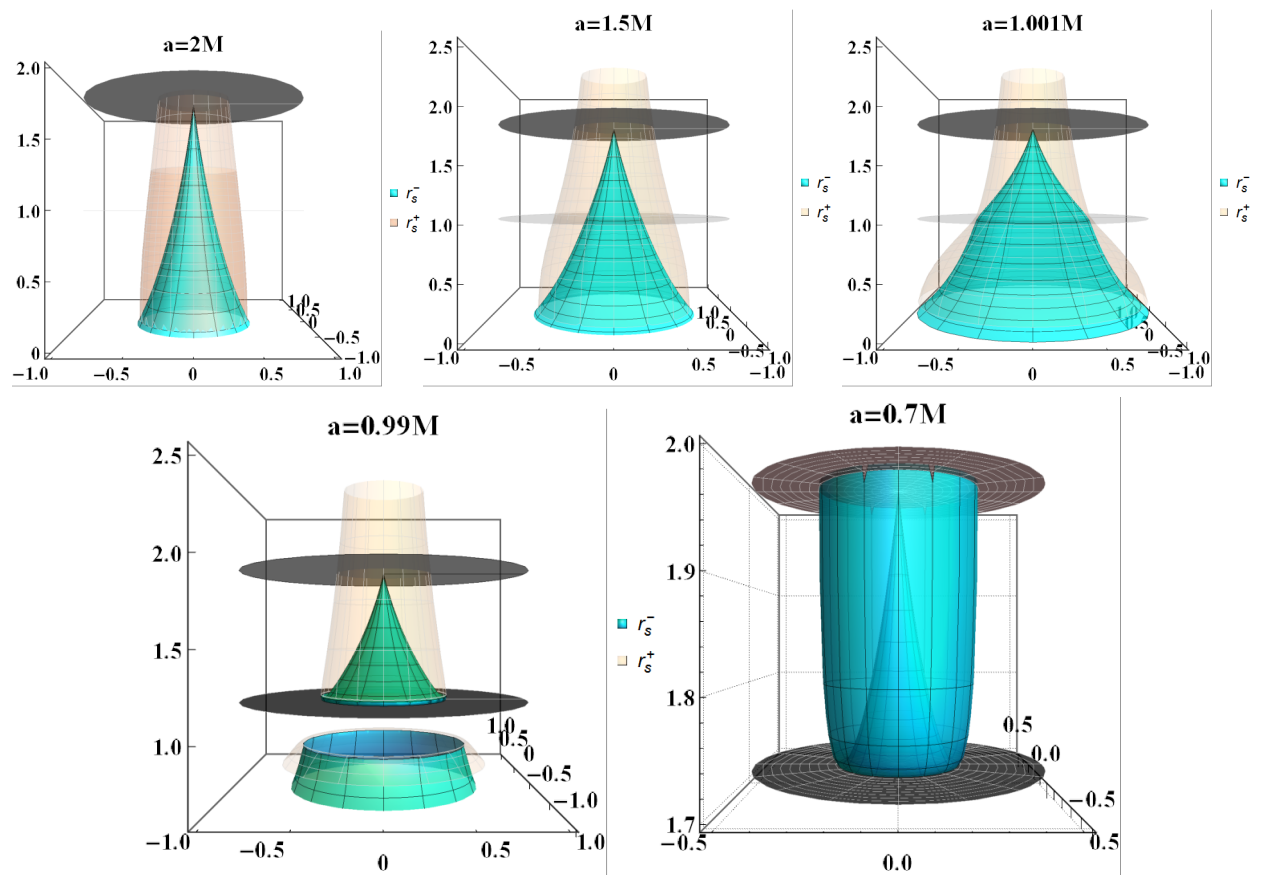


**Figure 7.9:** Plots of the surfaces  $r_s^\pm$  (in units of mass) versus the frequency  $\omega$  for different spin values  $a/M$ , including **BH** and **NS** geometries—see also Figs. 7.6. The surfaces  $r_s^\pm$  are represented as revolution surfaces with height  $r_s^\pm$  (vertical axes) and radius  $\omega$  (horizontal plane). Surfaces are generated by rotating the two-dimensional curves  $r_s^\pm$  around an axis (revolution of the function curves  $r_s^\pm$  around the “z” axis). Thus,  $r = \text{constant}$  with respect to the frequency  $\omega$  is represented by a circle under this transformation. The disks in the plots are either  $r = M$ ,  $r = r_+$  or  $r = r_e^+ = 2M$ . The surfaces  $r_s^\pm$  are green and pink colored, respectively (as mentioned in the legend). In the last panel ( $a = 0.7M$ ), both radii  $r_s^\pm$  are green colored

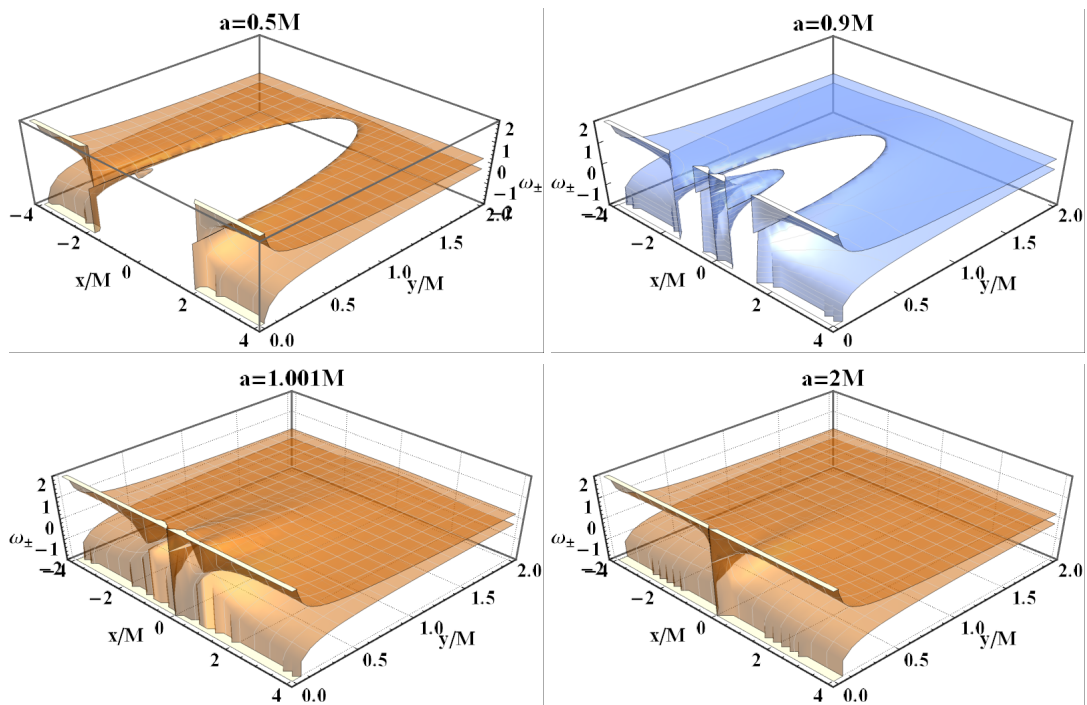


**Figure 7.10:** Plots of frequency surfaces  $\omega_{\pm}(r, \theta)$  as functions of the radial distance  $r$  in Cartesian coordinates  $(x, y)$  for different spin values  $a$ , including BHs and NSs –see also Figs. 7.6.

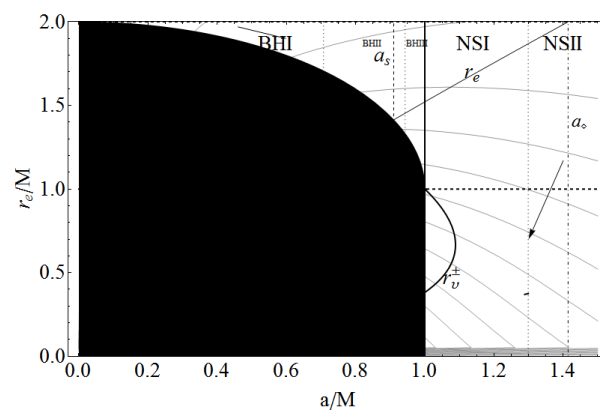


**Figure 7.11:** The plot shows the orbits (gray curves) of constant ZAMOs velocity  $\omega_Z = \text{constant}$  in the **BH** and **NS** regions. The radius  $r_e$  and the spin  $a_s : r_e = r_+$  are marked by dashed lines. The arrows show the increasing of the angular velocity.

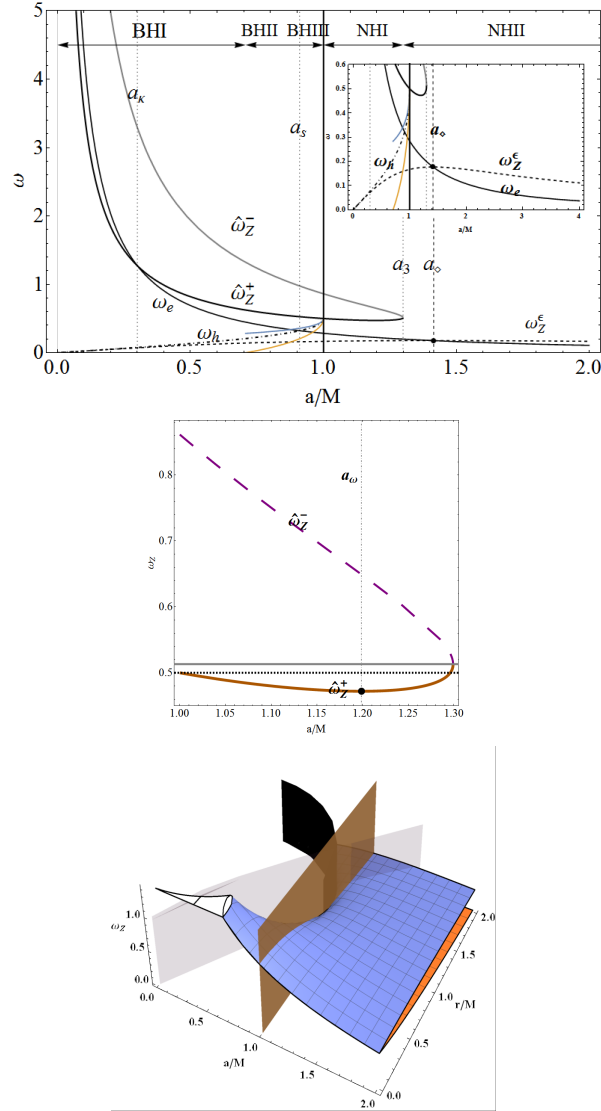


**Figure 7.12:** Upper panel: The angular velocity  $\omega_e \equiv \omega_Z(r_e)$  as a function of  $a/M$ . The angular velocities  $\omega_Z^\epsilon \equiv \omega_Z(r_e^+)$  (dashed curve),  $\omega_h \equiv \omega_\pm(r_+) = \omega_Z(r_+)$  (dot-dashed curve),  $\hat{\omega}_Z^\pm \equiv \omega_Z(\hat{r}_\pm)$  as functions of the spacetime rotation  $a/M$  for different **BH** and **NS** classes. Dotted lines are  $a_\kappa \approx 0.3002831060M$  :  $\omega_e = \hat{\omega}_Z^+$ ,  $a_s \approx 0.91017M$  :  $\omega_e = \omega_h$ ,  $a_3$  :  $\hat{\omega}_Z^+ = \hat{\omega}_Z^- = 8/9\sqrt{3}$ , and finally the spin  $a_\diamond = \sqrt{2}M$  :  $\omega_Z^\epsilon = \omega_2$  (dashed line) which is a maximum for  $\omega_Z^\epsilon$  (the maximum point is marked with a point). The inset plot is a zoom. The radius  $r_e/M$  is a maximum for  $\omega_e$ . The angular velocities  $\omega_\pm$  on the **BH** photon orbit  $r_\gamma \in \Sigma_e^+$  are also plotted (colored lines). Center panel:  $\hat{\omega}_Z^\pm \equiv \omega_Z(\hat{r}_\pm)$  as functions of  $a/M$  for different **NS** classes. The minimum point of the ZAMOs frequency  $\hat{\omega}_Z^+$  is marked with a point at spin  $a_\omega = 1.19866M$ . Bottom panel: The ZAMOs angular velocity  $\omega_Z$  is plotted as a function of the spin  $a/M$  and the radius  $r/M$ . The plane  $a = M$  and the horizon surface  $r = r_+$  are black surfaces. The gray surface denotes the orbit  $r_e$ . For both **NS** and **BH** spacetimes, the ZAMOs have a maximum frequency which is a function of  $a/M$ . The black thick curve corresponds to  $\mathcal{E} = 0$ . The black region denotes the region inside the outer horizon  $r < r_+$ .

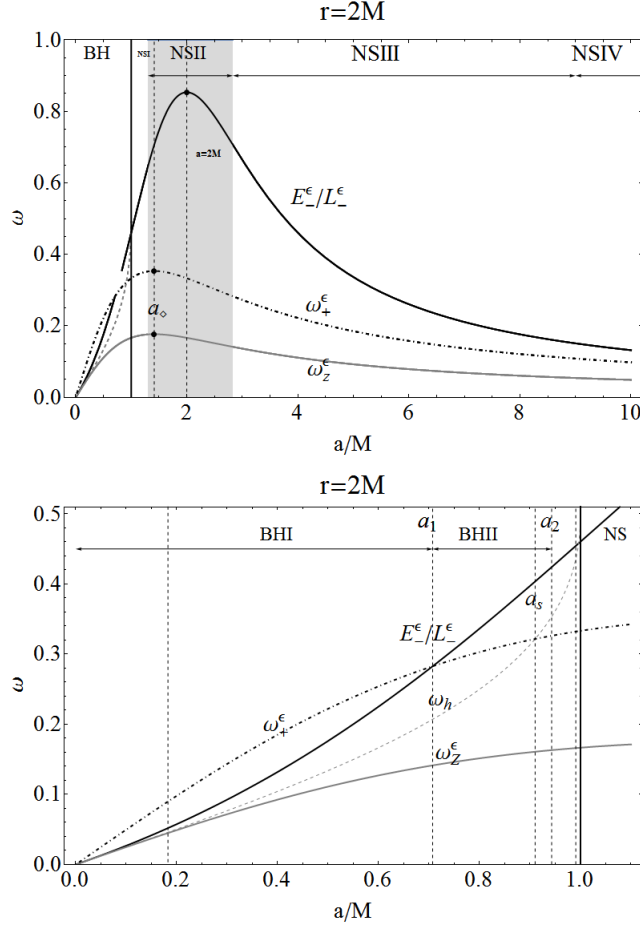


**Figure 7.13:** Upper panel: The ratio  $\mathcal{E}_-^\epsilon / \mathcal{L}_-^\epsilon$  and the angular momentum of the ZAMOs  $\omega_Z^\epsilon$  as a function of  $a/M$  in the static limit  $r = r_\epsilon^+$ . The angular momentum  $\omega_+^\epsilon \equiv \omega_+(r_\epsilon^+)$  which is a boundary frequency for the stationary observer (outer light surface) is plotted (gray curve). The radius  $r_\epsilon^+$  is defined by the condition  $\omega_-(r_\epsilon^+) = 0$ ,  $\omega_h$  is the ZAMOs angular velocity on  $r = r_+$ , i.e.  $\omega_\pm(r_\pm) = \omega_h$ . The maxima are denoted by points. The **NSII** region is in light-gray. A zoom of this plot in the **BH** region is in the bottom panel.

# Bibliography

- [1] H. Stephani, D. Kramer, M. MacCallum, C. Hoenselaers, and E. Herlt, *Exact solutions of Einstein's field equations*, Cambridge University Press, Cambridge UK, 2003.
- [2] F. J. Ernst, *New formulation of the axially symmetric gravitational field problem*, *Phys. Rev.* **167** (1968) 1175; F. J. Ernst, *New Formulation of the axially symmetric gravitational field problem II* *Phys. Rev.* **168** (1968) 1415.
- [3] H. Quevedo and B. Mashhoon, *Exterior gravitational field of a rotating deformed mass*, *Phys. Lett. A* **109** (1985) 13; H. Quevedo, *Class of stationary axisymmetric solutions of Einstein's equations in empty space*, *Phys. Rev. D* **33** (1986) 324; H. Quevedo and B. Mashhoon, *Exterior gravitational field of a charged rotating mass with arbitrary quadrupole moment*, *Phys. Lett. A* **148** (1990) 149; H. Quevedo, *Multipole Moments in General Relativity - Static and Stationary Solutions-*, *Fort. Phys.* **38** (1990) 733; H. Quevedo and B. Mashhoon *Generalization of Kerr spacetime*, *Phys. Rev. D* **43** (1991) 3902.
- [4] H. Weyl, *Zur Gravitationstheorie*, *Ann. Physik (Leipzig)* **54** (1917) 117.
- [5] T. Lewis, *Some special solutions of the equations of axially symmetric gravitational fields*, *Proc. Roy. Soc. London* **136** (1932) 176.
- [6] A. Papapetrou, *Eine rotationssymmetrische Lösung in der Allgemeinen Relativitätstheorie*, *Ann. Physik (Leipzig)* **12** (1953) 309.
- [7] F. J. Hernandez, F. Nettel, and H. Quevedo, *Gravitational fields as generalized string models*, *Grav. Cosmol.* **15**, 109 (2009).
- [8] H. Quevedo, *General Static Axisymmetric Solution of Einstein's Vacuum Field Equations in Prolate Spheroidal Coordinates*, *Phys. Rev. D* **39**, 2904–2911 (1989).

- [9] G. Erez and N. Rosen, *Bull. Res. Council. Israel* **8**, 47 (1959).
- [10] B. K. Harrison, *Phys. Rev. Lett.* **41**, 1197 (1978).
- [11] H. Quevedo, *Generating Solutions of the Einstein–Maxwell Equations with Prescribed Physical Properties*, *Phys. Rev. D* **45**, 1174–1177 (1992).
- [12] W. Dietz and C. Hoenselaers, *Solutions of Einstein’s equations: Techniques and results*, (Springer Verlag, Berlin, 1984).
- [13] V. A. Belinski and V. E. Zakharov, *Soviet Phys. – JETP*, **50**, 1 (1979).
- [14] C. W. Misner, *Harmonic maps as models for physical theories*, *Phys. Rev. D* **18** (1978) 4510.
- [15] D. Korotkin and H. Nicolai, *Separation of variables and Hamiltonian formulation for the Ernst equation*, *Phys. Rev. Lett.* **74** (1995) 1272.
- [16] J. Polchinski, *String Theory: An introduction to the bosonic string*, Cambridge University Press, Cambridge, UK, 2001.
- [17] D. Nuñez, H. Quevedo and A. Sánchez, *Einstein’s equations as functional geodesics*, *Rev. Mex. Phys.* **44** (1998) 440; J. Cortez, D. Nuñez, and H. Quevedo, *Gravitational fields and nonlinear sigma models*, *Int. J. Theor. Phys.* **40** (2001) 251.
- [18] R. Geroch, *J. Math. Phys.* **11**, 2580 (1970).
- [19] R. O. Hansen, *J. Math. Phys.* **15**, 46 (1974).
- [20] D. Bini, A. Geralico, O. Luongo, and H. Quevedo, *Generalized Kerr space-time with an arbitrary quadrupole moment: Geometric properties vs particle motion*, *Class. Quantum Grav.* **26**, 225006 (2009).
- [21] Carminati, J., McLenaghan, R.G.: Algebraic invariants of the Riemann tensor in a four-dimensional Lorentzian space, *Journal of Mathematical Physics* **32**(11), 3135–3140 (1991).
- [22] Doroshkevich, A., Zeldovich, Y.B., Novikov, I.: Gravitational collapse of nonsymmetric and rotating masses, *Journal of Experimental and Theoretical Physics (Soviet Physics JETP)* **22**(1), 122–130 (1966).

- [23] Erez, G., Rosen, N.: The gravitational field of a particle possessing a multipole moment. *Bulletin of the Research Council Israel* **8F**, 47–50 (1959).
- [24] Ernst, F.J.: New formulation of the axially symmetric gravitational field problem, *Phys. Rev.* **167**, 1175–1178 (1968).
- [25] Ernst, F.J.: New formulation of the axially symmetric gravitational field problem. II, *Phys. Rev.* **168**, 1415–1417 (1968).
- [26] Fodor, G., Hoenselaers, C., Perjés, Z.: Multipole moments of axisymmetric systems in relativity, *Journal of Mathematical Physics* **30**(10), 2252–2257 (1989).
- [27] Geroch, R.: Multipole moments. II. Curved space. *Journal of Mathematical Physics* **11**(8), 2580–2588 (1970).
- [28] Gürsel, Y.: Multipole moments for stationary systems: The equivalence of the Geroch-Hansen formulation and the Thorne formulation. *General Relativity and Gravitation* **15**(8), 737–754 (1983).
- [29] Gutsunayev, T.I., Manko, V.S.: On the gravitational field of a mass possessing a multipole moment. *General Relativity and Gravitation* **17**(11), 1025–1027 (1985).
- [30] Hansen, R.O.: Multipole moments of stationary space-times. *Journal of Mathematical Physics* **15**(1), 46–52 (1974).
- [31] Hernández-Pastora, J.L.: Relativistic gravitational fields near the Schwarzschild solution. Ph.D. thesis, University of Salamanca, Spain (1996).
- [32] Hernández-Pastora, J.L., Martín, J.: Monopole-quadrupole static axisymmetric solutions of Einstein field equations. *General Relativity and Gravitation* **26**(9), 877–907 (1994).
- [33] Hoenselaers, C., Perjés, Z.: Multipole moments of axisymmetric electrovacuum spacetimes. *Classical and Quantum Gravity* **7**(10), 1819–1825 (1990).

- [34] Malafarina, D.: Physical properties of the sources of the gamma metric. In: *Dynamics and Thermodynamics of Black Holes* (Conf. Proc. C0405132), 273 (2004).
- [35] Manko, V.S.: On the description of the external field of a static deformed mass. *Classical and Quantum Gravity* **7**(9), L209–L211 (1990).
- [36] Quevedo, H.: On the exterior gravitational field of a mass with a multipole moment. *General Relativity and Gravitation* **19**(10), 1013–1023 (1987).
- [37] Quevedo, H.: General static axisymmetric solution of Einstein's vacuum field equations in prolate spheroidal coordinates. *Phys. Rev. D* **39**, 2904–2911 (1989).
- [38] Quevedo, H.: Mass quadrupole as a source of naked singularities. *International Journal of Modern Physics D* **20**(10), 1779–1787 (2011).
- [39] Ryan, F.D.: Gravitational waves from the inspiral of a compact object into a massive, axisymmetric body with arbitrary multipole moments. *Phys. Rev. D* **52**, 5707–5718 (1995).
- [40] Schwarzschild, K.: Über das Gravitationsfeld eines Massenpunktes nach der Einsteinschen Theorie. *Sitzungsberichte der Königlich Preussischen Akademie der Wissenschaften*, 7, 189–196 (1916)
- [41] Simon, W., Beig, R.: The multipole structure of stationary space-times. *Journal of Mathematical Physics* **24**(5), 1163–1171 (1983).
- [42] Thorne, K.S.: Multipole expansions of gravitational radiation. *Rev. Mod. Phys.* **52**, 299–339 (1980).
- [43] Voorhees, B.H.: Static axially symmetric gravitational fields. *Phys. Rev. D* **2**, 2119–2122 (1970).
- [44] Zipoy, D.M.: Topology of some spheroidal metrics. *Journal of Mathematical Physics* **7**(6), 1137–1143 (1966).
- [45] R. M. Wald, *General Relativity*, (The University of Chicago Press, Chicago, 1984).

- [46] D. Pugliese and H. Quevedo, *Eur. Phys. J. C* **75**, 5, 234 (2015).
- [47] Jacob D. Bekenstein, *Phys. Rev. D* **7**, 2333 (1973).
- [48] Robert M. Wald, *Living Rev Relativ.* 4(1), 6 (2001).
- [49] T. M. Fiola, J. Preskill, A. Strominger and S. P. Trivedi, *Phys. Rev. D* **50**, 3987 (1994).
- [50] H. Nikolic, *Phys. Lett. B* **678**, 218 (2009).
- [51] K. Bradler and C. Adami, *JHEP* **1405**, 095 (2014).
- [52] L. Susskind, *Scientific American* **276**, 4, 52-57 (1997).
- [53] S.W.Hawking, *Comm. Math. Phys.* 43, 199 (1975) Erratum - *ibidem* 46, 206 (1976).
- [54] S.W.Hawking, *Mon. Not. R. astr. Soc.*152, 75-78 (1971).
- [55] R. Penrose, *Revista del Nuovo Cimento* (1969).
- [56] J.D. Bekenstein, *Physical Review D*, 12, 3077 (1975).
- [57] R. Penrose, and R. M. Floyd, *Science* **229**, 177179 (1971).
- [58] F. Gray, S. Schuster, A. VanBrunt and M. Visser, *Class. Quant. Grav.* **33**, 11, 115003, (2016).
- [59] M. Bejger, T. Piran, M. Abramowicz and F. Hakanson, *Phys. Rev. Lett.* **109**, 121101 (2012).
- [60] Z. Stuchlik, P. Slany, G. Torok and M. A. Abramowicz, *Phys. Rev. D* **71**, 024037 (2005).
- [61] D. L. Meier, *Black Hole Astrophysics The Engine Paradigm*, (Springer-Verlag, Berlin Heidelberg, 2012).
- [62] V. P. Frolov, A. Zelnikov, *Introduction to Black Hole Physics*, (Oxford University Press, 488, 2011).
- [63] J. Gariel, G. Marilhacy and N. O. Santos, *Astrophys. J.* **774**, 109 (2013).
- [64] R. Znajek, *Nature*, **262**, 270 (1976).

- [65] A. R. Prasanna and R. K. Varma, *Pramana* **8**, 3 229 (1977).
- [66] A. R. Prasanna and C. V. Vishveshwara, *Pramana* **11**, 359 (1978).
- [67] A. N. Aliev and N. Özdemir, *Mon. Not. Roy. Astron. Soc.* **336**, 241 (2002).
- [68] G. Preti, *Class. Quantum Grav.* **21**, 3433 (2004).
- [69] P. Bakala, E. Šrámková, Z. Stuchlík, and G. Török, *Class. Quantum Grav.* **27**, 045001 (2010).
- [70] V. P. Frolov and A. A. Shoom, *Phys. Rev. D* **82**, 084034 (2010).
- [71] T. Igata, T. Harada, M. Kimura, *Phys. Rev. D* **85**, 104028 (2012).
- [72] R. Shiose, M. Kimura, T. Chiba, *Phys. Rev. D* **90**, 124016 (2014).
- [73] S. Hussain, I. Hussain, M. Jamil, *Eur. Phys. J. C* **74** 12, 3210 (2014).
- [74] G. Pei, S. Nampalliwar, C. Bambi and M. J. Middleton, *Eur. Phys. J. C* **76**, 10, 534 (2016).
- [75] S. S. Komissarov, *J. Korean Phys. Soc.* **54**, 2503 (2009).
- [76] J.-P. Lasota, E. Gourgoulhon, M. Abramowicz, A. Tchekhovskoy and R. Narayan, *Phys. Rev. D* **89**, 2, 024041 (2014).
- [77] Z. Stuchlik and J. Kovar, *Class. Quant. Grav.* **23**, 3935 (2006).
- [78] Z. Stuchlik, D. Pugliese, J. Schee and H. Kuckov, *Eur. Phys. J. C* **75**, 9, 451 (2015).
- [79] A. Kotrlouk, G. Trk, E. Sramkov and Z. Stuchlik, *Astron. Astrophys.* **572**, A79 (2014).
- [80] K. Boshkayev, E. Gasporn, A. C. Gutierrez-Pierres, H. Quevedo, and S. Toktarbay *Phys. Rev. D* **93**, 024024 (2015).
- [81] M. Kolos and Z. Stuchlik, *Phys. Rev. D* **88** 065004, (2013).
- [82] J. Schee and Z. Stuchlik, *JCAP* **1304**, 005 (2013).
- [83] Z. Stuchlik, J. Schee, *Class. Quant. Grav.* **30**, 7, 075012 (2013).

- [84] G. Torok and Z. Stuchlik, *Astron. Astrophys.* **437**, 775 (2005).
- [85] Z. Stuchlik, *Bull. Astron. Inst. Czech*, **32**, 2, 68-72 (1981).
- [86] Z. Stuchlik, S. Hledik, K. Truparov, *Class. Quant. Grav.* **28**, 15 155017 (2011).
- [87] Z. Stuchlik and J. Schee, *Class. Quant. Grav.*, **29**, 6, (2012).
- [88] Z. Stuchlik and J. Schee, *Class. Quant. Grav.* **27**, 215017 (2010).
- [89] M. Patil and P. S. Joshi, *Class. Quant. Grav.* **28**, 235012 (2011).
- [90] Z. Stuchlik and J. Schee, *Class. Quant. Grav.* **29** 065002, (2012).
- [91] Z. Stuchlik and J. Schee, *Class. Quant. Grav.* **30**, 075012 (2013).
- [92] K. i. Nakao, P. S. Joshi, J. Q. Guo, P. Kocherlakota, H. Tagoshi, T. Harada, M. Patil and A. Krolak, arXiv:1707.07242 [gr-qc].
- [93] M. J. Lake and B. Carr, *JHEP* **1511**, 105 (2015).
- [94] B. J. Carr, arXiv:1703.08655 [gr-qc].
- [95] B. J. Carr, J. Mureika and P. Nicolini, *JHEP* **1507**, 052 (2015).
- [96] B. J. Carr, *Springer Proc. Phys.* **170**, 159 (2016).
- [97] Y. Prok *et al.* [CLAS Collaboration], *Phys. Lett. B* **672** (2009) 12
- [98] D. Pugliese, H. Quevedo and R. Ruffini, *Eur. Phys. J. C* **77**, 4, 206 (2017).
- [99] D. Pugliese, H. Quevedo and R. Ruffini, *Phys. Rev. D* **83**, 104052 (2011).
- [100] D. Pugliese, H. Quevedo and R. Ruffini, *Phys. Rev. D* **88**, 024042 (2013).
- [101] D. Pugliese, H. Quevedo and R. Ruffini, *Phys. Rev. D* **84**, 044030 (2011).
- [102] R. Goswami, P. S. Joshi and P. Singh, *Phys. Rev. Lett.* **96**, 031302 (2006).
- [103] C. Vaz and L. Witten, *Phys. Lett. B* **442**, 90 (1998).
- [104] H. Iguchi, T. Harada and K. i. Nakao, *Prog. Theor. Phys.* **101**, 1235 (1999).

- [105] H. Iguchi, K. i. Nakao and T. Harada, *Phys. Rev. D* **57**, 7262 (1998).
- [106] H. Iguchi, T. Harada and K. i. Nakao, *Prog. Theor. Phys.* **103**, 53 (2000).
- [107] Stuart L. Shapiro and Saul A. Teukolsky, *Phys. Rev. Lett.* **66**, 994 (1991).
- [108] T. A. Apostolatos K. S. Thorne, *Phys. Rev. D* **46**, 2435 (1992).
- [109] T. Jacobson, T. P. Sotiriou, *Phys. Rev. Lett.* **103**, 141101 (2009).
- [110] T. Jacobson and T. P. Sotiriou, *J. Phys. Conf. Ser.* **222**, 012041 (2010).
- [111] E. Barausse, V. Cardoso, and G. Khanna *Phys. Rev. Lett.* **105**, 261102 (2010).
- [112] B. Giacomazzo, L. Rezzolla and N. Stergioulas, *Phys. Rev. D* **84**, 024022 (2011).
- [113] V. Cardoso, P. Pani, M. Cadoni and M. Cavaglia, *Phys. Rev. D* **77**, 124044 (2008).
- [114] N. Comins and B. F. Schutz, *Proc. R. Soc. A* **364**, 1717 211-226 (1978).
- [115] A. Helou, I. Musco and J. C. Miller, arXiv:1601.05109 [gr-qc].
- [116] R. M. Wald and V. Iyer, *Phys. Rev. D* **44**, 3719 (1991).
- [117] P. S. Joshi, *Gravitational Collapse and Spacetime Singularities*, Cambridge Monographs on Mathematical Physics, New York 2007.
- [118] B. P. Abbott et al. (LIGO Scientific Collaboration and Virgo Collaboration) *Phys. Rev. Lett.* **116**, 061102 (2016).
- [119] B. P. Abbott *et al.* [LIGO Scientific and Virgo Collaborations], *Phys. Rev. Lett.* **119**, 16, 161101 (2017).
- [120] B. P. Abbott *et al.* [LIGO Scientific and Virgo and Fermi-GBM and INTEGRAL Collaborations], *Astrophys. J.* **848**, 2, L13 (2017).
- [121] M. Blaschke and Z. Stuchlk, *Phys. Rev. D* **94**, 8, 086006 (2016).
- [122] D. Pugliese, H. Quevedo and R. Ruffini, *Phys. Rev. D* **83**, 024021 (2011).
- [123] David B. Malament, *Journal of Mathematical Physics* **18**, 1399 (1977).

- [124] S. W. Hawking, A. R. King, and P. J. McCarthy, *Journal of Mathematical Physics* **17**, 174 (1976).
- [125] Robert P. Geroch, *Journal of Mathematical Physics*, **8**, 782 (1967).
- [126] F. de Felice, *A&A* **34**, 15 (1974).
- [127] F. de Felice, *Nature* **273**, 429-431 (1978).
- [128] Z. Stuchlik and J. Schee, *Int. J. Mod. Phys. D* **24**, 1550020 (2015).
- [129] J. Schee and Z. Stuchlik, *JCAP* **1506** 048, (2015).
- [130] J. Gariel, N. O. Santos and J. Silk, *Phys. Rev. D* **90**, 063505 (2014).
- [131] N. Pelavas, N. Neary and K. Lake, *Class. Quant. Grav.* **18**, 1319 (2001).
- [132] C. Herdeiro and E. Radu, *Phys. Rev. D* **89**, 124018 (2014).
- [133] Z. Stuchlik, *Bull. Astron. Inst. Czech* **31**, 129 (1980).
- [134] S. Gao and Y. Zhang, *Phys. Rev. D* **87**, 4 044028 (2013).
- [135] Z. Stuchlik, *Bull. Astron. Inst. Czech.* **32**, 68 (1981).
- [136] Z. Stuchlik, S. Hledik and K. Truparova, *Class. Quant. Grav.* **28**, 155017 (2011).
- [137] M. H. P. M. van Putten, *Prog. Theor. Phys.* **127**, 2 331-354 (2012).
- [138] C. F. Gammie, S. L. Shapiro and J. C. McKinney, *Astrophys. J.* **602**, 312 (2004).
- [139] P. Abolmasov *Mon. Not. R. Astron. Soc.* **432**, 761-768 (2013).
- [140] M. Kesden, *Phys. Rev. D* **83**, 104011 (2011).
- [141] R. M. Wald, *Ann. Phys.* **82**, 548 (1974).
- [142] P. Pradhan and P. Majumdar, *Eur. Phys. J. C* **73**, 6 2470 (2013).
- [143] D. Pugliese and G. Montani, *Phys. Rev. D* **91**, 8, 083011 (2015).
- [144] D. Pugliese and Z. Stuchlik, *Astrophys. J. Suppl.* **221**, 25 (2015).

- [145] D. Pugliese and Z. Stuchlik, *Astrophys. J. Suppl.* **229**, 2, 40 (2017).
- [146] D. Pugliese and Z. Stuchlik, *Astrophys. J. Suppl.* **223**, 2, 27 (2016).
- [147] D. Pugliese and Z. Stuchlik, *JHEAp* **17**, 1 (2018).
- [148] Z. Li and C. Bambi, *Phys. Rev. D* **87**, 124022 (2013).
- [149] J. Biák, Z. Stuchlik, and V. Balek, *Bull. Astron. Inst. Czech* **40**, 2 6592 (1989).
- [150] V. Balek, J. Bicak, Z. Stuchlik, *Bull. Astron. Inst. Czech* **40**, 3 133-165 (1989).
- [151] J. Kovar, O. Kopacek, V. Karas and Z. Stuchlik, *Class. Quant. Grav.* **27**, 135006 (2010).
- [152] S. W. Hawking & G. F. R. Ellis, *The large scale structure of space-time*, (Cambridge University Press, Cambridge, 1973).
- [153] C. Chakraborty, M. Patil, P. Kocherlakota, S. Bhattacharyya, P. S. Joshi and A. Krlak, *Phys. Rev. D* **95**, 8, 084024 (2017).
- [154] A. V. Frolov and V. P. Frolov, *Phys. Rev. D* **90**, 12, 124010 (2014).
- [155] J. B. Griffiths & J. Podolský, *Exact space-times in Einstein's General Relativity*, (Cambridge University Press, Cambridge, 2009).
- [156] L.D. Landau, E.M. Lifshitz, *The Classical Theory of Fields*, (Oxford, Pergamon Press, 1980).
- [157] Eric Poisson, *A Relativist's Toolkit: The Mathematics of Black-Hole Mechanics*, 1st Edition 2004, Cambridge University Press.
- [158] M. R. R. Good and Y. C. Ong, *Phys. Rev. D* **91**, 4, 044031 (2015).
- [159] P. T. Chrusciel, J. Lopes Costa and M. Heusler, *Living Rev. Rel.* **15**, 7 (2012).
- [160] B. Carter, gr-qc/9712038.
- [161] R. M. Wald, *Living Rev. Rel.* **4**, 6 (2001).

- [162] R. M. Wald, *Class. Quant. Grav.* **16**, A177 (1999).
- [163] S. Chandrasekhar, *The Mathematical Theory of Black Holes*, Oxford University Press (1983).
- [164] C. W. Misner, K. S. Thorne, J. A. Wheeler, *Gravitation*, (Freeman, San Francisco, 1973).
- [165] Jan Schee, Zdenek Stuchlik and Josef Juran Proceedings of RAG-time 6/7: Workshops on black holes and neutron stars, Opava, 1618/1820 September, 2004/2005
- [166] J. Schee and Z. Stuchlik, *Int. J. Mod. Phys. D* **18**, 983 (2009).
- [167] Takahashi, R.; Takahashi, M. *Astronomy and Astrophysics*, 513, A77, 7 (2010)
- [168] J. Schee and Z. Stuchlik, *Gen. Rel. Grav.* **41**, 1795 (2009).

